8-2014

Synthesis, Design, and Environmental Fate of Metallic Nanoparticles

Ashley E. Hart
Clemson University

SYNTHESIS, DESIGN, AND ENVIRONMENTAL FATE OF METALLIC NANOPARTICLES

A Dissertation
Presented to
the Graduate School of
Clemson University

In Partial Fulfillment
of the Requirements for the Degree
Doctor of Philosophy
Chemical Engineering

---

by
Ashley E. Hart
August 2014

Accepted by:
Dr. Christopher L. Kitchens, Committee Chair
Dr. David Bruce
Dr. Mark Roberts
Dr. Brian A. Powell
Dr. O. Thompson Mefford

ABSTRACT

Rational design of nanoparticle surface chemistry offers the ability to control nanoparticle characteristics such as size, polydispersity, shape, dispersibility in various solvents, functionality and end fate. Ligand exchange has proved to be is a versatile method for modifying the surface of plasmonic nanoparticles. Ligand exchange has provided a "green" alternative to traditional biphasic syntheses that require large amounts of phase transfer catalysts. Ligand exchange can also be used to reduce the amount of post synthesis processing and waste when it is conducted on nanoparticles that have been synthesized with a method that affords control over nanoparticle size and polydispersity. Ligand exchange is also an important reaction to consider when determining the end fate of nanomaterials due to the fact that when nanoparticles enter the natural environment, they will be exposed to a variety of natural ligands and electrolytes. We have conducted a comprehensive review of ligand exchange literature and used isothermal titration calorimetry to investigate ligand binding and exchange on gold nanoparticles experimentally. We have also investigated the impact that citrate and natural organic matter surface chemistries have on the transport properties of silver nanoparticles. This work has led to a greater understanding of the influencing factors on the mechanism of nanoparticle ligand binding and exchange.

DEDICATION

I would like to dedicate this dissertation to the people who sparked my interest in science, chemistry, and engineering; Jack Starr, Sean Muller and Tray Sleeper. Without their encouragement and drive to make a difference in a young woman's life, I would not have had the motivation to complete this dissertation. Thank you for always challenging me and providing me with the experiences that have made me the scientist I am today.

ACKNOWLEDGEMENTS

I would first like to thank my family for providing the support I needed get through graduate school. To my mother, you are my rock. You are always there to give me advice when I needed it most. To my father, thank you for telling me "just get it done." And finally to my brothers, thank you for giving me the motivation to get better grades than you simply by telling me I would be "the smartest doctor at McDonalds." I love all of you!

Second, I would like to thank Max, my best friend and partner in life. I wouldn't have stayed sane throughout the past 4 years with you. Thank you for your support, encouragement and most of all your patience, I love you.

Dr. Christopher L. Kitchens, I would like to thank you for giving me the opportunity to be a part of your research group, you have been an inspiring adviser. Thank you for your guidance, direction and patience with me as I like to leave things to the last possible moment! I would especially like to thank your for standing by me when my heart wasn't in it and for giving me the encouragement to keep going.

I would like to thank my dissertation committee, Dr. Powell, Dr. Mefford, Dr. Bruce and Dr. Roberts, for taking the time to read my dissertation and providing feedback on my work.

To my lab mates, past and present, Fiaz for telling me to be confident in myself, Jose for always having a snack ready for me, I would also like to thank the people who started this journey called graduate school with me; Nolan Wilson and Jesse Kelly.

I would like to thank of my collaborators; Hilary Emerson thank your for talking through problems with me and helping me come up with solutions, Kathleen Davis thank you for lending me lab supplies and helping me with my review paper. I would also like to thank Dr. Powell and Dr. Mefford for giving me unlimited access to your labs and for your guidance in my projects.

Lastly, I would like to acknowledge all of the people who have helped me in various ways during my time in graduate school including (but not limited to) Serita Aker, Bethany Carter, Dan D'Unger, Roland Stone, Steven Saville, Shanna Estes, Sam Gorosh, Scott Cole, and Elizabeth Amaddio.

TABLE OF CONTENTS

Page

TABLE OF CONTENTS (Continued)

Page

TABLE OF CONTENTS (Continued)

Page

TABLE OF CONTENTS (Continued)

Page

LIST OF TABLES

Page

LIST OF TABLES (Continued)

Page

LIST OF FIGURES

LIST OF FIGURES (Continued)

Page

LIST OF FIGURES (Continued)

Page

LIST OF FIGURES (Continued)

Page

CHAPTER ONE

INTRODUCTION AND BACKGROUND

The earliest, commonly accepted definition of nanotechnology, as defined by Eric Drexler, stated that nanotechnology is the study of precisely manipulating atoms and molecules for the fabrication of "nanomachines".[1] Drexler stated that "[nanomachines] will change our world in more ways than we can imagine."[1] The National Nanotechnology Initiative subsequently established a more generalized description which defined nanotechnology as the understanding and control of matter with at least one dimension of size 1 to 100 nanometers.[2] The unique properties of nano-materials arise from quantum and physical effects.[3] Quantum-mechanical rules predicted that nanoparticles in the diameter range of 1-10 nm would display electronic band structures resulting in properties that their bulk counterparts do not display.[4] The behavior of nanoparticles strongly depends on particle size, shape, interparticle distance and the nature of the nanoparticle surface chemistry.[5] In this dissertation, we will focus on how nanoparticle surface chemistry can be modified and its effects on nanoparticle properties and the overall impact of nanomaterials. We will also present a green, novel technique to synthesize nanoparticles of controllable size and discuss the implications of materials used during synthesis, purification and processing on the overall impact of nanomaterials. In order to fully understand the influence of surface chemistry on nanomaterial properties we will first present the use of nanomaterials throughout history.

Nano-materials and processes naturally occur in the environment and in the body. Most biological processes occur at the nanoscale and give scientists a template to fabricate new processes and materials for the advancement of many technological fields. Examples of Nanotechnology have been found throughout history, as early as the 4th century. The Lycurgus Cup from Roman times contains colloidal silver and gold to look green when lit from the outside, and red when lit from the inside.[3] Soluble gold was used to treat various ailments throughout the middle ages as detailed in what is considered the first book on colloidal gold written by Francisci Antonii in 1618.[6] Silver has been used for centuries to treat burns and chronic wounds.[7] By 1718 Hans Heinrich Helcher discovered the importance of surface chemistry when he stated that the use of boiled starch in drinkable gold preparation enhanced its stability.[8] In 1857, Michael Faraday demonstrated that nano-gold dispersions could produce different colored solutions at certain lighting conditions.[9]

Scientists have been able to design and control nanoparticles in order to take advantage of size[10], shape,[11] and morphology[12] and dependent properties that can vary greatly from bulk material. Silver and gold nanoparticles exhibit a localized surface plasmon resonance, LSPR, which their bulk counter parts do not. This phenomenon exists when photons of incident light match the natural frequency of surface electrons on nanoparticles. This causes plasmonic nanoparticles to exhibit a strong extinction band in the UV-vis spectrum that is not present in the spectrum of their bulk materials. The wavelength of this strong extinction band will shift depending on nanoparticle size, shape, dispersing media and surface chemistry.[13,14] In fact, the surface chemistry

dependent shift of the LSPR of nanoparticles has been used to investigate the kinetics and thermodynamics of ligand exchange.[15,16] The plasmonic properties of gold and silver nanoparticles have made them attractive in sensing,[17] and targeting applications.[18-20] Silver nanoparticles are used widely in many consumer products such as cosmetics, paints, cleaning supplies, and clothing, which take advantage of silver's antimicrobial properties.[7,21] Gold nanoparticles (GNPs) are utilized in catalysis[22-24] and biomedical applications[25-27] that include drug delivery,[19,28-31] sensing, and bioimaging.[32-36]

Nanoparticle surface chemistry will also have a significant impact on nanoparticle properties such as size, shape, function, and dispersity in various solvents. Many synthesis methods employ the use of a sacrificial ligand that allows for better control of nucleation and growth. The sacrificial ligand can then be displaced with a ligand possessing more desirable properties for the applications listed above. This surface modification procedure is commonly known as ligand exchange. Ligand exchange allows for the use of molecules that are not compatible with synthesis conditions such as heat or the presence of strong reducing agents. Ligand exchange can also be used as a green alternative to biphasic synthesis methods by eliminating the need for a phase transfer catalyst which is usually toxic and required in large quantities.[37,38] While ligand exchange provides a facile method of nanoparticle surface modification, there are many factors that must be taken into account that will affect the kinetics and extent of ligand exchange. Chapter 2 of this dissertation reviews the factors that affect ligand exchange such as nanoparticle size, shape, surface effects, age and ligand structure as well as others. This

chapter will also review applications of and methods to monitor and quantify ligand exchange.

With the increase in research and application of silver and gold nanoparticles, the risk of these materials must be evaluated. The increase in interest of these materials led to the publication of a book in 2012 by the National Research Center, outlining a research plan to determine the environmental and biological impact of nanomaterials. Two important contributing factors to the risk of nanoparticles are toxicity and exposure. While the use of gold and silver nanoparticles in biomedical applications is promising, the toxicity of these materials must be determined before they can be used in practical, real-world examples. Catherine Murphy and Michael Wyatt have studied the effect of surface chemistry, cetyltrimethylammonium bromide (CTAB) in particular, size,[39] shape (gold nanorods)[40] and exposure[41] of gold nanoparticles on their toxicity. The findings of these studies summarized that gold nanoparticle cores, regardless of size or shape, are not the cause of toxicity, but the precursors of the nanoparticle synthesis and the nanoparticle surface chemistry is responsible for the toxicity. In another study, the effect of aspect ratio of gold nanorods on the toxicity in human colon carcinoma cells was investigated.[40] This study demonstrated that while surface chemistry of gold nanoparticles may not directly affect toxicity, it will affect the amount of nanoparticle uptake in cells, and this has been demonstrated by other groups as well.[42] The charge of a gold nanoparticle, which is also determined by nanoparticle surface chemistry, can have a significant effect on their toxicity. Rotello et al demonstrated that cationic GNPs are moderately toxic while anionic GNPs are non-toxic. [43] The increased toxicity was due to the electrostatic

interactions between cationic GNPs and the anionic lipid bilayer of cell walls, which increased GNP uptake.[43] One aspect of the cytotoxicity of gold nanoparticles that requires further investigation is determining if a change in surface chemistry of the particles occurs once they have been taken up by a cell. This would require an investigation of the binding strengths of various functional groups in order to determine if a change in surface chemistry can take place. In Chapter 3 of this dissertation we investigate the binding strengths of thiol, amine, and carboxylic acid functionalized polyethylene glycol in order to develop a hierarchy of binding strengths. Polyethylene glycol was chosen as the ligand back bone due to its ease of fabrication, control over molecular weight and end group, and because of its stability in biological fluids.

It is well known that silver exhibits antimicrobial properties, and as stated above, has been used throughout history as a disinfectant for food and in healing purposes. More recently, silver nanoparticles have emerged as useful antimicrobial agents because of their high surface area to volume ratio. This has led to the emergence of numerous consumer products containing nano-silver and concurrently concern over the environmental impact of nano-silver when these products reach their end of life.[21] Silver sulfadiazine is a broad spectrum antibiotic because the silver ions bind to base pairs in DNA and inhibits transcription. [44] Silver released into the environment has the potential to bind to the DNA in microbes in the natural environment and subsequently affect an entire ecosystem. Several reviews[31,45,46] (and references within) have called for a better understanding of the environmental impact of nano-silver. Silver nanoparticles are not as stable as gold nanoparticles, which have metal bond dissociation energies of 160 ± 3.4

kJ/mol and 218 ± 6 kJ/mol, respectively.[47] Therefore, silver nanoparticles are more prone to dissolution. While there is still debate on whether silver nanoparticles themselves or their released ions cause toxicity, it is more likely that the ions are responsible. Steve Klaine's group at Clemson University conducted a study on the effect of natural organic matter on the dissolved ion concentration of silver nitrate (AgNO3) and AgNPs with gum Arabic (AgGA), polyethylene glycol (AgPEG), and polyvinylpyrrolidone (AgPVP) surface chemistries and the toxicity to *Daphnia magna.*[48] The results of this study demonstrated that silver nitrate ($AgNO_3$) was the most toxic and silver nanoparticles coated with polyvinylpyrrolidone (PVP) were the least toxic. Other surface chemistries studied were gum arabic (GA) and polyethylene glycol (PEG). The toxicity of $AgNO_3$ and GA and PEG coated nanoparticles also decreased when Suwannee River natural organic matter (NOM) was present in solution, while the toxicity of PVP coated AgNPs was unchanged. This study provided evidence

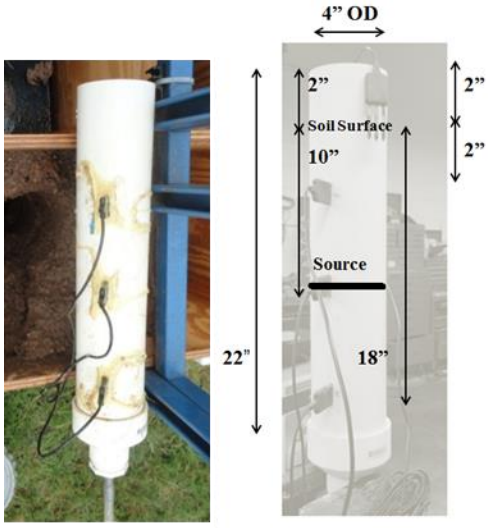

Figure 1-1: Schematic and demonsions of lysimeters used in the study by Emerson et al.

that the toxicity and antimicrobial activity of silver is a function of silver ion concentration and that the extent of AgNP dissolution can be controlled with surface chemistry and the presence of NOM.[48] NOM reduces the toxicity of silver by binding to Ag^+ but will also bind to and enhance the transport of AgNPs, increasing their exposure potential. These two outcomes can have opposite impacts on toxicology.

Few studies on AgNPs transport have been conducted under environmentally relevant conditions, which is the next step in determining their environmental impact. In collaboration with Brian Powell's group at Clemson University we conducted an intermediate scale field transport study on the physical transformations of silver and iron oxide nanoparticles in Savannah River Site sandy loam soil. [49] Lysimeters, which are field testing apparatuses used to test contaminant transport under environmentally relevant conditions, were used in this study to examine silver nanoparticle fate, Figure 1-1. Lysimeters were spiked with AgNPs stabilized by citrate, Suwanee River natural organic matter (SR-NOM), or dodecanethiol and exposed to environmental conditions for 1 year. The AgNP spiked and control lysimeters were then cored into 1 cm segments and each segment was analyzed for silver content on inductively coupled plasma-mass spectroscopy, ICP-MS. The results of this study demonstrated that in unsaturated conditions, 99 % of the silver nanoparticles travelled less than 5 cm from the nanoparticle source, Figure 2-2. [49]

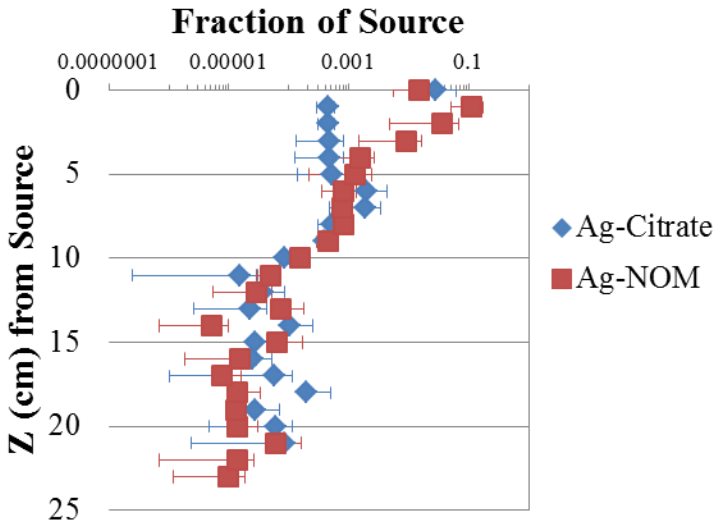

Figure 1-2: Transport profiles for SR-NOM (red) and citrate (blue) capped AgNPs

The most notable NP transformations observed were homoaggregation of the particles themselves and heteraggregation of the particles with colloidal-sized soil particles, Figure 1-3.

A significant finding of this work was the heterogeneity of the AgNPs after 1 year, as the source was originally homogenous. Figure 1-3 portrays digital images of the AgNP sources taken during the coring procedure. Nanoparticles may undergo a number of transformations including sorption, complexation, aggregation, oxidation/reduction reactions, and dissolution/precipitation when exposed to different conditions. Conditions in the lysimeters were largely unsaturated as only 5.2 pore volumes of liquid passed through the column over 1 year's exposure, which complicates the system further with

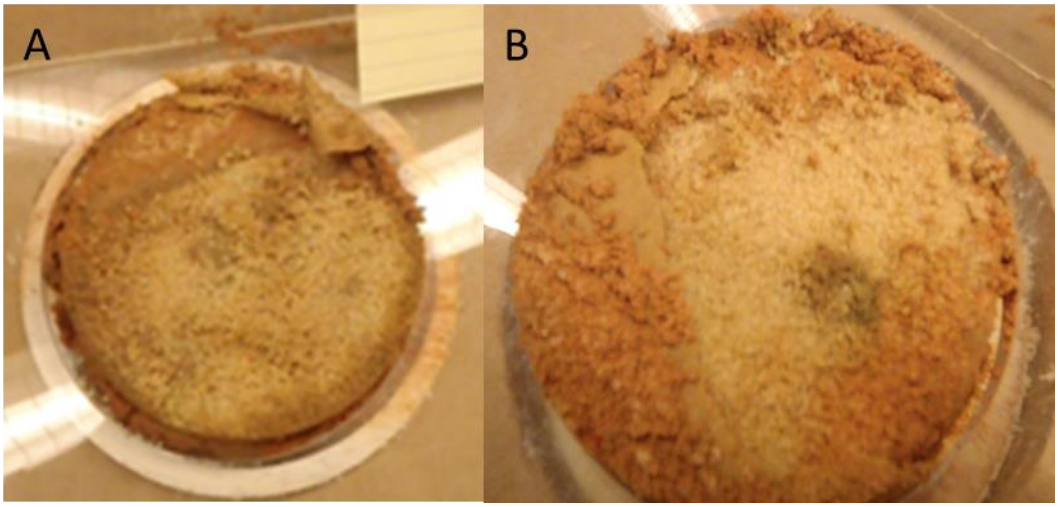

Figure 1-3: Digital imaged of lysimeter sources of A.) SR-NOM, and B.) Citrate capped AgNPs

additional transformations including capture by air–water interfaces[50] and agglomeration due to drying.[51,52]

Drastic changes in pore water chemistry caused by intermittent drying and rehydrating of soils can enhance the interactions expected under saturated conditions due to pH, ionic strength, and counter ion concentrations. In order to understand these transformations, it is necessary to isolate and test the factors that influence each type of transformation. Chapter 4 of this dissertation isolates the effects of SR-NOM and 3 different electrolytes (NaCl, $NaClO_4$, and $(CH_3)_4NClO_4$) on the mobility, sorption and dissolution of citrate stabilized AgNPs in saturated quartz columns.

Implications of materials used during synthesis, purification and processing is another aspect to consider when assessing the impact of nanomaterials. In order to reduce the environmental impact of nanomaterials, safe synthesis and processing procedures must be investigated and implemented. Size dependent properties of nanoparticles

require narrow size distributions with standard deviations of less than 5 %. A common synthesis protocol for hydrophilic spherical silver and gold nanoparticles was developed by Turkevich.[53] An adaptation of this method produces relatively monodispersed populations of nanoparticles, in which the surface chemistry can be easily modified. In this method, aqueous metal salts are added to hot or boiling solutions of trisodium citrate and varying the reaction time offers control over nanoparticle size.[53] Varying the ratio of metal salt to citrate also provides control over nanoparticle size and the addition of reducing agents such as sodium borohyrdide ($NaBH_4$) allows for rapid nucleation.[54] While these methods afford control over size, only microgram quantities of nanoparticle can be produced.[53] A protocol for synthesizing milligram quantities of spherical gold and silver nanoparticles is the Brust method.[37] On the other hand this method does not offer as much control over size as the Turkevich method and hence requires post synthesis processing to achieve very narrow size distributions. In this synthesis, metal salt dissolved in an aqueous phase and stirred vigorously with a solution of tetraoctylammonium bromide (TOAB), a phase transfer catalyst, in chloroform or toluene until all of the metal ions are transferred to the organic phase. An alkyl-thiol is then added to the organic phase, and this phase is stirred rapidly with an aqueous solution of sodium borohydride to facilitate the nucleation of nanoparticles.[37]

Surfactant-mediated methods for producing hydrophobic nanoparticles are also prevalent and afford control over nanoparticle size and surface chemistry. In particular, the surfactant sodium bis(2-ethylhexyl) sulfosuccinate (AOT) is used in concentrations such that a reverse micelle water-in-oil microemulsion is formed.[55] The AOT reverse

micelle system has been used widely for the synthesis of metallic nanoparticles including silver. Synthesis variables in the system that have been investigated include the type and concentration of surfactant, metal precursor, and reducing agent, as well as the temperature, pH, bulk solvent and water-to-surfactant molar ratio (W-value). This method usually leads to excess surfactant in the final nanoparticle product and post synthesis processing is needed for purification and further reduction in nanoparticle polydispersity.

A common post synthesis processing method for removing excess surfactants and precursors and for isolating nanoparticles of a particular size is the utilization of recursive antisolvent addition and centrifugation steps.[56] For example, toluene/ethanol or chloroform/ethanol solvent/antisolvent pairs are used to purify and fractionate gold and silver nanoparticles. Increasing the composition of antisolvent in nanoparticle dispersions weakens the solvent strength and induces nanoparticle precipitation. Since larger particles have greater van der Waals forces of attraction, these particles will precipitate first, and subsequent additions of antisolvent induces the precipitation of smaller nanoparticles.[37] While this process is common due to its simplicity, it is typically, time, solvent and energy intensive. To purify and fractionate 214 mg of Brust method prepared gold nanoparticles would require over 800mL of ethanol in addition to multiple centrifugations step, and it not easily scalable. As nanoparticles become more attractive for consumer product applications, the need for a scalable, rapid, and environmentally friendly method to synthesize nanoparticles of controllable size and polydispersity becomes more apparent.

Recently, CO_2 has been employed as an effective antisolvent for hydrophobically stabilized nanoparticles. CO_2 is a weak, non-polar solvent that will readily dissolve into and change the properties of organic solvents (toluene, hexane, pentane, etc.). The solvent properties change as a function of CO_2 composition i.e. pressure and as the CO_2 composition increases, the liquid volume also increases creating a system known as gas expanded liquids, GXLs.[57] Mcleod et al. utilized GXLs to facilitate the fractionation of polydispersed dodecanethiol stabilized silver nanoparticles using CO2 expanded hexane.[58] These advances led to the investigation of tuning solvents properties of an AOT reverse micelle microemulsion with CO_2 to control the size of nanoparticles in-situ and this work constitutes Chapter 5 of this dissertation.[59] This synthesis method essentially combines nanoparticle synthesis and processing into a single step.

The primary objective of the work presented in this dissertation was to determine the influence of nanoparticle surface chemistry in order to better predict and design how nanoparticles will behave during their intended application, end fate and overall impact. Another objective was to provide a technique to synthesize nanoparticles of controllable size that would have less impact on the environment than traditional methods. This work is motivated by the constant increase in interest of gold and silver nanoparticles and the lack of definitive knowledge of nanoparticle fate and impact.

Dissertation Outline

Nanoparticle surface chemistry has a significant impact on how these materials behave during their intended function and at their end of life. The primary motivation of

this dissertation is to provide insight on the interactions between ligands and nanoparticles in order to assess the fate of nanoparticles of these materials. In Chapter 2, we provide a comprehensive review of literature on ligand exchange and binding. This work aimed to consolidate current research on ligand exchange mechanisms and kinetics and extrapolate trends from the data. This work also aimed to identify areas of research that are lacking and provide recommendations to fill these gaps.

In order to fill the gaps in research on ligand exchange and binding, understanding of how various functional groups will bind to nanoparticles, in this case, gold nanoparticles. Chapter 3 of this dissertation discusses how isothermal titration calorimetry is used to probe the binding of functionalized polyethylene glycol to bare, citrate stabilized, and polyethylene glycol-amine stabilized gold nanoparticles. Age must be taken into account when assessing risks of nanomaterials as nanoparticle age also affects nanoparticle behavior such as binding, reactivity, aggregation potential and dissolution. These effects are potentially important for applications in catalysis, drug delivery, sensing and others. By understanding the mechanism and strength of nanoparticle-ligand interactions, nanoparticle systems can be designed to perform desired functions while reducing adverse effects.

When a nanomaterial has performed its intended function, reached its end of life, and is ultimately disposed of, these materials will come into contact with a wide range of natural molecules and electrolytes in the ecosystem. As motivated by the collaboration with Hilary Emerson and Dr. Powell in the EE&S department at Clemson University,

Chapter 4 describes how natural organic matter and electrolytes (sodium chloride, sodium perchlorate, and tetramethylsodium perchlorate) affects the mobility, dissolution and sorption of silver nanoparticles.

Adverse environmental effects can arise not only from nanomaterials themselves, but from synthesis and processing materials as well. A secondary motivation of this dissertation was to design a method to synthesize nanoparticles of controllable size with minimal effects on the environment. As stated previously, synthesis methods for organically stabilized nanoparticles require time, solvent, waste and energy intensive post synthesis processing to obtain monodispersed nanoparticle populations. Chapter 5 of this dissertation describes the use of gas expanded liquids to control the size of dodecane stabilized silver nanoparticles in-situ.

Finally, in Chapter 6 the conclusions of this dissertation are made along with recommendations of future work. The most important conclusion of this dissertation is that nanoparticle surface chemistry, age and synthesis conditions has a profound effect on nanoparticle stability, function and overall environmental impact.

References

(1) Drexler, K. E.: *Engines of Creation: The Coming Era of Nanotechnology*; Doubleday Dell Publishing Group inc.: New York, 1986.

(2) National Nanotechnology Initiative. Nano.gov; Vol. 2014.

(3) Daniel, M.-C.; Astruc, D.: Gold Nanoparticles: Assembly, Supramolecular Chemistry, Quantum-Size-Related Properties, and Applications toward Biology, Catalysis, and Nanotechnology. *Chemical Reviews* **2003**, *104*, 293-346.

(4) Alivisatos, A. P.: Semiconductor Clusters, Nanocrystals, and Quantum Dots. *Science* **1996**, *271*, 933-937.

(5) Mathias Brust, C. J. K.: Some recent advances in nanostructure preparation from gold and silver particles: a short topical review. *Colloids and Surfaces A: Physicochemical and Engineering Aspects* **2002**, *202*, 175-186.

(6) Antonii, F.: *Panacea Aurea-Auro Potabile*; Bibliopolio Frobeniano: Hamburg, 1618.

(7) Rai, M., A. Yadav, and A. Gade: Silver nanoparticles as a new generation of antimicrobials. *Biotechnol Adv* **2009**, *27*, 76-83.

(8) Helcher, H. H.: *Aurum Potabile oder Gold Tinstur*; J. Herbord Klossen: Breslau and Leipzig, 1718.

(9) Faraday, M.: The Bakerian Lecture: Experimental Relations of Gold (and Other Metals) to Light. *Philosophical Transactions of the Royal Society of London* **1857**, *147*, 145-181.

(10) M. J. Hostetler, J. E. W., C. J. Zhong, J. E. Harris, R. W. Vachet, M. R. Clark, J. D. Londono, S. J. Green, J. J. Stokes, G. D. Wignall, G. L. Glish, M. D. Porter, N. D. Evans and R. W. Murray: *Langmuir* **1998**, *14*, 17.

(11) Mahmoud, M. A.; O'Neil, D.; El-Sayed, M. A.: Shape and Symmetry Dependent Mechanical Properties of Metallic Gold and Silver on the Nanoscale. *Nano Letters* **2013**.

(12) Murray, R. W.: Nanoelectrochemistry: Metal Nanoparticles, Nanoelectrodes, and Nanopores. *Chemical Reviews* **2008**, *108*, 2688-2720.

(13) Jain, P. K.; Lee, K. S.; El-Sayed, I. H.; El-Sayed, M. A.: Calculated Absorption and Scattering Properties of Gold Nanoparticles of Different Size, Shape, and

Composition: Applications in Biological Imaging and Biomedicine. *The Journal of Physical Chemistry B* **2006**, *110*, 7238-7248.

(14) Haiss, W.; Thanh, N. T. K.; Aveyard, J.; Fernig, D. G.: Determination of Size and Concentration of Gold Nanoparticles from UV−Vis Spectra. *Analytical Chemistry* **2007**, *79*, 4215-4221.

(15) Reyes, E. n.; Madueño, R.; Blázquez, M.; Pineda, T.: Facile Exchange of Ligands on the 6-Mercaptopurine-Monolayer Protected Gold Clusters Surface†. *The Journal of Physical Chemistry C* **2010**, *114*, 15955-15962.

(16) Kumar, A., Mandal, Saikat, Pasricha, Renu, Mandale, A. B., Sastry, Murali: Investigation into the Interaction between Surface-Bound Alkylamines and Gold Nanoparticles. *Langmuir* **2003**, *19*, 6277-6282.

(17) Lee, K.-S. a. M. A. E.-S.: Gold and Silver Nanoparticles in Sensing and Imaging:,Äâ Sensitivity of Plasmon Response to Size, Shape, and Metal Composition. *Journal of Physical Chemistry B* **2006**, *110*, 19220-19225.

(18) Dixit, V.; Van den Bossche, J.; Sherman, D. M.; Thompson, D. H.; Andres, R. P.: Synthesis and grafting of thioctic acid-PEG-folate conjugates onto Au nanoparticles for selective targeting of folate receptor-positive tumor cells. *Bioconjugate Chemistry* **2006**, *17*, 603-609.

(19) Shakeri-Zadeh, A., Mansoori, G.A, Hasemian, A. R., Eshghi, H., Sazgarnia, A., Montazerabadi, A. R.: Cancerous Cells Targeting and Destruction Using Folate Conjugated Gold Nanoparticles. *Dynamic Biochemistry, Process Biotechnology and Molecular Biology* **2010**, *4*, 6-12.

(20) Mansoori, G. A.; Brandenburg, K. S.; Shakeri-Zadeh, A.: A Comparative Study of Two Folate-Conjugated Gold Nanoparticles for Cancer Nanotechnology Applications. *Cancers* **2010**, *2*, 1911-1928.

(21) Scholars, W. W. I. C. f.: Consumer Products Inventory. In *The Project on Emerging Nanotechnologies*, 2014.

(22) LaLonde, A. D. G. N., M.; Zhang, D.; Ganadean, D.; Alkhateeb, A.; Padmanabhan, R.; McIlroy, D. N.: *J. Mater. Res.* **2005**, *20*, 3021–7.

(23) Ni, C.; Hassan, P. A.; Kaler, E. W.: Structural Characteristics and Growth of Pentagonal Silver Nanorods Prepared by a Surfactant Method. *Langmuir* **2005**, *21*, 3334-3337.

(24) Zhang, S.-H.; Jiang, Z.-Y.; Xie, Z.-X.; Xu, X.; Huang, R.-B.; Zheng, L.-S.: Growth of Silver Nanowires from Solutions: A Cyclic Penta-twinned-Crystal Growth Mechanism. *The Journal of Physical Chemistry B* **2005**, *109*, 9416-9421.

(25) Scarberry, K. E. D., E. B.; McDonald, J. F.; Zhang, Z. J.: Magnetic Nanoparticle−Peptide Conjugates for in Vitro and in Vivo Targeting and Extraction of Cancer Cells. *Journal of the American Chemical Society* **2008**, *130*, 10258–10262.

(26) Park, H. Y., J.; Seo, S.; Kim, K.; Suh, J.; Kim, D.; Haam, S.;; Kyung-Hwa, Y.: Multifunctional Nanoparticles for Photothermally Controlled Drug Delivery and Magnetic Resonance Imaging Enhancement. *Small* **2008**, *4*, 192–196.

(27) Bhattacharya, R. P., C. R.; Earl, A.; Wang, S.; Katarya, A.; Lu, L.; Kizhakkedathu, J. N.; Yaszemski, M. J.; Greipp, P. R.;Mukhopadhyay, D.; Mukherjee, P.: Attaching folic acid on gold nanoparticles using noncovalent interaction via different polyethylene glycol backbones and targeting of cancer cells. *Nanomedicine: Nanotechnology, Biology and Medicine* **2007**, *3*, 224–238.

(28) Wuelfing, W. P.; Gross, S. M.; Miles, D. T.; Murray, R. W.: Nanometer Gold Clusters Protected by Surface-Bound Monolayers of Thiolated Poly(ethylene glycol) Polymer Electrolyte. *Journal of the American Chemical Society* **1998**, *120*, 12696-12697.

(29) Lowe, A. B.; Sumerlin, B. S.; Donovan, M. S.; McCormick, C. L.: Facile Preparation of Transition Metal Nanoparticles Stabilized by Well-Defined (Co)polymers Synthesized via Aqueous Reversible Addition-Fragmentation Chain Transfer Polymerization†. *Journal of the American Chemical Society* **2002**, *124*, 11562-11563.

(30) Mandal, T. K.; Fleming, M. S.; Walt, D. R.: Preparation of Polymer Coated Gold Nanoparticles by Surface-Confined Living Radical Polymerization at Ambient Temperature. *Nano Letters* **2002**, *2*, 3-7.

(31) Levard, C.; Hotze, E. M.; Lowry, G. V.; Brown, G. E.: Environmental Transformations of Silver Nanoparticles: Impact on Stability and Toxicity. *Environmental Science & Technology* **2012**, *46*, 6900-6914.

(32) Yong, K. T., Swihart, M. T., Ding, H. and Prasad, P. N.: Preparation of Gold Nanoparticles and their Applications in Anisotropic Nanoparticle Synthesis and Bioimaging. *Plasmonics* **2009**, *4*, 79-93.

(33) Krishnendu Saha, S. S. A., Chaekyu Kim, Xiaoning Li, and Vincent M. Rotello: Gold Nanoparticles in Chemical and Biological Sensing. *Chemical Reviews* **2012**, *112*, 2739−2779.

(34) Burgi, C. G. a. T.: Chiral Inversion of Gold Nanoparticles. *Journal of the American Chemical Society* **2009**, *130*.

(35) Shang, J.; Liu, C.; Wang, Z.; Wu, H.; Zhu, K.; Li, J.; Liu, J.: In-Situ Measurements of Engineered Nanoporous Particle Transport in Saturated Porous Media. *Environmental Science & Technology* **2010**, *44*, 8190-8195.

(36) Takara, M.; Toyoshima, M.; Seto, H.; Hoshino, Y.; Miura, Y.: Polymer-modified gold nanoparticles via RAFT polymerization: a detailed study for a biosensing application. *Polymer Chemistry* **2014**, *5*, 931-939.

(37) Brust, M., Walker, M., Bethell, D., Schiffrin, D. J., Whyman, R.: *Chemical Communications* **1994**, 801.

(38) Sastry, M.: Phase Transfer Protocals in Nanoparticle Synthesis. *Current Science* **2003**, *85*, 1735-1745.

(39) Connor, E. E.; Mwamuka, J.; Gole, A.; Murphy, C. J.; Wyatt, M. D.: Gold Nanoparticles Are Taken Up by Human Cells but Do Not Cause Acute Cytotoxicity. *Small* **2005**, *1*, 325-327.

(40) Alkilany, A. M.; Nagaria, P. K.; Hexel, C. R.; Shaw, T. J.; Murphy, C. J.; Wyatt, M. D.: Cellular Uptake and Cytotoxicity of Gold Nanorods: Molecular Origin of Cytotoxicity and Surface Effects. *Small* **2009**, *5*, 701-708.

(41) Alkilany, A.; Murphy, C.: Toxicity and cellular uptake of gold nanoparticles: what we have learned so far? *J Nanopart Res* **2010**, *12*, 2313-2333.

(42) Hauck, T. S.; Ghazani, A. A.; Chan, W. C. W.: Assessing the Effect of Surface Chemistry on Gold Nanorod Uptake, Toxicity, and Gene Expression in Mammalian Cells. *Small* **2008**, *4*, 153-159.

(43) Goodman, C. M.; McCusker, C. D.; Yilmaz, T.; Rotello, V. M.: Toxicity of Gold Nanoparticles Functionalized with Cationic and Anionic Side Chains. *Bioconjugate Chemistry* **2004**, *15*, 897-900.

(44) Bishara S. Atiyeh, M. C., Shady N. Hayek, Saad A. Dibo: Effect of silver on burn wound infection control and healing: Review of the literature. *Burns* **2007**, *33*, 139-148.

(45) Hotze, E. M.; Phenrat, T.; Lowry, G. V.: Nanoparticle aggregation: Challenges to understanding transport and reactivity in the environment. *Journal of environmental quality* **2010**, *39*, 1909-1924.

(46) Wiesner, M. R.; Lowry, G. V.; Alvarez, P.; Dionysiou, D.; Biswas, P.: Assessing the Risks of Manufactured Nanomaterials. *Environmental Science & Technology* **2006**, *40*, 4336-4345.

(47) Weast, R. C.: *Handbook of Chemistry and Physics*; 57 ed.; CRC Press: Cleveland, 1976.

(48) Newton, K. M.; Puppala, H. L.; Kitchens, C. L.; Colvin, V. L.; Klaine, S. J.: Silver nanoparticle toxicity to Daphnia magna is a function of dissolved silver concentration. *Environmental Toxicology and Chemistry* **2013**, *32*, 2356-2364.

(49) Hilary P. Emerson, A. E. H., Jonathon A. Baldwin, Tyler C. Waterhouse, Christopher L. Kitchens, O. Thompson Mefford, Brian A. Powell: Physical transformations of iron oxide and silver nanoparticles from an intermediate scale field transport study. *J Nanopart Res* **2014**, *16*.

(50) Gao, B.; Saiers, J. E.; Ryan, J.: Pore-scale mechanisms of colloid deposition and mobilization during steady and transient flow through unsaturated granular media. *Water Resources Research* **2006**, *42*, W01410.

(51) Eran Rabani, D. R. R., Phillip L. Geissler, Louis E. Brus: Drying-mediated self-assembly of nanoparticles. *Nature* **2003**, *426*, 271-274.

(52) Gilbert, B.; Ono, R. K.; Ching, K. A.; Kim, C. S.: The effects of nanoparticle aggregation processes on aggregate structure and metal uptake. *J Colloid Interface Sci* **2009**, *339*, 285-295.

(53) J. Turkevich, P. C. S., J. Hillier: A study of the nucleation and growth processes in the synthesis of colloidal gold. *Discussions of the Faraday Society* **1951**, *11*, 55-75.

(54) Brown, K. R., Walter, D. G., Natan, M. J.: Seeding of Colloidal Au Nanoparticle Solutions. 2. Improved Control of Particle Size and Shape. *Chemical Materials* **2000**, *12*, 306-313.

(55) Wanzhong Zhang, X. Q., Jianguo Chen: Synthesis of silver nanoparticles—Effects of concerned parameters in water/oil microemulsion. *Materials Science and Engineering: B* **2007**, *142*, 1-15.

(56) Korgel, B. A.; Fullam, S.; Connolly, S.; Fitzmaurice, D.: Assembly and Self-Organization of Silver Nanocrystal Superlattices: Ordered "Soft Spheres". *The Journal of Physical Chemistry B* **1998**, *102*, 8379-8388.

(57) Jessop, P. G.; Subramaniam, B.: Gas-Expanded Liquids. *Chemical Reviews* **2007**, *107*, 2666-2694.

(58) McLeod, M. C.; Anand, M.; Kitchens, C. L.; Roberts, C. B.: Precise and Rapid Size Selection and Targeted Deposition of Nanoparticle Populations Using CO2 Gas Expanded Liquids. *Nano Letters* **2005**, *5*, 461-465.

(59) Hart, A. E., Akers, David B., Gorosh, Samuel, Kitchens, Christopher L.: Reverse micelle synthesis of silver nanoparticles in gas expanded liquids. *The Journal of Supercritical Fluids* **2013**, *76*, 236-243.

CHAPTER TWO

LIGAND BINDING AND EXCHANGE KINETICS ON THE SURFACE OF PLASMONIC NANOPARTICLES

Abstract

Ligand exchange is a versatile method for modifying the surface of plasmonic nanoparticles. A detailed understanding of the influencing factors on the mechanism of nanoparticle ligand binding and exchange is pertinent for the robust design of nanoparticles. This chapter reviews the work of several research groups in order to compile the work done to date on nanoparticle ligand binding and exchange to make conclusions about the overall mechanism of ligand exchange and to build a hierarchy of functional groups in order of preferential binding. Nanoparticle properties that affect ligand binding and exchange include size, shape, crystalline structure, charge, oxidation state and age. Ligand properties that affect ligand exchange and binding include structure, i.e. multivalent ligands, chain length, extent of branching and chirality, and chemistry; end group and perhaps most importantly head group, through which ligands bind to nanoparticle surfaces. A major conclusion from this work suggests that the mechanism of ligand exchange is an S_N2, associative mechanism in which an incoming ligand binds to a nanoparticle surface while an outgoing ligand desorbs from the surface in a simultaneous process. Ligand binding and exchange is initiated and occurs rapidly at highly reactive defect sites and then slows as defect site-bound ligands migrate to less reactive terrace sites to allow more ligands to bind.

Introduction

Applications of plasmonic nanoparticles have expanded across a plethora of research areas and emerging technologies; becoming materials of opportunity with size dependent properties that differ from those of their bulk materials. [1-4] With each of these applications, a nanoparticle core material may be chosen based on the inherent properties of that nanomaterial of a given size, shape, or composition. For example, nanomaterials have found extensive applications in catalysis, targeted drug delivery, cell targeting, sensors, and optics.[2,5] Particle size,[6,7] shape,[2,8] and morphology[1,9,10] all influence the inherent nanomaterial properties. In order to fully exploit these desirable properties it is necessary to impart specific functionality into the engineered nanomaterials, which is achieve through the design of surface ligand chemistry.[11] A primary role of the nanoparticle ligand is to provide stability in a colloidal dispersion, suspension, powder or composite. Preservation of the nanoscale dimensions and prevention of irreversible agglomeration or other destructive phenomena that results in the loss of desired nanoscale features and hence, unique properties, is imperative. Furthermore, ligand chemistry can be used to tailor the surface properties of nanomaterials, rendering them hydrophobic[12-16] or hydrophilic; anionic[17-19], cationi [20-22], nonionic [23,24], or zwitterionic [24-31]; or combinations of the above in patchy particles.[2] In biomedical therapeutic and diagnostic applications, specific surface functionalities can impart biocompatibility or selective binding sites for cellular or extracellular proteins, peptides, DNA, etc.[32-34] In nanocomposite and nanofluidic applications, the ligand provides compatibility with the dispersing media.[2] In catalysis, ligand functionality provides preferential binding while

leaving specific catalytic sites exposed[35] and chiral ligands afford chiral chemistry in chemical production.[12] In other applications, ligand functionality can provide control of ionic release in anti-microbial activity, and chelating chemistry in environmental remediation.[36] Ligands can also impart functionality that is desired for interfacial phenomena such as the air/water interface and immiscible fluids i.e. nanoparticle stabilized-emulsions, pickering emulsions and oil recovery.[37-41]

Ligand properties can be used to control the size,[42,43] shape,[44] and polydispersity[45,46] of synthesized nanoparticles; however a ligand that can control size, shape or polydispersity during synthesis may be incompatible with the desired end application. For example, high-yield gold nanorod synthesis can be achieved using a cetyltrimethyl ammonium bromide (CTAB) surfactant, but if these nanorods are to be used for biomedical applications, the cytotoxicity of the CTAB is an issue.[47] Thus, extensive post-synthesis purification may be necessary to remove the synthesis ligand or isolate the nanoparticles of desired size or shape.[13] A common nanoparticle synthesis approach is to employ 1) a sacrificial ligand that can either be displaced by a new ligand with desired functionality using a post-synthesis ligand exchange reaction or 2) a reactive ligand that provides sites for reactive modification, via grafting-to or -from the nanoparticle surface by interfacial polymerization,[48-51] click chemistry[52,53] or layer by layer deposition. The former approach has the benefit of higher yields of nanomaterials with desired nanoscale morphology and inherent material properties. A fundamental understanding of ligand exchange is pertinent in order to take advantage of these benefits. The focus of this review is to compile the experimental methods and results obtained in

recent studies that will help enhance our fundamental understanding of nanoparticle – ligand interactions and the implications ranging from nanomaterial synthesis to application.

Background

In this review, we intend to focus our investigation on silver and gold nanoparticles due to their wide use in consumer products and research in biomedical applications, as well as their characteristic optical properties[54-56] that facilitate the study of interfacial reactions and interactions. Silver nanoparticles are used widely in many consumer products such as cosmetics, paints, cleaning supplies, and clothing.[57,58] Gold nanoparticles (GNPs) are utilized in catalysis[59-61] and biomedical applications[62-64] that include drug delivery,[32,65-68] sensing, and bioimaging.[12,69-72]

Nanoparticles have a tendency to aggregate in solution, thus it is important to design a surface chemistry that provides repulsion forces strong enough to overcome Van der waals or magnetic forces of attraction. The Derjaguin, Landau, Verwey and Overbeek, (DLVO) theory [73] is a useful tool to model the interparticle interaction forces and dispersion phenomena. [74-78] The particle-particle interaction potential is calculated by summing the potentials of van der Waals forces of attraction, V_a, with the potentials of electrostatic, V_e, repulsions, Eq 1.

$$V_{Total} = V_a + V_e$$

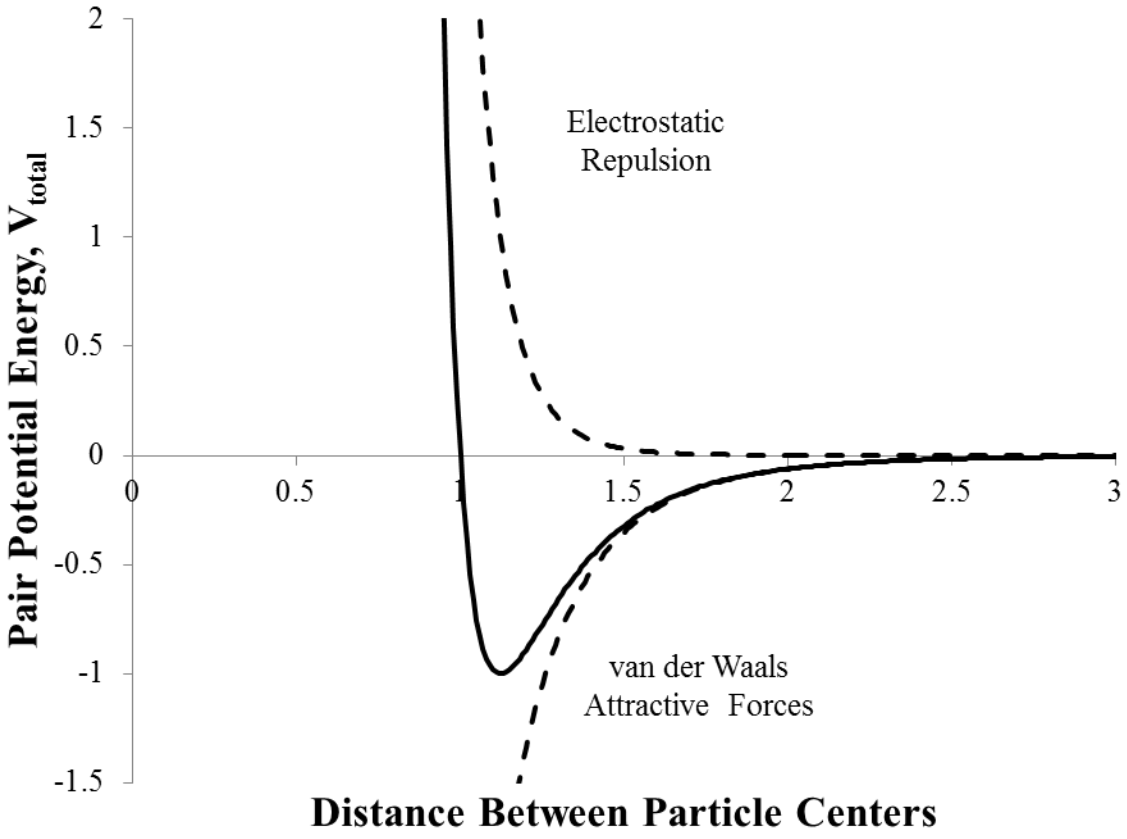

Figure 2-1: Schematic of the interaction energy potentials for soft spherical molecules with repulsive overlap and attractive dispersion forces

According to the DLVO theory, colloidal stability is determined by balancing the double layer repulsion with van der Waals attraction. Double layer repulsion increases exponentially with increasing distance between particles, Figure 2.1.

By varying the factors that contribute to these forces, the interactions between particles can be controlled.[77-79] One way to alter interparticle interactions is through the use of stabilizing ligands. Ligands provide two mechanisms of repulsion to prevent aggregation, steric and electrostatic, or a combination of both. Charged ligands, such as sodium citrate,[80] provide electrostatic repulsion that inhibit coalescence of particles when

their surfaces to collide. Electrostatic repulsion can come from positive, negative, or zwitterionic ligands such as polyethyleneimine,[21] triphenyl phosphine,[81] or a zwitterionic disulfide, [27] respectively. Electrostatic stabilization is import for particles that are dispersed in a dielectric (polar) solvent. Some ligands, such as polyelectrolytes, 1,2-dipalmitoyl-sn-glycero-3-phosphocholine (DPPC) or natural organic matter provide both steric and electrostatic stabilization. Steric repulsion occurs when the outer segments of a ligand on the surface of a nanoparticle begin to overlap when two particles get closer than a few radii of gyration. This leads to a repulsive osmotic force due to the unfavorable entropy associated with compressing the chains between the particles.[82-84] Large ligands such as 10,000 MW PEG-SH or the previously mentioned CTAB provide this type of stabilization.

Ligands not only provide a mechanism of stabilization to nanoparticles but can also impart functionality to the surface of nanoparticles. Ligand tails determine the hydrophobicity of a nanoparticle and may contain an active functional group to provide additional functionality to the nanoparticle surface. Bifunctional ligands typically have one polar end and one non-polar end. Sulfur preferentially binds to gold through a nonpolar thiol group and[85] therefore it is advantageous to use a bifunctional ligand with a thiol [86] head group and a polar –X end group (X-R-SH) that could be –COOH, -OH, etc especially for biological applications that require the nanoparticles to be stable in aqueous dispersions. End groups may also be non-polar, such as to impart specialized functionality in non-polar solvents. End group functionalities also determine the binding capabilities of nanoparticles with other molecules while the thiol head group maintains a

strong bond to the nanoparticle surface, ensuring that the ligand is not displaced. Examples of bifunctional ligands include (but are not limited to) bovine serum albumin (BSA) or single stranded DNA.[87,88] PEG-thiol ligands [65,89-92] can be used to disperse thiol stabilized GNPs in water instead of using a weaker ligand such as citrate which can easily be destabilized. Targeting ligands are bifunctional ligands that are attached to the surface of nanoparticles to ensure that the particles are directed to a specific environment or cell. A common approach is to functionalize GNPs with a folic acid-PEG-thioctic acid conjugate to selectively target and destroy cancer cells. [48] Cancerous cells require 500+ times more folate than healthy cells and express this great need in the amount of folate receptors on the cell surface. Thus it is postulated that the folate conjugated GNPs preferentially target cancerous cells over healthy ones. [48,93-100] Ligands also can be described as synthetic, natural, or biological molecules. Synthetic or engineered ligands are designed in a laboratory for a specific function, such as the folic acid-PEG-thioctic acid conjugate mentioned above. Natural ligands are molecules found in the natural environment that are capable of binding to and stabilizing nanoparticles. For example, humic acid, Figure 2-2, which is a model form of natural organic matter, (NOM) is found in soil and the sediment of natural waters. Biological ligands are molecules found in the body, i.e. proteins, enzymes, peptides, DNA, etc.

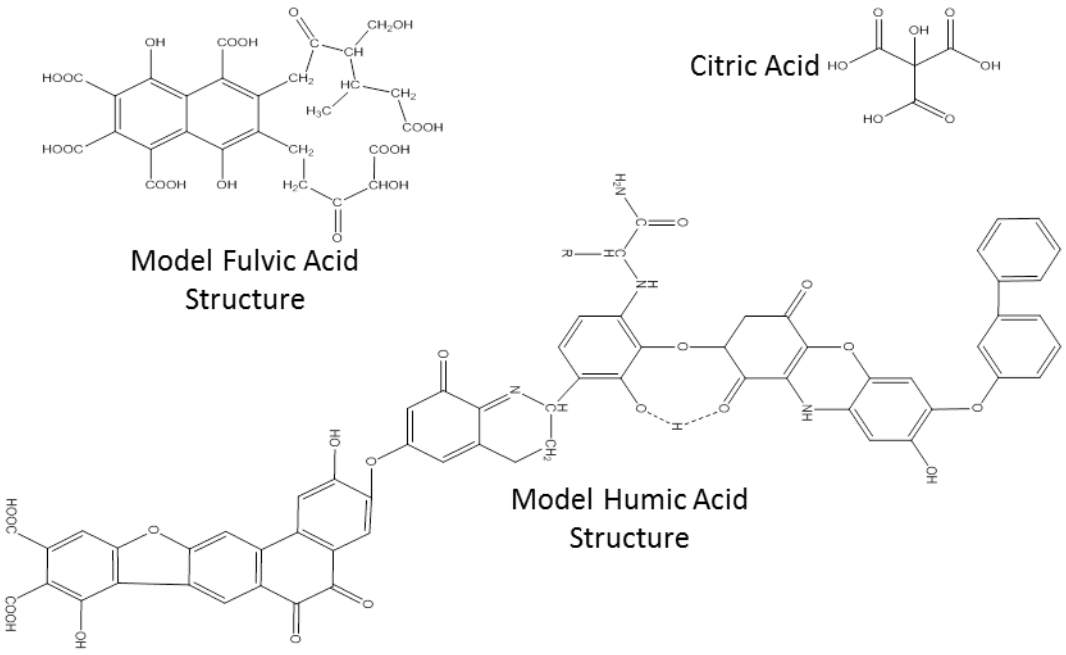

Figure 2-2: Representative structures of molecules commonly found in nature

Methods to modify the surface of nanoparticles with the aforementioned ligands include; in-situ ligand introduction, ligand exchange, which will be the focus of this review,[101,102] atom transfer radical polymerization, (ATRP),[87,103-110] reversible-addition-fragmentation chain-transfer, (RAFT),[72,111] click chemistry[52,53,112-115] EDC coupling,[116] layer by layer (LBL) deposition,[80,117] as well as other methods not mentioned. Ligand exchange is a versatile method of surface modification because it allows for the rapid alteration of chemical functionality and solubility of nanoparticles, without changing particle size or shape.[16,118,119] Since the unique properties of nanoparticles come from their shape, size and polydispersity, it is important to be able to modify the surface without compromising these properties. Ligand exchange is a simple process that involves rapid mixing of a ligand-nanoparticle complex with a free ligand in solution that

has a higher affinity to the nanoparticle surface than the original ligand. The original ligand is displaced on the nanoparticle surface by the free ligand in solution.

Applications of Nanoparticle Ligand Exchange

One robust technique for controlling surface chemistry is through the use of multiphase ligand exchange, depicted in Figure 2-3.[120-122] Processing of nanoparticles in non-polar solvents is usually much easier than in polar solvents, due to low interfacial energies in non-polar organic solvents, and allows for longer term storage.[122] In multiphase ligand exchange, nanoparticles are synthesized in an aqueous or high polarity solvent with a polar ligand, due to the solubility of common metal salt precursors and reducing agents. Following nanoparticle synthesis, the polar ligand is then displaced by a non-polar ligand and the nanoparticles subsequently transfer to the non-polar phase. This technique is advantageous because there are numerous methods to synthesize water-soluble nanoparticles of various shapes and sizes that cannot be achieved in non-polar media synthesis. One example is the commonly used and robust citrate synthesis of GNPs originally developed by Turkevitch,[123] which produces nanoparticles with relatively low size polydispersity. Frens [124] modified Turkevitch's method to obtain nanoparticles of different sizes (16-147nm) by adjusting the molar ratio of sodium citrate to gold salt. Other researchers have adapted this method to produce nanoparticles of silver, iron and other metal cores. [17,18,125] Nanoparticle syntheses in non-polar solvents often require a phase transfer catalyst to transfer metal ions to the non-polar phase. Phase transfer catalysts are expensive, typically toxic, and potentially harmful to the environment and

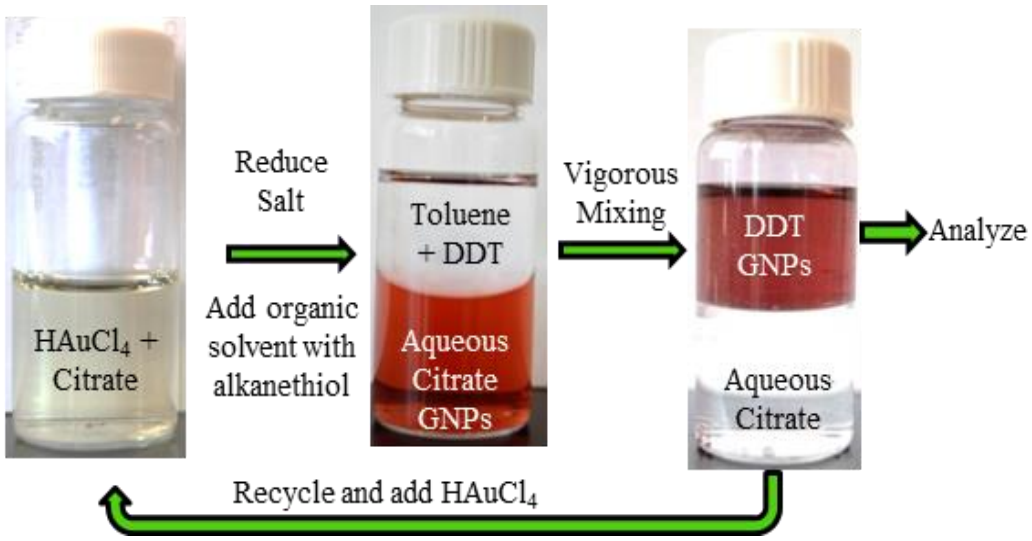

Figure 2-3: Schematic of biphasic ligand exchange of aqueous citrate stabilized AgNPs with dodecanethiol in an organic phase

can cause complications during synthesis and processing. Ligand exchange can be implemented as a greener alternative to non-polar solvent syntheses. [126] For example, citrate coated GNPs can be synthesized via the reduction of gold salt with either sodium borohydride or heat in the presence of trisodium citrate. The sacrificial citrate ligand can then be displaced with more desirable surface chemistry in an organic phase through a ligand exchange process without the use of a harsh phase transfer catalyst. [119,127-129] White *et al.* used this method to obtain 3.9 ± 0.7 nm stearylamine capped GNPs in toluene. [130] Direct synthesis of stearylamine GNPs would require a biphasic synthesis and a phase transfer catalyst to transfer the gold ions into an organic phase. [126] Biphasic synthesis methods do not always produce nanoparticles with narrow size distributions whereas the citrate synthesis is a robust synthesis technique with narrow size distributions. In another example, Lennox *et al.* synthesized citrate stabilized GNPs and SNPs in water with diameters ranging from 3 to 100 nm. The solubility of these NPs was

then altered via ligand exchange with polystyrene-thiol, PS-SH in an acetone/water mixture. The PS-SH nanoparticles were then precipitated out of solution and easily dispersed into non-polar solvents.[119]

In contrast, multiphasic ligand exchange can also be performed to transfer particles from non-polar to polar solvents.[131,132] Aqueous-based synthesis of metallic nanoparticles is typically performed in low concentrations to overcome aggregation/precipitation problems associated with ionic interactions. By synthesizing metallic nanoparticles in non-polar media, larger concentrations can be obtained, however the hydrophobicity of these particles limit their used in biomedical applications.[121,122] Hydrophobic nanoparticles can be ligand exchanged to allow for dispersions in polar or aqueous media in higher concentrations and this has been crucial for the widespread use of quantum dots.[133-135] Schmid *et al.* was one of the first groups to attempt the phase transfer of GNPs from an organic phase to an aqueous phase with ligand exchange. Triphenylphosphane chloride was exchanged with $12Ph_2PC_6H4_SO_3Na$ of the surface of GNPs. They found that the GNPs were more stable in the aqueaous phase due to the high ionic charge of $12Ph_2PC_6H4_SO_3Na$.[136] Later Rotello *et al.* exchanged octanethiol (OT) stabilized GNPs with 11-thioundecanoic acid to create water soluble particles with mixed monolayers.[137,138] Mixed monolayer stabilized GNPs feature a wide range of functionality that has potential use in a variety of applications.

Mixed Monolayer GNPs are used in many applications such as nanomedicine,[138-140] nanoelectronics[141] and interfacial phenomena.[37,38] Ligand exchange is a facile method

to obtain nanoparticles with mixed monolayers, as introducing a mixture of ligands during synthesis can compromise the size distribution.[16,142-145] Zambori fabricated vapor sensing flexible films with mixed monolayer GNPs by first synthesizing particles with a modified Brust method to control NP size.[126,141] Ligand exchange was then used to incorporate conductive polymer linkers to provide bridges for electron tunneling.[141] Sandhu synthesized mixed monolayer GNPs to transfect DNA as a method for gene transfer.[145] Murray and coworkers also used GNPs with mixed monolayers of tiopronin/ethidium and trimethyl-(mercaptoundecyl)- ammonium/ethidium to bind the NPs to DNA.[146,147] These methods are advantageous because of the ease of fabrication of GNPs versus complex high-generation dendrimers and the reduced risk of cytotoxicity and immune responses.[148] GNPs for use in coatings were produced by first synthesizing GNPs using the Brust method with hexanethiolate as the original ligand, then incorporating mercaptoundecanoic acid and 4-aminothiolphenol onto the GNP surface with ligand exchange. The mixed monolayer GNPs were then attached to a glass surface functionalized with 3-mercaptopropyl trimethoxy silane, again using ligand exchange to create a GNP coating.[149]

Ligand exchange has also made it possible to modify nanoparticle surface chemistry with molecules that could not be introduced during nanoparticle synthesis because of chemical incompatibility, harsh synthesis conditions, or without compromising the size distribution. In this case, a sacrificial ligand is used during nanoparticle synthesis and then the surface chemistry is modified via ligand exchange to incorporate reactive molecules on the surface. One example is “click chemistry” reactions

which typically call for reactive azide molecules that would reduce to amine groups in the presence of $NaBH_4$ or other strong reducing agents. Therefore, the ligand exchange is necessary to introduce azide functionality post synthesis as a reactive platform for click-chemistry. Kadnikova's group used this method to modify GNPs with an azidothiol group as a precursor for a "click" reaction with good reproducibility.[53] Ketones are another functional group that will react with strong reducing agents to form alcohols and ligand exchange makes ketone surface chemistry possible. Kell saw this in his work investigating ligand exchange dependence on nanoparticle size.[150]

Control over ligand chirality can also be achieved with ligand exchange. Burgi and co-workers found that chiral inversion of thoil ligands on GNP surfaces reverses the optical activity in metal-based electronic transitions, MBET.[12] Chiral nanoparticles have potential applications in heterogeneous enantioselective catalysis,[151] enantiodiscriminiation,[152] enantioselective crystallization,[153] liquid crystal displays [154] and in optics.[12]

Mechanisms of Nanoparticle Ligand Exchange

Mechanistic studies have been conducted[16,49,107,155-157] and the fundamental mechanisms of nanoparticle ligand exchange are still being investigated. A comprehensive review written by Chechik and Caragheorgheopol on the mechanism of ligand exchange on GNPs summarized the potential pathways for ligand exchange.[16] They used classic inorganic chemistry to describe the ligand exchange process as associative, dissociative, or interchange mechanisms, which are shown in Figure 2-4 and

possess distinctions first suggested by Langford and Gray. [43] In an associative mechanisms exchange occurs in one step where the incoming binds and the outgoing ligand desorbs in a simultaneous process, and this type of mechanism is generally used to describe ligand exchange. In a dissociative mechanism the outgoing ligand desorbs before the incoming ligands coordinated in the associative mechanism and the outgoing ligand is dissociated in the dissociative mechanism. These mechanisms of ligand exchange tend to be rapid processes. Chechik and Caragheorgheopol described the interchange mechanism as a concerted, one-step process that is subdivided into "intimate" mechanisms; interchange associative (I_a) and interchange dissociate (I_d). In the I_a mechanism, an intermediate is formed in which the incoming ligand is bound strongly to the NP surface while the outgoing ligand is weakly bound, then eventually desorbs. In an I_d mechanism, both the incoming and outgoing

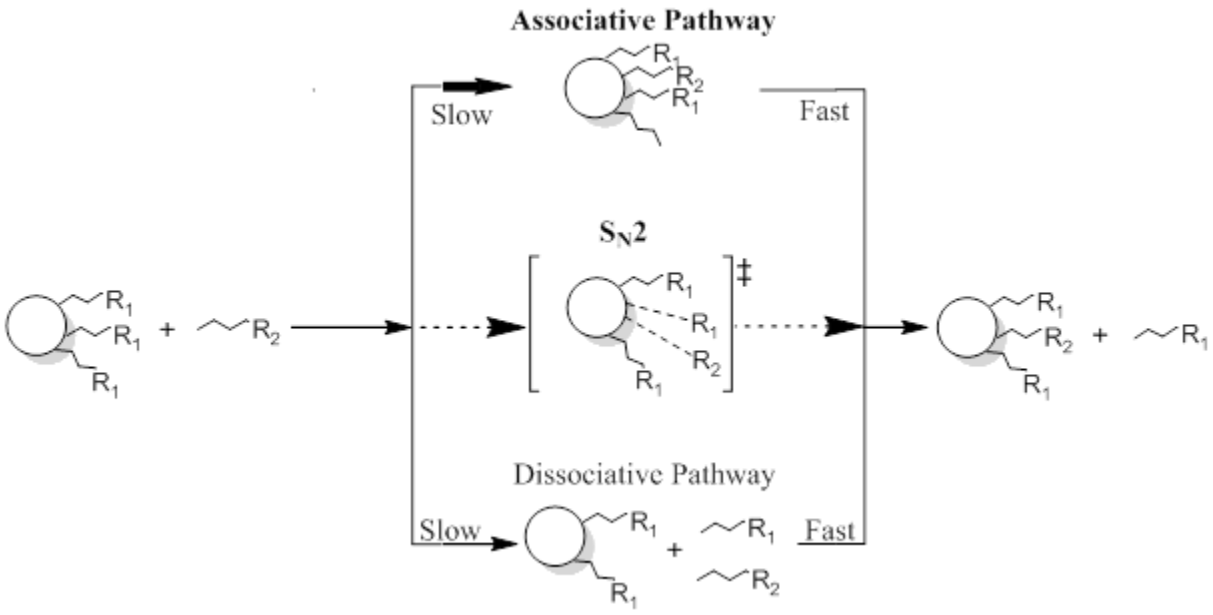

Figure 2-4: Flow diagram of the possible mechanisms of ligand exchange adapted from Chechik et al. IA and Id denote interchange associative and interchange dissociative mechanisms, resepectively

ligands are weakly bound to the surface and the incoming ligand can bind strongly only when the outgoing ligand has completely desorbed.

Traditional organic S_N2 and S_N1 type reaction mechanisms have also been used to describe ligand exchange with similarities to associative, dissociative and interchange mechanisms.[16] In an S_N2 mechanism, one bond if formed while a preexisting one is broken simultaneously while in and S_N1 these 2 processed occur separately. Ligand exchange on GNPs is generally considered to be an associative, S_N2 mechanism in which an incoming ligand attaches to a GNP surface and the bound ligand leaves the surface in a simultaneous process.[6,155,158,159] In general, nanoparticle surfaces contain more vertices, edges, defect sites and grain boundaries than flat surfaces, which increase electron density and reactivity.[115,157,160,161] Edges and vertices are also less sterically hindered making these sites more accessible for the incoming ligand and facilitating exchange, especially for bulky molecules. [14,162,163] The reactivity and steric accessibility of these sites makes an associative mechanism possible, [107,155] although associative reactions can be inhibited by tight packing on the nanoparticle surface. [7] Ligand exchange is initially rapid at these core defect sites, followed by the migration of these bound species to terrace site allowing for more ligand to bind at the defect sites. This migration becomes harder further away from defect sites and subsequently slows the exchange reaction as it progresses. This process is consistent with a second order, associative mechanism. [142,157] Murray and coworkers used HNMR to study the effect of particle size on the mechanism of exchange. Phenylethanethiolate was exchanged with p-substituted arylthiols (p-X-PhSH) where X = NO_2, Br, CH_3, OCH_3 or OH on Au_{38} and Au_{140} GNPs.

Table 2-1: Pseudo 1st order rate constants determine from ligand exchange of phenylethylenethiol with various bifunctional ligands in Murrays study

NO2pHSH		BrPhSH		CH3PhSH		OCH3PhSH	
(M)	K1, (s-1)*10^-4	**(M)**	K1, (s-1)*10^-4	**(M)**	K1, (s-1)*10^-4	**(M)**	K1, (s-1)*10^-4
0.0089	1.02 ± 0.06	0.0201	0.64 ± 0.04	0.0272	0.49 ± 0.03	0.0126	0.32 ± 0.02
0.0185	1.75 ± 0.09	0.0309	1.05 ± 0.05	0.0378	0.64 ±0.04	0.0202	0.51 ± 0.03
0.0234	2.28 ± 0.11	0.0395	1.41 ± 0.10	0.0485	0.77 ± 0.03	0.0265	0.63 ± 0.04
0.028	2.80 ± 0.14	0.0435	1.48 ± 0.10	0.059	0.91 ± 0.06	0.0399	0.91 ± 0.06

The results of this investigations demonstrated that the first-order rate constants for the first 25% of ligand exchange varied linearly with the incoming arylthiol concentration, suggesting an overall second-order reaction mechanism as seen in Table 2-1. [163] These results showed that the second-order rate constants for the initial stages of exchange of the both Au_{38} and Au_{140} were very similar, Table 2.2. On the other hand, later stages of exchange were slower on Au_{140} particles due to a higher terrace site concentration on Au_{140} particles. [163] Murray also studied the reverse exchange reactions to further characterize the mechanism of exchange. Rate constants determined for both forward and reverse exchanges were very similar, suggesting a concurrent bonding of both in-coming and out-going ligands to the GNP surface providing evidence of an associative mechanism.[163] The effect of end group on the rate of exchange will be discussed later. A dissociative mechanism is proposed for ligand exchange with disulfide molecules for weakly bound ligands such as short-chain alkylthiols, amines and sulfides.[156,157] The presence of molecular oxygen in solution can create a competing dissociative pathway for ligand exchange that most likely involves the formation of Au(I) thiolate species in solution. [157]

Table 2-2: First order rate constants determined for ligand exchange of phenylethylenthiol with various bifunctional ligand on small and large GNPs in Guo's study

MPC	Incoming ligand	Ratio	kPE(I) (10-3 M-1 s-1)
$Au_{38}(SC2Ph)_{24}$	NO_2pHSH	4.2:1	8.5
	BrPhSH	6.7:1	1.8
	CH_3PhSH	4.3:1	1.1
	CH_3OPhSH	4.0:1	1.3
	HOPhSH	7.1:1	1
$Au_{140}(SC2Ph)_{53}$	NO_2pHSH	1.3:1	1.7
	BrPhSH	2.2:1	0.6
	CH_3PhSH	3.3:1	0.6

Methods to Monitor Nanoparticle Ligand Exchange

Analytical techniques can be used to monitor ligand exchange and binding processes, determining extent of ligand exchange, surface composition, mechanisms, and kinetics and binding strengths. Here we will describe how to monitor ligand exchange with various techniques that include, but are not limited to; fluorescence spectroscopy,[14,88,107,164,165] electron paramagnetic resonance spectroscopy (EPR),[156,166] UV-vis spectroscopy,[104,105,167,168] NMR,[104,120,141,150,157,163,169-175] surface enhanced raman spectroscopy (SERS),[176,177] Fourier transform infrared spectroscopy (FTIR),[6,120,155,168] isothermal titration calorimetry(ITC), and x-ray photoemission spectroscopy (XPS).[178,179]

Fluorescence Spectroscopy

Fluorescence spectroscopy is a popular technique to monitor ligand exchange on GNPs because the exchange reactions can be observed in real time without perturbing the experiment [14,88,104,164,165,180] because GNPs quench the fluorescence of fluorescent dye

molecules, a phenomenon known as Forester resonant energy transfer, FRET, Figure 2.5. [107,181,182] The use of fluorescence allows for a sensitive measurement of ligand exchange on the surface of GNPs. This method is convenient because ligands and GNPs can easily be functionalized with fluorescent molecules and real time measurements can be obtained. An experimental scenario begins with GNP's functionalized with a fluorescent dye molecule, such as fluorescein or a fluorescently tagged ligand, FL-ligand. When a fluorescent molecule is bound to the particle, the gold core absorbs the photons emitted by the dye molecule. When a new non-fluorescent ligand binds to the particle surface and subsequently displaces a dye molecule, the fluorescence is no longer quenched. The reverse scenario can also be used where FL-ligands are titrated into a solution of non-labeled GNPs and the intensity will decrease as the FL-ligands displace the non-tagged ligands, and are quenched by the gold core. A scenario with multiple ligands tagged with different dyes can be also used to investigate ligand exchange. In this case two dyes can be bound to the nanoparticle and an untagged ligand would be titrated into the NP solution in order to demonstrate competitive displacement of one ligand over another. Alternatively, one FL- ligand can also be used to displace a different FL-ligand and the fluorescence intensity for the unbound ligand would decrease as the intensity for the bound ligand increased as the reaction progressed. Rotello and coworkers employed these methods to study the exchange alkanethiols tagged with tryptophan, dithiothreitol (DTT), dihydrolipoic acid (DHLA), and glutathione (GSH), which are the most abundant thiols in living cells.

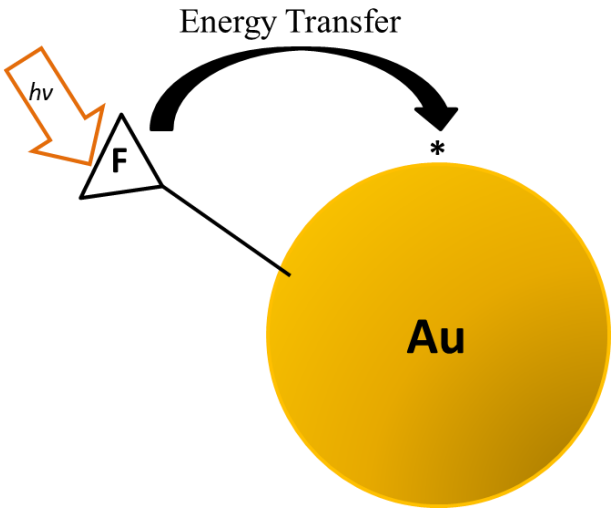

Figure 2-5: Schematic of Forester resonant energy transfer. When incident light hits a fluorescent molecule on a GNP surface energy is transferred to the gold core and fluorescence is quenched

The fluorescence of tryptophan tagged ligands originally bound to GNPs is quenched until displaced by another, non-tagged ligand. As more tryptophan was released, fluorescence intensity increased over time until equilibrium was reached.

Table 2-3: First and second order rate constants determined in Rotello'sstudy. Stuctures of the incoming ligands are presented in Figure 2-6.

Original Ligand	Rate Constants	Incoming Ligand DDT	DHLA	GSH
NP-Sec	k_1 (10^{-2} min^{-1})	2.86 ± 0.25	2.19 ± 0.02	0.33 ±0.02
	k_2 (dm^3 mol^{-1} min^{-1})	28.6 ± 2.5	21.9 ± 0.2	0.66 ± 0.04
NP-Nor	k_1 (10^{-2} min^{-1})	2.38 ± 0.13	1.96 ± 0.11	0.18 ± 0.02
	k_2 (dm^3 mol^{-1} min^{-1})	23.8 ± 1.3	19.6 ± 1.1	0.36 ± 0.04
NP-Iso	k_1 (10^{-2} min^{-1})	1.76 ± 0.09	1.57 ± 0.07	0.11 ± 0.04
	k_2 (dm^3 mol^{-1} min^{-1})	17.6 ± 0.9	15.7± 0.7	0.22 ± 0.08

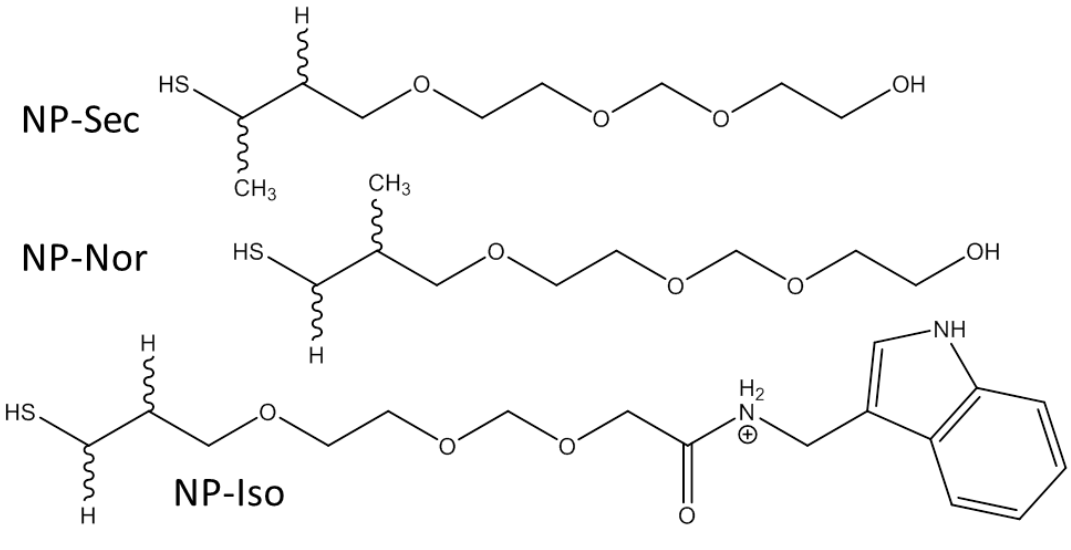

Figure 2-3: Structures of the ligands used in Rotello's work studying ligand exchange with fluorescence spectroscopy

The kinetic rate constants calculated by the Stern Volmer equation for this experiment can be seen in Table 2-3.[183] The reaction rates of the incoming ligands decrease in the order of DTT > DHLA >> GSH. The explanation of this trend is due to the fact that DTT and DHLA carry two mercapto groups and will interact more strongly with GNPs that GSH, which only carries one mercapto group. Graf and coworkers also used fluorescence spectroscopy to investigate the effect of multidentate ligands on ligand exchange kinetics with monothiols on different size GNPs. Kinetic rate constants for this investigation are listed in Table 2-4.[165] Results from this study demonstrated that multidentate ligands exchange on the surface much more rapidly that monodentate ligands. Results also showed that multidentate ligands exchanged more rapidily on medium sized (3.2nm) than small (2.2nm) GNPs because of their steric bulk.

Table 2-4: Rate constants of ligand exchange with multidentate ligand calculated with biexponential and Langmuir models in Graf's study

Size (nm)	Model	Rate Constant	1,1,1-tris(mercaptomethyl) nonane	2-octylpropane-1,3-thiol	Dodecanthiol
3.2 ± 0.7	Biexponential	k_1*10^{-3} (s^{-1})	5.75±0.85	5.25±0.35	2.55±0.56
		k_2*10^{-5} (s^{-1})	11.20±2.02	6.45±3.14	5.30±1.47
	Langmuir	k_L*10^{-3} (s^{-1})	61.5±5.8	50.8±7.7	34.7±3.6
2.2 ± 0.4	Biexponential	k_1*10^{-3} (s^{-1})	0.85±0.07	3.93±0.63	0.94±0.03
		k_2*10^{-5} (s^{-1})	5.58±1.28	15.80±2.45	9.0±0.82
	Langmuir	k_L*10^{-3} (s^{-1})	22.7±2.8	66.3±8.4	29.4±1.2

UV-Vis spectroscopy

Plasmonic nanoparticles exhibit a strong UV-visible extinction band that is not present in the spectrum of bulk materials. The extinction band occurs when the frequency of incident light matches the natural frequency of surface electrons on nanoparticles, and this is known as the localized surface plasmon resonance, LSPR. The peak wavelength of the LSPR spectrum is dependent on size, shape, core material, surface chemistry and local environment of a nanoparticle.[166,184-188] Time studies can be conducted to monitor the kinetics of exchange and can be fit with a Langmuir isotherm to obtain binding constants. Reyes *et al.* used UV-Vis spectroscopy to monitor the exchange of 6-mercaptopurine (6MP) with 11-mercapto-1-undcanol (MUA).[168] The change in the LSPR peak was monitored over time as the exchange reaction progressed. Kinetics were investigated as a function of the ratio of incoming to outgoing ligand. The first and second order rate constants of this experiment can be found in Table 2.5.[168]

Table 2-5: First and second order rate constants of ligand exchange of 6-mercaptopurine (6MP) with 11-mercaptoundecanoic acid (MUA) as a function of the ratio incoming to outgoing ligand monitored by UV-Vis spectroscopy

[MUA]/[6MP]	k_1 ($s^{-1}*10^2$)	k_2 ($s^{-1}*10^3$)
55:27.2	1.8	2.44
50:39.4	2.5	2.96
45:42.0	3.5	4.1

These results indicated a second-order mechanism due to the fact that the constants increased linearly with an increase in the incoming to outgoing ratio.

Other groups have used similar experiments to monitor ligand exchange either to determine if ligand exchange took place and/or to determine exchange kinetics. [105,167] Kumar *et al.* used UV-Vis spectroscopy to determine if ligand exchange reactions could occur between alylamine molecules. Laurylamine protected GNPs were mixed with ethylenediamine in chloroform. The diamine was chosen because if ligand exchange occurred, the diamine stabilized GNPs would crosslink and cause a visible change in optical properties. Broadening in the plasmon band indicated aggregation caused by crosslinking, confirming that the amine-amine exchanges are possible. [189] UV-vis can be particularly useful in biphasic ligand exchange due to the transfer of color from one phase to the other. [190]

FTIR

FTIR analysis is a method commonly employed to monitor and confirm ligand exchange on gold nanoparticle surfaces.[191-193] Like other spectroscopic techniques, exchange of ligands on nanoparticles is investigated by observing changes in IR peaks

over time. Reyes et al. used FTIR in addition to UV-Vis, to monitor the exchange of 6-mercaptopurine (6MP) stabilized GNPs with 11-mercaptoundecanoic acid (MUA) and 11-mercapto-1-undecanol (MUOH) as a function of the ration of incoming to outgoing ligand concentration and nanoparticle size.[168] The IR peak for 6MP was monitored to study the kinetics and extent of the exchange reaction. Results showed that exchange reactions were slower on larger GNPs and on 2D surfaces indicating that nanoparticle defect sites are responsible for higher reactions rates.[168]

NMR/HNMR

NMR and HNMR have been used by many groups studying ligand exchange.[104,150,163,194] NMR can confirm that an exchange has taken place and the composition of surface chemistry however, real time data is often difficult to obtain. Early methods involved isolating and purifying the exchanged nanoparticles at specific time intervals and then determining the monolayer composition by NMR.[169,174] Sharma characterized the kinetics and mechanism of deuterated triphenylphosphine exchange on triphenylphosphine capped GNPs.[169] The exchange kinetics were monitored by obtaining HNMR spectra at various time intervals and the average rate constant was calculated by plotting the normalized intensity peaks of each ligand over time. The average rate constant obtained for the exchange was 0.17 ± 0.04 min^{-1} and the data obtained suggested a dissociative mechanism for exchange. As mentioned earlier Murray and coworkers studied the effect of particle size and ligand end group[163] on the rate and mechanism of ligand exchange.[157] These studies enabled researchers to obtain information about ligand

exchange in-situ by selecting ligands that have NMR peaks that don't overlap for the exchange process.[163]

Electron Paramagnetic Resonance spectroscopy

Electron Paramagnetic Resonance spectroscopy, EPR is a technique where an unbound ligand is functionalized with a spin label. [156,166] The EPR peaks from the spin label will disappear as the spin labeled-ligand replaces the bound ligand on the GNP surface. This method can also provide real time information about ligand exchange. Caragheorgheopol *et al.* used EPR to monitor the exchange of n-butanethiol-protected GNPs with a diradical disulfide to determine the mechanism of exchange.[156] They first obtained EPR spectra of the original nanoparticles then added the disulfide and additional spectra were obtained after 4, 8, 14, 21, 29, and 60 minutes after mixing. Decreasing height, then disappearance of peaks from the disulfide indicated ligand exchange was occurring. This experiment was performed to determine the mechanism of ligand exchange with disulfide molecules. From the EPR data, they proposed a zeroth order mechanism in which the disulfide bond is broken and the molecule binds to the GNP as two separate ligands.[156] Chechik performed the same experiment to determine how aging effects the kinetics of ligand exchange and found that ligand exchange occurs much more slowly on aged GNPs.[166] Zachary et al. discovered that thiols can hop from one GNP to another using spin labeled molecules and calculated rate constants for exchange of spin labeled ligands with octanethiol, Table 2.6, which also provided evidence that the exchange follows a dissociative mechanism.[195]

Table 2-6: Kinetic rate constants of ligand exchange of triphenyl phosphine with bis-nitroxide disulfide on gold nanoparticles, performed by Zachary et al. and monitored by EPR

Ratio of Spin labeled octanethiol (mM:mM)	Rate constant, k, ($s^{-1}*10^{-4}$)	Extent of Reaction, %
0.01:0.07	1.1	18.4
0.01:0.1	1.1	20.2
0.01:0.2	1.4	17.2
0.014:0.1	1.2	24.7
0.01:0.1	1.4	24.2
0.005:0.1	1.6	21.8

Surface enhanced Raman spectroscopy

Surface enhanced raman spectroscopy (SERS) is a technique where the Raman signal of a molecule is enhanced when it is bound to a metal surface. [196-198] The enhancement gained from GNPs allows SERS to detect single molecules on their surface. [199,200] Feng *et al.* utilized SERS to investigate the mechanism exchange of citrate on GNP with 3 different ligands; naphthalenethiol, 22'-bipyrdine, and octanethiol. [177] Control experiments in the study demonstrated that citrate is SERS inactive and an increase in intensity of the Raman peak of the incoming ligand of interest gradually increased as the exchange reaction was carried out. The SERS peak of naphthalenethiol and 22'-bipyrdine increased occurred rapidly in the first 15 minutes of exchange and then continued to gradually increase after the first 15 minutes. This indicated a two-step exchange process where ligands initially bind to the surface at highly reactive sites, and then when the ligand density at these sites reaches a critical value the ligand would migrate and reorganize to allow more ligands to bind. [177] Ansar *et al.* used SERS to determine the binding affinity, packing and conformation of mercaptobenzimidazole

(MBI) thiolate (S^-), thiol (SH) and thione (S) ligands exchanged onto citrate stabilized GNPS.[176] The different forms of MBI were produced by changing the pH of the solution; thiolate at pH 7.9 and 12.5, thione at pH 1.4. From the SERS spectra the thiol conformation was not dominant in these experiments.[176] A disadvantage of using SERS for quantitative measurements is that aggregation can enhance signal intensity disproportionally and care must be taken to ensure that signal enhancement is due molecules on the nanoparticle surface and not due to aggregation.[201,202]

X-Ray Photoemission Spectroscopy

X-ray photoemission spectroscopy, XPS, is generally not used to monitor ligand exchange but can measure binding energies of functional groups to the surface of gold nanoparticles. This analytical technique can identify elemental composition, stoichiometry, chemical and electron state of molecules bound to gold and iron oxide surfaces. [203-205] XPS spectra are obtained by irradiating a material with X-rays and measuring the kinetic energy and the number of electrons that are emitted from the top 1-10nm of the surface being analyzed, therefore, this technique is suitable for measuring the binding energy of ligands bound to GNPs. The binding energy is proportional to the difference in energy of the X-ray irradiation and electrons emitted from the surface of the GNP. XPS can ensure that ligand exchange has taken place and determine the extent of ligand displacement. Brown *et al.* used XPS to monitor and determine the extent of exchange of phosphine stabilized GNPs with octadecanethiol. [206] The binding energy for thiol was found to be 163.3 to 163.9 eV[206] which agreed with other values reported in

literature.[207,208] Lee *et al.* used XPS to determine the binding energy and stability of multidentate thiols exchanged for citrate on GNPS. [127] In this study citrate was exchanged with hexadecanethiol (*n*-C16), 2,2-dimethylhexadecane-1-thiol (DMC16), 2-tetradecylpropane-1,3-dithiol (C16C2), 2-methyl-2-tetradecylpropane-1,3-dithiol (C16C3), or 1,1,1-tris-(mercaptomethyl)pentadecane (t-C16) and the binding energies of these compounds to GNPs was measured with XPS to be 162 eV regardless of chain structure. Results also showed that $C_{16}C_2$, $C_{16}C_3$, and t-C_{16} ligands enhanced the stability of 50 nm GNPs in toluene more effectively than the other ligands studied.[127] Kumar *et al.* measured the binding energies of alkylamines to GNPs and found that amines can bind to gold surfaces in two different modes; an electrostatically and a through a stronger, near covalent bond.[209]

Isothermal Titration Calorimetry

Isothermal titration calorimetry, ITC, has been very useful in studying the thermodynamics of binding in biological systems such as protein-protein interactions,[210] protein-DNA interactions, [211] and protein-lipid interactions. [212,213] Recently, this method had been used to study ligand binding to the surface of nanoparticles due to the temperature sensitivity of this technique as ITC can detect nanoWatts of heat change. ITC can be used to study ligand binding and exchange by titrating a known concentration of unbound ligand into a solution of nanoparticles of known concentration. The binding/exchange reaction will evolve heat which is measured by ITC as a function of the amount of ligand added and then this data is modelled thermodynamically to determine a

binding constant and heats of binding. Sastry *et al.* use ITC to determine the heat of binding of lysine and aspartic acid to bare GNPs at different pH's, and discovered that amino acids bring more strong to GNPs when they are unprotonated.[178] Sastry also observed that PNA monomers bind much more strongly to GNPs than DNA bases and require a concentration 10 times less than DNA bases to reach saturation of the GNP surface. The strength of interaction of the PNA bases increased in the order thymine < adenine < guanine < cytosine.[214]

MALDI

Matrix-assisted laser desorption/ionization, MALDI, is a soft ionization form of mass spectroscopy that allows for the analysis of large organic molecules that tend to be fragile when ionized. MALDI can be used to determine distribution and composition of ligands in a mixed monolayer on GNPs, however, fragmentation may occur.[215,216] Murray and coworkers used MALDI to monitor ligand exchange and determine the binding conformation of multidentate thiols with monovalent thiols on GNPs. [217] A laser pulse intensity threshold approach was used to avoid fragmentation in a trans-2-[3-(4-tert-butylphenyl)-2-methyl-2-propenylidene] malononitrile (DCTB)35 matrix.[218] Low concentrations were used to slow the reaction and the progress was monitored by measuring samples at various times intervals. Results indicated that dithiols replace 2 monothiols. The mass spectrums obtained suggest that chelation is the major binding mechanism for multidentate ligands on NP surfaces. Products were assigned as dithiols that bind to adjacent GNP-bound dithiols to create a semi-ring around the nanoparticle.[217]

A downside to using MALDI to monitor ligand exchange is that in-situ observations are not possible.

Chromatography: GPC/GC

Chromatography is a facile method to study ligand exchange reactions where there are differences in ligand structure. Lennox *et al.* used this technique to investigate the exchange of decanethiol with dodecanethiol. [219] Ligand exchange was studied by adding small aliquots of dodecanethiol to decanethiol coated GNPs, precipitating the NPs after each addition with ethanol and centrifugation, then analyzing the supernatant on GC to determine the ligand concentrations in solution. The presence of decanethiol in the supernatant indicated ligand exchange had occurred. The results quantified surface coverage which was modeled with a second order diffusion limited Langmuir isotherm to determine the binding constant for thiol bound to a GNP to be $0.0137 \pm 0.0006\ s^{-1/2}$. [219] Murray and coworkers also used this technique to examine ligand exchange reaction products to determine the surface coverage and extent of ligand exchange as a function of chain length. [155] This study demonstrated that ligand exchange proceeds through an associative pathway and the rate of exchange decreases with increasing chain length of the initially bound ligand. [155] While chromatography is a facile method to monitor ligand exchange, it does not provide in-situ observations of the process.

Methods to Calculate Rate Constants

Many groups monitor ligand exchange reactions simply to confirm that the reaction occurred. Research is lacking in the area of investigating rate and binding

constants of exchange of specific functional groups, especially for competitive binding. In this section we discuss methods to determine kinetic rate constants of ligand exchange. The methods discussed in this paper are the most common and convenient ones to calculate rate constants in conjunction with traditional instrumental methods.

The Langmuir isotherm model is based on the assumptions in the Langmuir model of adsorption. To describe the model, consider adsorption of a monatomic ideal gas in equilibrium onto a solid substrate. The surface has a certain number of equivalent sites and only one adsorbate can bind on each site. The model also assumes that the molecules bound to the surface do not interact. Lennox *et al.* used a second order diffusion limited form of the Langmuir model to fit kinetic data of the exchange of decanethiol with dodecanethiol and obtained a second order rate constant of $0.013\pm0.008*10^{-6}$ s^{-1}. [219]

The Stern-Volmer model is used in conjunction with fluorescence spectroscopy. The model describes kinetics of intermolecular deactivation, for example; when one chemical species, Q, is in the presence of another species in an excited state, A*; Q becomes activated, and A is deactivated:

$$A^* + Q \rightarrow A + Q^*$$

In order to monitor ligand exchange via fluorescence spectroscopy, a ligand with is labeled with a fluorescent dye, and then bound to a GNP. When the labeled ligand is replaced with a new ligand through an exchange reaction, the dye will fluoresce and intensity is measured. The fluorophore is quenched by gold, and therefore it does not

fluoresce until it breaks off. This is a phenomena know as fluorescence resonance energy transfer, FRET. Intensity is plotted against ligand concentration or surface coverage and the date is fit to the following equation;

$$\frac{I_f^0}{I_f} = 1 + k_q \tau_0 \cdot [Q]$$

Where I_f^0 is the intensity of fluorescence without a quencher, I_f is the intensity with a quencher, k_q is the quencher rate coefficient, τ_0 is the fluorescence lifetime of A and [Q] is the concentration of the quencher. A plot of $\log\left[\frac{I_f^0 - I_f}{I_f}\right]$ vs. $\log[Q]$ will determine the binding constant, K_b (intercept) and the number of binding sites, n (slope).

$$\log\left[\frac{I_f^0 - I_0}{I_0}\right] = \log K_b + n \log[Q]$$

A second order mechanism has been adopted by many groups to describe ligand exchange. [155,157,163,168,174,183] This mechanism describes ligand exchange as a 2-step process in which the incoming ligand attached to the surface, rearrangement of the ligands takes place and then the original bound ligand is then desorbed from the surface. The rate constants in this model are strongly dependent on the incoming ligand concentration.[220] Graf and coworkers took the presence of defect sites on a GNP surface into account when studying ligand exchange. As discussed before, ligand exchange occurs more rapidly at defect sites then on smooth surfaces. This discovery motivated the

development of a biexponential model that describes two distinct kinetic processes in ligand exchange, the rapid exchange at defect sites and the subsequent exchange at the remaining non-defect sites. Fluorescence spectroscopy was used to monitor ligand exchange and a modified version of the biexponential was employed to model kinetic data. Graf found that the biexponetial model fit experimental data much better than monoexponetial models and rate constants obtain with this model can be found in Table 2-4.[220]

Factors Affecting Nanoparticle Ligand Exchange

Nanoparticle Properties

Size and Surface Effects

Nanoparticles are largely not perfectly spherical, but have both flat terraces, and defect sites; edges, vertices, and grain boundaries.[115,160,161,221] The defect sites have different electron densities and steric accessibilities that can affect the rate of exchange.[14,162,163,222,223] Defect sites are more reactive than smooth surfaces and therefore ligand exchange occurs rapidly at these sites then slows as bound ligands migrate from the defect sites to smooth terrace sites. This migration is slow and becomes increasingly more difficult father away from defect sites.[150] This can lead to incomplete exchange on larger particles. Kell *et al.* found that the relative number of edge and vertex sites is proportional to the number of terrace sites and therefore dependent on size.[150] But since very small particles have very high surface curvatures, and a large number of atoms with incomplete valence shells, ligand exchange cannot reach equilibrium on these surfaces.

Kell found that ligand exchange rates increase and reach equilibrium faster as particle size increases up to 5 nm in diameter.[150] Graf *et al.* also observed this trend, stating the number of defect sites is size dependent, and smaller particles have a higher ratio of defect sites to non-defect sites than larger particles due to higher surface curvature.[165] As the size continues to increase above 5nm, terrace sites start to greatly outnumber defect sites and ligand exchange rates decrease along with the extent of reaction. Larger nanoparticles have tighter packing arrangement of ligands on the surface due to smaller surface curvature and more terrace sites.[165] Tighter packing on terrace surfaces will restrict ligand exchange, but will also make the destabilization of surrounding bound ligands by an incoming ligand easier. Surface curvature plays an important role in ligand exchange. Smaller particles are less tightly packed due to high surface curvature, and this can increase the rate and extent of ligand exchange.[150] Nanorods are a good example of this trend. Different exchange rates have been observed on the sides and ends attributed to differing surface curvature.[44,224]

The structure of crystalline faces also affects the rate of exchange and strength of binding. As stated previously nanoparticles are not perfectly spherical and can be synthesized in a variety of shapes including blocks, cubes and tetrapods.[47] Gold has a face-centered cubic (FCC) structure which has 3 faces, 100, 110, and 111. [225] Preference for a given crystal face is based on steric accessibility and the size of the binding group compared interatomic spacing.[11,226] Murphy found that head group size on CTAB, a common surfactant used in the synthesis of gold nanorods, is more comparable to side faces, 110 or 100 therefore promoting the growth of the nanorod shape.[44] Gold atoms are

too closely packed in the 111 face for larger head groups to bind and this finding had been reported by other groups as well for gold[227] and for silver.[60,61,226]

Oxidation State and Charge

The oxidation state and charge of both the nanoparticle core and ligand can affect ligand exchange kinetics and binding strength. For gold nanoparticles, ligand exchange is accelerated by the oxidative charging of gold nanoparticle surfaces.[157] This charging can be achieved electrochemically[174] or by admitting dioxygen.[228] Song and Murray studied the effect of nanoparticle core charge and observed that a positive charge placed on the surface with electrolysis increased both the initial rate and extent of reaction, Table 2-8 as both the first and second order rate constants increased with an increase in nanoparticle charge.[174] This work was significant because charged nanoparticle cores have the potential for use as electron donors or acceptors in capacitor applications [229] and the chemical consequences of nanoparticle charging are relatively unknown. [174] Porter *et al.* showed that thiolate ligands can be desorbed when a sufficiently negative potential is applied to flat gold surfaces. This work was done in order to quantify surface coverage thiolates on GNPs.[230] This finding also explains why ligand exchange of thiols occurs more rapidly at electron dense defect sites.[174]

Table 2-7: Charge dependent first and second order rate constants of ligand exchange

Original ligand	**Rate contant**	**Charge**			
		As Prep	**0**	**1**	**3**
Hexanethiol	K_1 (S^{-1})	0.00012	0.00014	0.00015	0.0002
	K_2, (M^{-1} S^{-1})	0.0071	0.0082	0.0088	0.014

Nanoparticle Age

Research has shown that nanoparticles can change size and shape with age [231] and that their reactivity can also be altered with age. Chechik *et al.* [166] showed that age will all affect the reactivity of nanoparticles due to changes in surface morphology. The changes in surface morphology and chemistry can be monitored by size exclusion chromatography, SEC, and atomic force microscopy, AFM. [232,233] This is confirmed by a number of experiments, EPR to monitor reaction kinetics, TGA to determine the degradation temperature of bound ligands, and UV-vis spectroscopy to measure the max absorbance wavelength. The kinetic profiles obtained from EPR demonstrated that ligand exchange reactions took longer to come to completion on aged nanoparticles. Nanoparticle age may also result in poor reproducibly of ligand exchange experiments in the same batch of nanoparticles; however nanoparticles with the same aging history showed good reproducibility. UV-Vis spectrum analysis showed that spectra of fresh and aged GNPs had similar shape, but the plasmon peak for aged particles underwent a substantial red-shift. Thermal gravimetric analysis showed that decomposition of aged nanoparticles happened at a slightly higher temperature than fresh nanoparticles, indicating that ligands are more strongly bound to aged particles. Chechik concluded that the decrease in reactivity is due to the annealing[234] or stabilization of high-energy defect sites on the particle surface. The change in morphology can be attributed to the high surface mobility of thiol bound Au atoms, [235] which is confirmed by AFM measurements.[233]

Nanoparticle Environment

Depending on the end fate of nanoparticles, they will be exposed to different conditions. Nanoparticles may be exposed to various temperatures, pH's, salts, ionic strengths, and natural and biological molecules, all of which could impact nanoparticle stability and rates of ligand exchange.

pH, Salt Type and Ionic Strength

The effect of pH on nanoparticle ligand exchange is ligand dependent. An overall trend to remember is that the bonds of certain functional groups will change depending on the pH of solution, therefore altering the binding strength of the ligand to the particle surface. Woehrle *et al.* showed that ligand exchange reactions must occur in a solution with a pH at which the head groups are ionized, and the binding group is deprotonated. [236] X-ray photoemission spectroscopy, XPS, work performed by Sastry *et al.* showed that at a pH of 7, lysine binds weakly to GNPs, but at a pH of 11, strong binding occurred.[178] The pI of lysine is 9.4 and therefore, at a pH of 7, lysine would be protonated, making binding to gold difficult.

Salt type also influences the speed and strength of binding in ligand exchange reactions.[88] Rothberg *et al.*[88] studied the effect of salt type on the exchange of citrate with single stranded DNA (ssDNA). Rothberg hypothesized that the binding of the amine group in ssDNA is affected more by the DNA/solvent interactions than the amine/surface interactions. In this regard, the binding rate is related to the average number of water molecules hydrated each of the bases in the DNA molecule, which is termed the

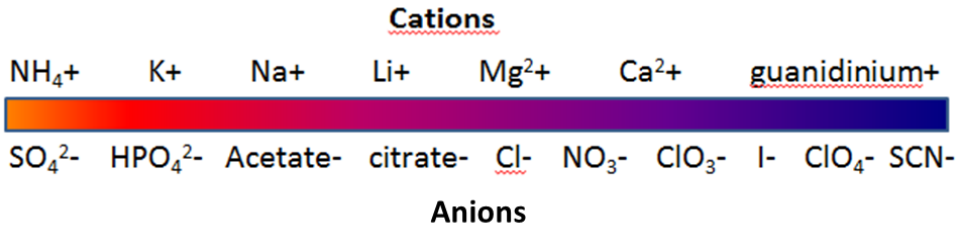

Figure 2-7: Hofmeister series of electolyte solutions

hydration number. The hydration number affects the secondary structure of ssDNA, and this structure affects the binding of ssDNA to GNPs. The salt type in an electrolyte solution will influence the hydration number of ssDNA, and therefore the binding rate to GNPs. Rothberg found that in the Hofmeister series of electrolyte solutions; cations high in the series increase binding rates and anions high in series decrease binding rates, Figure 7 due to their ionic charge. They also showed that chaotropic anions resulted in faster binding and strongly hydrated kosmotropic anions slowed reactions down. [88]

Ligand Properties:

Ligand Structure; Multivalency, Chain length, Branching and Chirality

Multidentate ligands bind to a nanoparticle surface at multiple binding sites and tend to have bulkier headgroups, which leads to more complex interactions with the nanoparticle surface than monovalent ligands. Many biological molecules, DNA, BSA, proteins, and carbohydrates and many polymers have multiple binding groups and behave like multivalent ligands. Multivalent ligands are known to have much stronger interactions with nanoparticles than monovalent ligands because of an entropy-driven

chelating effect. [127,175,183,203,237] Increased spacing between the tail groups of multivalent ligand allows for more conformational freedom, better solvation of the tails, and contributes to the strong interaction between ligand and nanoparticle.[127] Multivalent ligands effective in dispersing larger particles and binding to them during ligand exchange due to their strong interaction with GNPs through multiple functional groups. [127,217,238] Multivalent ligands also exhibited higher extents of ligand exchange than monovalent ligand on large (>15nm) GNPs. The extent of multivalency will also affect the rate of ligand exchange. Exchange rates of trivalent ligands are similar or lower than divalent ligands due to steric hindrance of the bulky molecule.[165] Since small particles have smaller areas of smooth terraces and edges are shorter, the complete binding of multivalent ligands may not be possible.[165] Multivalent ligands provide numerous binding sites, but the number of ligand tails in solution to maintain dispersibility is a fraction of the number of binding sites and the enhanced spacing between ligand tails on very large (>50nm) particles can reduce their stability.[237]

Chain length has a significant effect on the rate of exchange. Longer chains behave similarly to multivalent ligands in that conformational changes may be required in order for binding to occur. Ingram *et al.*[171] investigated the effect of chain length on ligand exchange by exchanging thiol groups of five different chain lengths ranging from C8 to C16. They discovered that longer chains will displace short chains, but short chains will not displace long chains. This is due to entropic effects and additional steric stabilization provided by longer chains that short chains do not offer. [171] Rotello's group [14] studied the effect of branching and chirality on ligand exchange on GNPs, Figure 2-8.

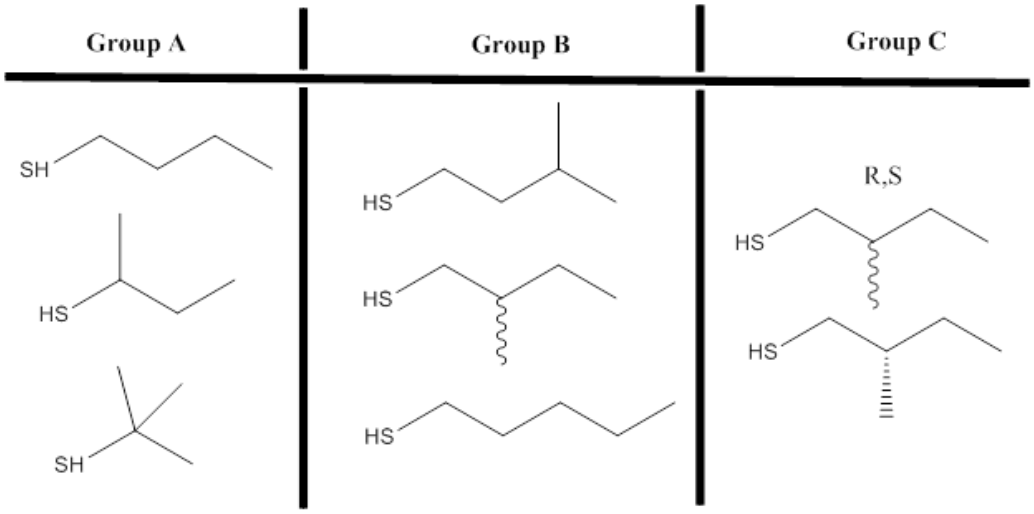

Figure 2-4: Structures of ligand used in Rotello's study

Group A consisted of primary, secondary and tertiary thiols, Group B included linear and branched thiols and Group C investigated thiol chirality. Rotello discovered that primary thiols are more successful at exchanging onto GNPs surfaces than secondary and tertiary thiols due to steric hindrance by branched chains. Conversely, they found that a thiol group with a one carbon branch was more active than a linear thiol group with the same molecular weight. They hypothesized that branched thiols may pack better and form a more stable monolayer on the surface. The branched thiol may also occupy more space than a linear chain, which allows it to destabilize surrounding bound thiol more easily. A branched carbon chain may also provide more steric protection of defect sites. They also found that even very subtle changes in the ligand structure can dramatically change the rate of ligand exchange. Exchange by racemic thiol mixture was significantly

faster than with a homochiral thiol, which may also be due to better packing on the surface. [14]

Ligand Chemistry: End group

A multitude of ligand variations exist for nanoparticle surface modification, which can include the ligand head group chemistry and end group chemistry. While the ligand head group determines the mechanism and strength of binding, the end group can have an impact on the rate and extent of exchange depending on its electronic characteristics. In the study conducted by Guo *et al.* mentioned earlier, phenylethanethiolate was exchanged with various p-X-substituted arylthiols, (X = NO2, Br and CH3) and the NMR peak for phenylethanethiolate was used to study exchange kinetics.[163] As the exchange reaction progressed phenylethanethiolate was liberated and the growth of its NMR peak relative to a ferrocene tracer was used to determine exchange kinetics, rate constants can be found in Table 2.1. The exchange rates differed for each of the p-X-substituted arylthiols with exchange rates increasing in the following order; $k_{(CH3)} < k_{(Br)} < k_{(NO2).}$ While these initial rates differed, equilibrium rate constants for each X-substituent were the same implying that ligand binding is not affected by X- groups rather there is an activation barrier to initiate exchange that is dependent on X.[163] This trend was also seen in an earlier study conducted by Donkers *et al.* demonstrated that the extent of ligand exchange is higher for thiol ligands with electron donating substituents, Table 2.9.[157]

Table 2-8: Second order rate constants determined from ligand exchange of phenylethylenethiol with various bifunctional ligands in Donkers' study

Incoming Ligand	KP-E, (M^{-1} s^{-1})
SH-R-NO2	0.014
SH-R-CN	0.009
SH-R-Br	0.006
SH-R-CH3	0.004
SH-R-OCH3	0.004
SH-R-OH	0.004

Ligand Head Group

Ligands bind to nanoparticles through their head groups and these groups have the largest impact on ligand binding and exchange reactions. Two common methods to modify the surface of NPs are physical and chemical adsorption. Certain functional groups, such as thiols that bind chemically will displace other groups, such as citrate, which binds physically, to the surface of GNPs very easily. The reverse reaction will not take place. The advantage of chemical over physical binding is the strength of binding to the particle. The heat of adsorption of a chemical bond is -40 to -1000kJ/mol, while the heat of adsorption for a physical bond is only -10 to -40 kJ/mol. [239] This is an area of research that is not fully understood and in which information is lacking. Gold preferentially binds to soft ligands such as sulfur and phosphines. [184,221,240] The sulfur-gold bond is considered nearly covalent. Competitive binding experiments have shown that thiols preferentially bind to gold surfaces. [241,242] Work done with self-assembled monolayers on flat surfaces (2D SAMs) has described the Au-S bond as polar or slightly ionic.[230,243] Density-functional theory, DFT, modelling performed by Andreoni *et al.* [244]

estimated the Au-S bond strength on Au(111) faces to be 37 to 55 kcal/mol, which compares to the bond energy calculated Nuzzo *et al.* of 45 kcal/mol.[207] Landman *et al.* also estimated the Au-S bond energy in Au_{38} nanocrystals to be ~32 to 50 kcal/mol.[222] The bond energy of disulfides to gold was also studied by Andreoni. Disulfides bond weakly in dimer form, about 20 kcal/mol, whereas when the S-S bond dissociates, the Au-S bond energy was calculated to be ~38 kcal/mol.[244] There is debate on whether disulfides bind to gold in the dimer or dissociated form,[245,246] nonetheless experimental evidence supports the claim that disulfides bind to gold in the dissociated form. [207,222,244,247] High resolution XPS results did not distinguish between SAMs formed from disulfide or thiols. [207,241] Amines are another functional group that has strong interactions with gold. The amine-gold bond is charge neutral and can be described as weakly covalent in non-polar solvents. [248] In highly polar solvents such as ethanol, the interaction of gold with amines must compete with the solvent – amine interaction. [249] This suggests that amines need to be deprotonated in order to bind to strongly to gold.[250] Leff *et al.* described the amine-gold bond is predominantly kinetic and nanoparticle size dependent in nature. [248] Phosphine groups can be used as precursors for ligand exchange with thiol ligands. [167,179,251] Citrate, another common ligand, binds weakly to gold through an electrostatic attraction. [252]

Conclusions

In this review, we have summarized applications, methods to perform and analyze, and effects on ligand exchange and binding. Ligand exchange has proved to be a

versatile and robust method for modifying nanoparticle surfaces regardless of core material. Overall, a S_N2, associative mechanism in which an incoming ligand binds to a nanoparticle surface while an outgoing ligand desorbes from the surface in a simultaneous process; can be used to describe ligand exchange on gold nanoparticles with thiols and amines. A dissociative mechanism describes ligand exchange involving disulfides or when molecular oxygen is present. In both cases ligand binding and exchange is initiated and occurs rapidly at highly reactive defect sites and then slows as defect site-bound ligands migrate to less reactive terrace sites to allow more ligands to bind. Many factors contribute to the strengths and kinetics of ligand binding and exchange. Nanoparticle properties that affect ligand binding and exchange include size, shape, crystalline structure, charge, oxidation state, and age. Ligand properties that affect ligand exchange and binding include structure, i.e. multivalency, chain length, extent of branching and chirality, and chemistry; end group and perhaps most importantly head group, through which ligands bind to nanoparticle surfaces. Thiols preferentially bind to GNPs but amines, phosphines and carboxylic acids are other common functional groups that bind to GNPs.

References

(1) Ferrando, R.; Jellinek, J.; Johnston, R. L.: Nanoalloys: From Theory to Applications of Alloy Clusters and Nanoparticles. *Chemical Reviews* **2008**, *108*, 845-910.

(2) Daniel, M.-C.; Astruc, D.: Gold Nanoparticles: Assembly, Supramolecular Chemistry, Quantum-Size-Related Properties, and Applications toward Biology, Catalysis, and Nanotechnology. *Chemical Reviews* **2003**, *104*, 293-346.

(3) Daniel, M.-C. a. D. A.: Gold Nanoparticles:‚Äâ Assembly, Supramolecular Chemistry, Quantum-Size-Related Properties, and Applications toward Biology, Catalysis, and Nanotechnology. *Chemical Reviews* **2003**, *104*, 293-346.

(4) Haberlen, O. D.; Sai-Cheong, C.: From clusters to bulk: A relativistic density functional investigation on a series of gold. *Journal of Chemical Physics* **1997**, *106*, 5189.

(5) Hao, R.; Yu, J.; Ge, Z.; Zhao, L.; Sheng, F.; Xu, L.; Li, G.; Hou, Y.: Developing Fe3O4 nanoparticles into an efficient multimodality imaging and therapeutic probe. *Nanoscale* **2013**, *5*, 11954-63.

(6) M. J. Hostetler, J. E. W., C. J. Zhong, J. E. Harris, R. W. Vachet, M. R. Clark, J. D. Londono, S. J. Green, J. J. Stokes, G. D. Wignall, G. L. Glish, M. D. Porter, N. D. Evans and R. W. Murray: *Langmuir* **1998**, *14*, 17.

(7) V. Chechik, R. M. C. a. C. J. M. S.: *Adv. Mater.*, *12*, 1161.

(8) Mahmoud, M. A.; O'Neil, D.; El-Sayed, M. A.: Shape and Symmetry Dependent Mechanical Properties of Metallic Gold and Silver on the Nanoscale. *Nano Letters* **2013**.

(9) Murray, R. W.: Nanoelectrochemistry: Metal Nanoparticles, Nanoelectrodes, and Nanopores. *Chemical Reviews* **2008**, *108*, 2688-2720.

(10) Huynh, W. U.; Dittmer, J. J.; Alivisatos, A. P.: Hybrid Nanorod-Polymer Solar Cells. *Science* **2002**, *295*, 2425-2427.

(11) Gai, P. L.; Harmer, M. A.: Surface Atomic Defect Structures and Growth of Gold Nanorods. *Nano Letters* **2002**, *2*, 771-774.

(12) Burgi, C. G. a. T.: Chiral Inversion of Gold Nanoparticles. *Journal of the American Chemical Society* **2009**, *130*.

(13) Hart, A. E., Akers, David B., Gorosh, Samuel, Kitchens, Christopher L.: Reverse micelle synthesis of silver nanoparticles in gas expanded liquids. *The Journal of Supercritical Fluids* **2013**, *76*, 236-243.

(14) Hong, R., Fernandez, J. M., Nakada, H., Arvizo, R., Emrick, T., Rotello, V. M.: In situ observation of place exchange reactions of gold nanoparticles. Correlation of monolayer structure and stability. *Chemical Communications* **2006**, *2006*, 2347 - 2349.

(15) Park, J.; An, K.; Hwang, Y.; Park, J. G.; Noh, H. J.; Kim, J. Y.; Park, J. H.; Hwang, N. M.; Hyeon, T.: Ultra-large-scale syntheses of monodisperse nanocrystals. *Nat Mater* **2004**, *3*, 891-5.

(16) Caragheorgheopol, A., Chechik, V.: Mechanistic aspects of ligand exchange in Au Nanoparticles. *Physical Chemistry Chemical Physics* **2008**, *10*, 5029-5041.

(17) Brown, K. R., Walter, D. G., Natan, M. J.: Seeding of Colloidal Au Nanoparticle Solutions. 2. Improved Control of Particle Size and Shape. *Chemical Materials* **2000**, *12*, 306-313.

(18) Jana, N. R., Gearheart, L., Murphy, C. J. : Seeding Growth for Size Control of 5-40 nm Diameter Gold Nanoparticles. *Langmuir* **2001**, *17*, 6782-6786.

(19) Toth, I. Y.; Illes, E.; Bauer, R. A.; Nesztor, D.; Szekeres, M.; Zupko, I.; Tombacz, E.: Designed polyelectrolyte shell on magnetite nanocore for dilution-resistant biocompatible magnetic fluids. *Langmuir : the ACS journal of surfaces and colloids* **2012**, *28*, 16638-46.

(20) Itoh, H.; Naka, K.; Chujo, Y.: Synthesis of Gold Nanoparticles Modified with Ionic Liquid Based on the Imidazolium Cation. *Journal of the American Chemical Society* **2004**, *126*, 3026-3027.

(21) Mohammed, F. S.; Cole, S. R.; Kitchens, C. L.: Synthesis and Enhanced Colloidal Stability of Cationic Gold Nanoparticles using Polyethyleneimine and Carbon Dioxide. *ACS Sustainable Chemistry & Engineering* **2013**.

(22) Badruddoza, A. Z. M.; Shawon, Z. B. Z.; Rahman, M. T.; Hao, K. W.; Hidajat, K.; Uddin, M. S.: Ionically modified magnetic nanomaterials for arsenic and chromium removal from water. *Chemical Engineering Journal* **2013**, *225*, 607-615.

(23) Lu, C.; Zu, Y.; Yam, V. W.-W.: Nonionic surfactant-capped gold nanoparticles as postcolumn reagents for high-performance liquid chromatography assay of low-molecular-mass biothiols. *Journal of Chromatography A* **2007**, *1163*, 328-332.

(24) Stobiecka, M. D., J.; Hepel, M.;: Ligand exchange effects in gold nanoparticle assembly induced by oxidative stress biomarkers: Homocyteine and cysteine. *Biophysical Chemistry* **2010**, *146*, 98-107.

(25) Ryouta Tatumi, H. F.: Remarkably stable gold nanoparticles functionalized with a zwitterionic liquid based on imidazolium sulfonate in a high concentration of aqueous electrolyte and ionic liquid. *Chemical Communications* **2005**, *2005*, 83-85.

(26) Qiao Jin, J.-P. X., Jian Ji, Jia-Cong Shen: Zwitterionic phosphorylcholine as a better ligand for stabilizing large biocompatible gold nanoparticlesElectronic supplementary information (ESI) available: Synthesis and characterization of HS-PC, synthesis and FTIR spectra of the HS-PC protected gold nanoparticles, Stability tests against pH values, salt concentrations, and gel electrophoresis. *Chemical Communications* **2008**, *2008*, 3058-3060.

(27) Susumu, K.; Oh, E.; Delehanty, J. B.; Blanco-Canosa, J. B.; Johnson, B. J.; Jain, V.; Hervey, W. J.; Algar, W. R.; Boeneman, K.; Dawson, P. E.; Medintz, I. L.: Multifunctional Compact Zwitterionic Ligands for Preparing Robust Biocompatible Semiconductor Quantum Dots and Gold Nanoparticles. *Journal of the American Chemical Society* **2011**, *133*, 9480-9496.

(28) Shuzhuo Zhang, X. K., Zhi Yang, Qihui Shi, Galen D. Stucky, Lingdong Sun, Jianfang Wang, Chunhua Yan Nanonecklaces assembled from gold rods, spheres, and bipyramidsElectronic supplementary information (ESI) available: TEM images of irregularly aggregated and linearly assembled Au nanorods, nanospheres, and bipyramids, and extinction spectra measured in the presence of varying amounts of cysteine, glycine, and 3-mercaptopropionic acid. *Chemical Communications* **2007**, *2007*, 1816-1818.

(29) Lim, I. I. S.; Ip, W.; Crew, E.; Njoki, P. N.; Mott, D.; Zhong, C.-J.; Pan, Y.; Zhou, S.: Homocysteine-Mediated Reactivity and Assembly of Gold Nanoparticles. *Langmuir* **2006**, *23*, 826-833.

(30) Zhang, L.; Xue, H.; Gao, C.; Carr, L.; Wang, J.; Chu, B.; Jiang, S.: Imaging and cell targeting characteristics of magnetic nanoparticles modified by a functionalizable zwitterionic polymer with adhesive 3,4-dihydroxyphenyl-l-alanine linkages. *Biomaterials* **2010**, *31*, 6582-8.

(31) Wei, H.; Insin, N.; Lee, J.; Han, H. S.; Cordero, J. M.; Liu, W.; Bawendi, M. G.: Compact zwitterion-coated iron oxide nanoparticles for biological applications. *Nano Letters* **2012**, *12*, 22-5.

(32) Shakeri-Zadeh, A., Mansoori, G.A, Hasemian, A. R., Eshghi, H., Sazgarnia, A., Montazerabadi, A. R.: Cancerous Cells Targeting and Destruction Using Folate Conjugated Gold Nanoparticles. *Dynamic Biochemistry, Process Biotechnology and Molecular Biology* **2010**, *4*, 6-12.

(33) Muthiah, M.; Park, I. K.; Cho, C. S.: Surface modification of iron oxide nanoparticles by biocompatible polymers for tissue imaging and targeting. *Biotechnol Adv* **2013**, *31*, 1224-36.

(34) Taratula, O.; Dani, R. K.; Schumann, C.; Xu, H.; Wang, A.; Song, H.; Dhagat, P.: Multifunctional nanomedicine platform for concurrent delivery of chemotherapeutic drugs and mild hyperthermia to ovarian cancer cells. *Int J Pharm* **2013**, *458*, 169-80.

(35) Lowry, G. V.; Gregory, K. B.; Apte, S. C.; Lead, J. R.: Transformations of Nanomaterials in the Environment. *Environmental Science & Technology* **2012**, *46*, 6893-6899.

(36) Newton, K. M.; Puppala, H. L.; Kitchens, C. L.; Colvin, V. L.; Klaine, S. J.: Silver nanoparticle toxicity to Daphnia magna is a function of dissolved silver concentration. *Environmental Toxicology and Chemistry* **2013**, *32*, 2356-2364.

(37) Elizabeth Glogowski, J. H., Thomas P. Russell and Todd Emrick: Mixed monolayer coverage on gold nanoparticles for interfacial stabilization of immiscible fluids. *Chemical Communications* **2005**, 4050-4052.

(38) Norgaard, K.; Weygand, M. J.; Kjaer, K.; Brust, M.; Bjornholm, T.: Adaptive chemistry of bifunctional gold nanoparticles at the air/water interface. A synchrotron X-ray study of giant amphiphiles. *Faraday Discussions* **2004**, *125*, 221-233.

(39) Zhang, T.; Davidson, D.; Bryant, S. L.; Huh, C.: Nanoparticle-Stabilized Emulsions for Applications in Enhanced Oil Recovery. Society of Petroleum Engineers.

(40) Zhang, T.; Roberts, M.; Bryant, S. L.; Huh, C.: Foams and Emulsions Stabilized With Nanoparticles for Potential Conformance Control Applications. Society of Petroleum Engineers.

(41) Suleimanov, B. A.; Ismailov, F. S.; Veliyev, E. F.: Nanofluid for enhanced oil recovery. *Journal of Petroleum Science and Engineering* **2011**, *78*, 431-437.

(42) Qi, W. H., Wang, M. P.: Size and shape dependent melting temperature of metallic nanoparticles. *Materials Chemistry and Physics* **2004**, *88*, 280-284.

(43) Gray, C. H. L. a. H. B.: *Ligand Substitution Processes*; W. A. Benjamin: New York, 1966.

(44) Catherine J. Murphy, T. K. S., Anand M. Gole, Christopher J. Orendorff, Jinxin Gao,; Linfeng Gou, S. E. H., and Tan Li: Anisotropic Metal Nanoparticles: Synthesis, Assembly, and Optical Applications. *Journal of Physical Chemistry B* **2005**, *109*, 13857-13870.

(45) M.B. Sigman, A. E. S., B.A. Korgel: Metal nanocrystal superlattice nucleation and growth. *Langmuir* **2004**, *20*, 978-983.

(46) Bock, C., Paquet, C., Couillard, M., Botton, G. A., MacDougall, B. R.: Size-Selected Synthesis of PtRu Nano-Catalysts: Reaction and Size Control Mechanism. *Jounral of the American Chemical Society* **2004**, *126*, 8028-8037.

(47) Sau, T. K.; Murphy, C. J.: Room Temperature, High-Yield Synthesis of Multiple Shapes of Gold Nanoparticles in Aqueous Solution. *Journal of the American Chemical Society* **2004**, *126*, 8648-8649.

(48) Dixit, V.; Van den Bossche, J.; Sherman, D. M.; Thompson, D. H.; Andres, R. P.: Synthesis and grafting of thioctic acid-PEG-folate conjugates onto Au nanoparticles for selective targeting of folate receptor-positive tumor cells. *Bioconjugate Chemistry* **2006**, *17*, 603-609.

(49) Jewrajka, S. K.; Chatterjee, U.: Block copolymer mediated synthesis of amphiphilic gold nanoparticles in water and an aqueous tetrahydrofuran medium: An approach for the preparation of polymer–gold nanocomposites. *Journal of Polymer Science Part A: Polymer Chemistry* **2006**, *44*, 1841-1854.

(50) Mondini, S.; Drago, C.; Ferretti, A. M.; Puglisi, A.; Ponti, A.: Colloidal stability of iron oxide nanocrystals coated with a PEG-based tetra-catechol surfactant. *Nanotechnology* **2013**, *24*, 105702.

(51) Basuki, J. S.; Esser, L.; Zetterlund, P. B.; Whittaker, M. R.; Boyer, C.; Davis, T. P.: Grafting of P(OEGA) Onto Magnetic Nanoparticles Using Cu(0) Mediated Polymerization: Comparing Grafting “from” and “to” Approaches in the Search for the Optimal Material Design of Nanoparticle MRI Contrast Agents. *Macromolecules* **2013**, *46*, 6038-6047.

(52) Bolley, J.; Guenin, E.; Lievre, N.; Lecouvey, M.; Soussan, M.; Lalatonne, Y.; Motte, L.: Carbodiimide versus Click Chemistry for Nanoparticle Surface Functionalization: A Comparative Study for the Elaboration of Multimodal Superparamagnetic Nanoparticles Targeting alphavbeta3 Integrins. *Langmuir : the ACS journal of surfaces and colloids* **2013**, *29*, 14639-47.

(53) Kadnikova, D. B. a. E. N.: Synthesis and characterization of azidoalkyl-functionalized gold nanoparticles as scaffolds for ‘‘click’’-chemistry derivatization. *Jounral of Materials Chemistry* **2011**, *21*, 6152-7157.

(54) Lin, S.; Cheng, Y.; Bobcombe, Y.; L. Jones, K.; Liu, J.; Wiesner, M. R.: Deposition of Silver Nanoparticles in Geochemically Heterogeneous Porous Media: Predicting Affinity from Surface Composition Analysis. *Environmental Science & Technology* **2011**, *45*, 5209-5215.

(55) Petosa, A. R.; Jaisi, D. P.; Quevedo, I. R.; Elimelech, M.; Tufenkji, N.: Aggregation and Deposition of Engineered Nanomaterials in Aquatic Environments: Role of Physicochemical Interactions. *Environmental Science & Technology* **2010**, *44*, 6532-6549.

(56) Sagee, O.; Dror, I.; Berkowitz, B.: Transport of silver nanoparticles (AgNPs) in soil. *Chemosphere* **2012**, *88*, 670-675.

(57) Rai, M., A. Yadav, and A. Gade: Silver nanoparticles as a new generation of antimicrobials. *Biotechnol Adv* **2009**, *27*, 76-83.

(58) Scholars, W. W. I. C. f.: Consumer Products Inventory. In *The Project on Emerging Nanotechnologies*, 2014.

(59) LaLonde, A. D. G. N., M.; Zhang, D.; Ganadean, D.; Alkhateeb, A.; Padmanabhan, R.; McIlroy, D. N.: *J. Mater. Res.* **2005**, *20*, 3021–7.

(60) Ni, C.; Hassan, P. A.; Kaler, E. W.: Structural Characteristics and Growth of Pentagonal Silver Nanorods Prepared by a Surfactant Method. *Langmuir* **2005**, *21*, 3334-3337.

(61) Zhang, S.-H.; Jiang, Z.-Y.; Xie, Z.-X.; Xu, X.; Huang, R.-B.; Zheng, L.-S.: Growth of Silver Nanowires from Solutions: A Cyclic Penta-twinned-Crystal Growth Mechanism. *The Journal of Physical Chemistry B* **2005**, *109*, 9416-9421.

(62) Scarberry, K. E. D., E. B.; McDonald, J. F.; Zhang, Z. J.: Magnetic Nanoparticle−Peptide Conjugates for in Vitro and in Vivo Targeting and Extraction of Cancer Cells. *Journal of the American Chemical Society* **2008**, *130*, 10258–10262.

(63) Park, H. Y., J.; Seo, S.; Kim, K.; Suh, J.; Kim, D.; Haam, S.;; Kyung-Hwa, Y.: Multifunctional Nanoparticles for Photothermally Controlled Drug Delivery and Magnetic Resonance Imaging Enhancement. *Small* **2008**, *4*, 192–196.

(64) Bhattacharya, R. P., C. R.; Earl, A.; Wang, S.; Katarya, A.; Lu, L.; Kizhakkedathu, J. N.; Yaszemski, M. J.; Greipp, P. R.;Mukhopadhyay, D.; Mukherjee, P.: Attaching folic acid on gold nanoparticles using noncovalent interaction via different polyethylene glycol backbones and targeting of cancer cells. *Nanomedicine: Nanotechnology, Biology and Medicine* **2007**, *3*, 224–238.

(65) Wuelfing, W. P.; Gross, S. M.; Miles, D. T.; Murray, R. W.: Nanometer Gold Clusters Protected by Surface-Bound Monolayers of Thiolated Poly(ethylene glycol) Polymer Electrolyte. *Journal of the American Chemical Society* **1998**, *120*, 12696-12697.

(66) Lowe, A. B.; Sumerlin, B. S.; Donovan, M. S.; McCormick, C. L.: Facile Preparation of Transition Metal Nanoparticles Stabilized by Well-Defined (Co)polymers Synthesized via Aqueous Reversible Addition-Fragmentation Chain Transfer Polymerization†. *Journal of the American Chemical Society* **2002**, *124*, 11562-11563.

(67) Mandal, T. K.; Fleming, M. S.; Walt, D. R.: Preparation of Polymer Coated Gold Nanoparticles by Surface-Confined Living Radical Polymerization at Ambient Temperature. *Nano Letters* **2002**, *2*, 3-7.

(68) Levard, C.; Hotze, E. M.; Lowry, G. V.; Brown, G. E.: Environmental Transformations of Silver Nanoparticles: Impact on Stability and Toxicity. *Environmental Science & Technology* **2012**, *46*, 6900-6914.

(69) Yong, K. T., Swihart, M. T., Ding, H. and Prasad, P. N.: Preparation of Gold Nanoparticles and their Applications in Anisotropic Nanoparticle Synthesis and Bioimaging. *Plasmonics* **2009**, *4*, 79-93.

(70) Krishnendu Saha, S. S. A., Chaekyu Kim, Xiaoning Li, and Vincent M. Rotello: Gold Nanoparticles in Chemical and Biological Sensing. *Chemical Reviews* **2012**, *112*, 2739−2779.

(71) Shang, J.; Liu, C.; Wang, Z.; Wu, H.; Zhu, K.; Li, J.; Liu, J.: In-Situ Measurements of Engineered Nanoporous Particle Transport in Saturated Porous Media. *Environmental Science & Technology* **2010**, *44*, 8190-8195.

(72) Takara, M.; Toyoshima, M.; Seto, H.; Hoshino, Y.; Miura, Y.: Polymer-modified gold nanoparticles via RAFT polymerization: a detailed study for a biosensing application. *Polymer Chemistry* **2014**, *5*, 931-939.

(73) Verwey, E. J. W. a. O., J. Th. G.: *Theory of the stability of lyophobic colloids*; Elsevier Publishing Company., 1947.

(74) Hunter, R. J.: *Foundations of Colloidal Science*; Clarendon Press: Oxford, UK, 1992.

(75) Verwey, E. J. W. a. O., J. Th. G.: *Theory of the Stability of Lyophobic Colloids*; Dover: Mineola, NY, 2000.

(76) Deryaguin, B. V. L., L. D.: *Acta Physicochem* **1941**, *14*, 633-652.

(77) Kim, T.; Lee, K.; Gong, M.-s.; Joo, S.-W.: Control of Gold Nanoparticle Aggregates by Manipulation of Interparticle Interaction. *Langmuir* **2005**, *21*, 9524-9528.

(78) Viudez, A. J.; Madueño, R.; Pineda, T.; Blázquez, M.: Stabilization of Gold Nanoparticles by 6-Mercaptopurine Monolayers. Effects of the Solvent Properties. *The Journal of Physical Chemistry B* **2006**, *110*, 17840-17847.

(79) Kitchens, C. L.; McLeod, M. C.; Roberts, C. B.: Solvent Effects on the Growth and Steric Stabilization of Copper Metallic Nanoparticles in AOT Reverse Micelle Systems. *The Journal of Physical Chemistry B* **2003**, *107*, 11331-11338.

(80) Gittins, D. I.; Caruso, F.: Tailoring the Polyelectrolyte Coating of Metal Nanoparticles. *The Journal of Physical Chemistry B* **2001**, *105*, 6846-6852.

(81) Woehrle, G. H.; Brown, L. O.; Hutchison, J. E.: Thiol-Functionalized, 1.5-nm Gold Nanoparticles through Ligand Exchange Reactions: Scope and Mechanism of Ligand Exchange. *Journal of the American Chemical Society* **2005**, *127*, 2172-2183.

(82) Korgel, B. A.; Fullam, S.; Connolly, S.; Fitzmaurice, D.: Assembly and Self-Organization of Silver Nanocrystal Superlattices: Ordered "Soft Spheres". *The Journal of Physical Chemistry B* **1998**, *102*, 8379-8388.

(83) de Gennes, P. G.: Polymers at an interface; a simplified view. *Advances in Colloid and Interface Science* **1987**, *27*, 189-209.

(84) Barrera, C.; Herrera, A. P.; Bezares, N.; Fachini, E.; Olayo-Valles, R.; Hinestroza, J. P.; Rinaldi, C.: Effect of poly(ethylene oxide)-silane graft molecular weight on the colloidal properties of iron oxide nanoparticles for biomedical applications. *J Colloid Interface Sci* **2012**, *377*, 40-50.

(85) Johnson, S. R.; Evans, S. D.; Brydson, R.: Influence of a Terminal Functionality on the Physical Properties of Surfactant-Stabilized Gold Nanoparticles. *Langmuir* **1998**, *14*, 6639-6647.

(86) Israelachvili, J.: *Intermolecular and surface forces1991*; Academic Press: London, 1991.

(87) Brewer, S. H. G., W. R.; Johnson, M. C.; Knag, M. K.; Franzen, S.;: Probing BSA binding to Citrate-Coated Gold Nanoparticles and Surfaces. *Langmuir* **2005**, *21*, 9303-9307.

(88) Nelson, E. M. R., L. J.; : Kinetics and Mechanism of Single-Stranded DNA Adsorption onto Citrate-Stabilized Gold Nanoparticles in Colliodal Solution. *Langmuir* **2011**, *27*, 1770-1777.

(89) Bartz, M.; Kuther, J.; Nelles, G.; Weber, N.; Seshadri, R.; Tremel, W.: Monothiols derived from glycols as agents for stabilizing gold colloids in water: synthesis, self-assembly and use as crystallization templates. *Journal of Materials Chemistry* **1999**, *9*, 1121-1125.

(90) Foos, E. E.; Snow, A. W.; Twigg, M. E.; Ancona, M. G.: Thiol-Terminated Di-, Tri-, and Tetraethylene Oxide Functionalized Gold Nanoparticles: A Water-Soluble, Charge-Neutral Cluster. *Chemistry of Materials* **2002**, *14*, 2401-2408.

(91) Kanaras, A. G.; Kamounah, F. S.; Schaumburg, K.; Kiely, C. J.; Brust, M.: Thioalkylated tetraethylene glycol: a new ligand for water soluble monolayer protected gold clusters. *Chemical Communications* **2002**, 2294-2295.

(92) Pengo, P.; Polizzi, S.; Battagliarin, M.; Pasquato, L.; Scrimin, P.: Synthesis, characterization and properties of water-soluble gold nanoparticles with tunable core size. *Journal of Materials Chemistry* **2003**, *13*, 2471-2478.

(93) Mansoori, G. A.; Brandenburg, K. S.; Shakeri-Zadeh, A.: A Comparative Study of Two Folate-Conjugated Gold Nanoparticles for Cancer Nanotechnology Applications. *Cancers* **2010**, *2*, 1911-1928.

(94) Garcia-Bennett, A.; Nees, M.; Fadeel, B.: In search of the Holy Grail: Folate-targeted nanoparticles for cancer therapy. *Biochemical Pharmacology* **2011**, *81*, 976-984.

(95) Zwicke, G. L.; Mansoori, G. A.; Jeffery, C. J.: Utilizing the folate receptor for active targeting of cancer nanotherapeutics. *Nano Reviews* **2012**, *3*.

(96) Eshghi, H.: Folate-conjugated gold nanoparticles. عملرز از والا هدایت فولاند اور ی و *International Journal of NanoScience and Nanotechnology* **2009**, *5*.

(97) Sonvico, F.; Mornet, S.; Vasseur, S.; Dubernet, C.; Jaillard, D.; Degrouard, J.; Hoebeke, J.; Duguet, E.; Colombo, P.; Couvreur, P.: Folate-conjugated iron oxide nanoparticles for solid tumor targeting as potential specific magnetic hyperthermia mediators: synthesis, physicochemical characterization, and in vitro experiments. *Bioconjugate Chemistry* **2005**, *16*, 1181-1188.

(98) Han, G.; Ghosh, P.; Rotello, V. M.: Functionalized gold nanoparticles for drug delivery. *Nanomedicine* **2007**, *2*, 113-123.

(99) Han, G.; Ghosh, P.; De, M.; Rotello, V. M.: Drug and gene delivery using gold nanoparticles. *NanoBiotechnology* **2007**, *3*, 40-45.

(100) Paciotti, G. F.; Kingston, D. G. I.; Tamarkin, L.: Colloidal gold nanoparticles: a novel nanoparticle platform for developing multifunctional tumor-targeted drug delivery vectors. *Drug development research* **2006**, *67*, 47-54.

(101) Binder, W. H.; Weinstabl, H.; Sachsenhofer, R.: Superparamagnetic Ironoxide Nanoparticles via Ligand Exchange Reactions: Organic 1,2-Diols as Versatile Building Blocks for Surface Engineering. *Journal of Nanomaterials* **2008**, *2008*, 1-10.

(102) Khoee, S.; Hemati, K.: Synthesis of magnetite/polyamino-ester dendrimer based on PCL/PEG amphiphilic copolymers via convergent approach for targeted diagnosis and therapy. *Polymer* **2013**, *54*, 5574-5585.

(103) Hongchen Dong, M. Z., Jeong Ae Yoon, Haifeng Gao, Rongchao Jin, and Krzysztof Matyjaszewski: One-Pot Synthesis of Robust Core/Shell Gold Nanoparticles. *Jounral of the American Chemical Society* **2008**, *130*, 12852–12853.

(104) Wang, X. R., O.; Yan, M.;: Quantitative Analysis of Multivalent Ligand Presentation on Gold Glyconanoparticles and the Impact on Lectin Binding. *Analytical Chemistry* **2010**, *82*, 9082-9089.

(105) Wang, Y. Z., O.; Gitis, V.; Neyman, A.; Weinstock, I. A.;: Reversible binding of an inorganic cluster-anion to the surface of a gold nanoparticle. *Inorganic Chimicia Acta* **2010**, *363*, 4416-4420.

(106) Kumar, A. J., H.; Pasicha, R.; Mandale, A. B.; Sastry, M.; : Phase transfer of silver nanoparticles from aqueous to organic solutions using fatty amine molecules. *J Colloid Interface Sci* **2003**, *264*, 396-401.

(107) Montalti, M. P., L.; Zaccheroni, N.; Baxter, R.; Teobaldi, G.; Zerbetto, : Kinetics of Place Exchange Reactions of Thiols on Gold Nanoparticles. *Langmuir* **2003**, *19*, 5172.

(108) Marutani, E.; Yamamoto, S.; Ninjbadgar, T.; Tsujii, Y.; Fukuda, T.; Takano, M.: Surface-initiated atom transfer radical polymerization of methyl methacrylate on magnetite nanoparticles. *Polymer* **2004**, *45*, 2231-2235.

(109) Zhou, Y.; Wang, S.; Ding, B.; Yang, Z.: Modification of magnetite nanoparticles via surface-initiated atom transfer radical polymerization (ATRP). *Chemical Engineering Journal* **2008**, *138*, 578-585.

(110) Galeotti, F.; Bertini, F.; Scavia, G.; Bolognesi, A.: A controlled approach to iron oxide nanoparticles functionalization for magnetic polymer brushes. *J Colloid Interface Sci* **2011**, *360*, 540-7.

(111) Janne Raula, J. S., Markus Nuopponen, Antti Niskanen, Hua Jiang, Esko I. Kauppinen, and Heikki Tenhu: Synthesis of Gold Nanoparticles Grafted with a Thermoresponsive Polymer by Surface-Induced Reversible-Addition-Fragmentation Chain-Transfer Polymerization. *Langmuir* **2003**, *19*, 3499-3504.

(112) Jennifer L. Brennan, N. S. H., T. Robert Tshikhudo, Nijole Dirvianskyte,§ Valdemaras Razumas, Shamkant Patkar, Jesper Vind, Allan Svendsen, Roeland J. M. Nolte, Alan E. Rowan, and Mathias Brust: Bionanoconjugation via Click Chemistry: The Creation of Functional Hybrids of Lipases and Gold Nanoparticles. *Bioconjugate Chemistry* **2006**, *17*, 1373-1375.

(113) Kanaras, D. B. a. A. G.: Preparation of Peptide-Functionalized Gold Nanoparticles Using One Pot EDC/Sulfo-NHS Coupling. *Langmuir* **2011**, *27*, 10119–10123.

(114) Ahn, J.; Moon, D. S.; Lee, J. K.: Arsonic Acid As a Robust Anchor Group for the Surface Modification of FeO. *Langmuir : the ACS journal of surfaces and colloids* **2013**.

(115) A. Ivanisevic, K. V. M. a. C. A. M.: Site-Directed Exchange Studies with Combinatorial Libraries of Nanostructues. *Journal of the American Chemical Society* **2002**, *124*, 11997.

(116) Bartczak, D.; Kanaras, A. G.: Preparation of Peptide-Functionalized Gold Nanoparticles Using One Pot EDC/Sulfo-NHS Coupling. *Langmuir* **2011**, *27*, 10119-10123.

(117) Mayya, K. S.; Schoeler, B.; Caruso, F.: Preparation and Organization of Nanoscale Polyelectrolyte-Coated Gold Nanoparticles. *Advanced Functional Materials* **2003**, *13*, 183-188.

(118) Rucareanu, S.; Gandubert, V. J.; Lennox, R. B.: 4-(N,N-Dimethylamino)pyridine-Protected Au Nanoparticles: Versatile Precursors for Water- and Organic-Soluble Gold Nanoparticles. *Chemistry of Materials* **2006**, *18*, 4674-4680.

(119) Goulet, P. J. G.; Bourret, G. R.; Lennox, R. B.: Facile Phase Transfer of Large, Water-Soluble Metal Nanoparticles to Nonpolar Solvents. *Langmuir* **2012**, *28*, 2909-2913.

(120) Hostetler, M. J. G., S. J. Stokes, J. J.; Murray, R. W.: *Journal of the American Chemical Society* **1996**, *118*, 4212.

(121) Sastry, M.: Phase Transfer Protocals in Nanoparticle Synthesis. *Current Science* **2003**, *85*, 1735-1745.

(122) Jim Yang Lee, J. Y. Y.: Phase transfer and its applications in nanotechnology. *Chemical Society Reviews* **2011**, *40*, 1672-1696.

(123) J. Turkevich, P. C. S., J. Hillier: A study of the nucleation and growth processes in the synthesis of colloidal gold. *Discussions of the Faraday Society* **1951**, *11*, 55-75.

(124) Frens, G.: Controlled nucleation for the regulation of the particle size in monodisperse gold suspensions. . *Nature Phys Sci* **1973**, *241*, 20-22.

(125) Li, L.; Mak, K. Y.; Leung, C. W.; Chan, K. Y.; Chan, W. K.; Zhong, W.; Pong, P. W. T.: Effect of synthesis conditions on the properties of citric-acid coated iron oxide nanoparticles. *Microelectronic Engineering* **2013**, *110*, 329-334.

(126) Brust, M., Walker, M., Bethell, D., Schiffrin, D. J., Whyman, R.: *Chemical Communications* **1994**, 801.

(127) Zhang, S. L., G.; Srisombat, L.; Lee, T. R.;: Rationally Designed Ligands that Inhibit the Aggregation of Large Gold Nanoparticles in Solution. *The Journal of the American Chemical Society* **2008**, *130*, 113-120.

(128) Schulzendorf, M.; Cavelius, C.; Born, P.; Murray, E.; Kraus, T.: Biphasic Synthesis of Au@SiO2 Core−Shell Particles with Stepwise Ligand Exchange. *Langmuir* **2010**, *27*, 727-732.

(129) Frimpong, R. A.; Hilt, J. Z.: Poly(n-isopropylacrylamide)-based hydrogel coatings on magnetite nanoparticles via atom transfer radical polymerization. *Nanotechnology* **2008**, *19*, 175101.

(130) White, G. V., Mohammed, F. S., Kitchens, C. L.: Small-Angle Neutron Scattering Investigation of Gold Nanoparticle Clustering and Ligand Structure Under Antisolvent Conditions. *The Journal of Physical Chemistry C* **2011**, *115*, 18397-18405.

(131) Gomez, S.; Philippot, K.; Colliere, V.; Chaudret, B.; Senocq, F.; Lecante, P.: Gold nanoparticles from self-assembled gold() amine precursors. *Chemical Communications* **2000**, 1945-1946.

(132) Gittins, D. I.; Caruso, F.: Spontaneous Phase Transfer of Nanoparticulate Metals from Organic to Aqueous Media. *Angewandte Chemie International Edition* **2001**, *40*, 3001-3004.

(133) Gerion, D.; Pinaud, F.; Williams, S. C.; Parak, W. J.; Zanchet, D.; Weiss, S.; Alivisatos, A. P.: Synthesis and Properties of Biocompatible Water-Soluble Silica-Coated CdSe/ZnS Semiconductor Quantum Dots†. *The Journal of Physical Chemistry B* **2001**, *105*, 8861-8871.

(134) Michalet, X.; Pinaud, F. F.; Bentolila, L. A.; Tsay, J. M.; Doose, S.; Li, J. J.; Sundaresan, G.; Wu, A. M.; Gambhir, S. S.; Weiss, S.: Quantum Dots for Live Cells, in Vivo Imaging, and Diagnostics. *Science* **2005**, *307*, 538-544.

(135) Chan, W. C. W.; Nie, S.: Quantum Dot Bioconjugates for Ultrasensitive Nonisotopic Detection. *Science* **1998**, *281*, 2016-2018.

(136) Schmid, G.; Klein, N.; Korste, L.; Kreibig, U.; Schönauer, D.: Large transition metal clusters—VI. Ligand exchange reactions on Au55(PPh3)12Cl6—the formation of a water soluble Au55 cluster. *Polyhedron* **1988**, *7*, 605-608.

(137) Joseph Simard, C. B., Andrew K. Boal and Vincent M. Rotello: Formation and pH-controlled assembly of amphiphilic gold nanoparticles. *Chemical Communications* **2000**, 1943-1944.

(138) Catherine M. McIntosh, E. A. E., III, Andrew K. Boal, Joseph M. Simard, Craig T. Martin, and Vincent M. Rotello: Inhibition of DNA Transcription Using Cationic Mixed Monolayer Protected Gold Clusters. *Journal of the American Chemical Society* **2001**, *123*, 7626-7629.

(139) Liu, Y.; Shipton, M. K.; Ryan, J.; Kaufman, E. D.; Franzen, S.; Feldheim, D. L.: Synthesis, Stability, and Cellular Internalization of Gold Nanoparticles Containing Mixed Peptide−Poly(ethylene glycol) Monolayers. *Analytical Chemistry* **2007**, *79*, 2221-2229.

(140) Yan, B.; Jeong, Y.; Mercante, L. A.; Tonga, G. Y.; Kim, C.; Zhu, Z. J.; Vachet, R. W.; Rotello, V. M.: Characterization of surface ligands on functionalized magnetic nanoparticles using laser desorption/ionization mass spectrometry (LDI-MS). *Nanoscale* **2013**, *5*, 5063-6.

(141) Zamborini, F. P. L., M. C.; Hicks, J. F.; Kulesza, P. J.; Malik, M. A.; Murray, R. W.: *Journal of the American Chemical Society* **2002**, *124*, 8958-8964.

(142) Hostetler, M. J.; Templeton, A. C.; Murray, R. W.: Dynamics of Place-Exchange Reactions on Monolayer-Protected Gold Cluster Molecules. *Langmuir* **1999**, *15*, 3782-3789.

(143) Templeton, A. C.; Hostetler, M. J.; Warmoth, E. K.; Chen, S.; Hartshorn, C. M.; Krishnamurthy, V. M.; Forbes, M. D. E.; Murray, R. W.: Gateway Reactions to Diverse, Polyfunctional Monolayer-Protected Gold Clusters. *Journal of the American Chemical Society* **1998**, *120*, 4845-4849.

(144) Templeton, A. C.; Cliffel, D. E.; Murray, R. W.: Redox and Fluorophore Functionalization of Water-Soluble, Tiopronin-Protected Gold Clusters. *Journal of the American Chemical Society* **1999**, *121*, 7081-7089.

(145) Sandhu, K. K., McIntosh, Catherine M., Simard, Joseph M., Smith, Sallie W., Rotello, Vincent M.: Gold Nanoparticle-Mediated Transfection of Mammalian Cells. *Bioconjugate Chemistry* **2001**, *13*, 3-6.

(146) Sandhu, K. K. M., C. M.; Simard, J. M.; Smith, S. W.; Rotello, V.: *Bioconjugate Chemistry* **2002**, *13*, 3-6.

(147) Wang, G. Z., J.; Murray, R. W.: *Analytical Chemistry* **2002**, *74*, 4320-4327.

(148) Morris, M. C.; Chaloin, L.; Heitz, F.; Divita, G.: Translocating peptides and proteins and their use for gene delivery. *Current Opinion in Biotechnology* **2000**, *11*, 461-466.

(149) Hicks, J. F. S.-S., Y.; Murray, R. W.: *Langmuir* **2002**, *18*, 2288-2294.

(150) Kell, K. J. D., R. L.; Workentin, M. S.;: Core Size Effects on the Reactivity of Organic Substrates as Monolayers on Gold Nanoparticles. *Langmuir* **2004**, *21*, 735-752.

(151) Bonnemann, H. B., G. A.: *Angewandte Chemie International Edition* **1996**, *35*, 1992-1995.

(152) Bieri, M. G., C.; Burgi, T.: *Chem. Phys. Phys. Chem.* **2007**, *9*, 671-685.

(153) Dressler, D. H. M., Y.: *Journal of Colloidal and Interface Science* **2007**, *310*.

(154) Hao Qi, T. H.: Formation of periodic stripe patterns in nematic liquid crystals doped with functionalized gold nanoparticlesElectronic supplementary information (ESI) available: Synthesis and spectroscopic details for thiol 3b, additional UV-vis, CD, XRD, and TEM data for Au1–Au4. *Journal of Materials Chemistry* **2006**, *16*, 4197-4205.

(155) M. J. Hostetler, A. C. T. a. R. W. M.: *Langmuir* **1999**, *15*, 3782.

(156) Ionita, P. C., A.; : EPR Study of Place-Exchange Reaction on Au Nanoparticles: Two Branches of a Disulfide Molecule Do Not Adsorb Adjacent to Each Other. *The Journal of the American Chemical Society* **2002**, *124*, 9048-9049.

(157) Donkers, R. L., Song, Yang, Murray, Royce W.: Substituent Effects on the Exchange Dynamics of Ligands on 1.6 nm Diameter Gold Nanoparticles. *Langmuir* **2004**, *20*, 4703-4707.

(158) Templeton, A. C. H., M. J.; Kraft, C. T.; Murray, R. W.;: Reactivity of Monolayer-Protected Gold Cluster Molecules: Steric Effects. *The Journal of the American Chemical Society* **1998**, *120*, 1906-1911.

(159) M. Hasan, D. B. a. M. B.: *Journal of the American Chemical Society* **2002**, *124*, 1132.

(160) G. G. Baralia, A.-S. D., B. Nysten and A. M. Jonas: *Langmuir* **2005**, *21*, 6825.

(161) N. Nishidal, M. H., H. Sasabe and W. Knoll: *Japan Jounral of Applied Physics* **1996**, *35*, 5866.

(162) R. Paulini, B. L. F. a. V. M. R.: *Langmuir* **2002**, *18*, 2368.

(163) Guo, R. S., Y.; Wang, G.; Murray, R. W.;: Does Core Size Matter in the Kinetics of Ligand Exchanges of Monolayer-Protected Au Clusters? *The Journal of the American Chemical Society* **2005**, *128*, 2752-2757.

(164) Joshi, P. C., S.; Dey, S.; Shanker, V.; Ansari, Z. A.; Singh, S. P.; Chakrabarti, P.;: Binding of chloroquine-conjugated gold nanoparticles with bovine serum albumin. *J Colloid Interface Sci* **2011**, *355*, 402-409.

(165) Perumal, S. H., A.; Scholz, N.; Ruhl, E.; Graf, C.;: Kinetics Study of the Binding of Multivalent Ligands on Size-Selected Gold Nanoparticles. *Langmuir* **2011**, *27*, 4456-4464.

(166) Chechik, V.: Reduced Reactivity of Aged Au Nanoparticles in Ligand Exchange Reactions. *The Journal of the American Chemical Society* **2004**, *126*, 7780-7781.

(167) Woerhrle, G. H. W., M. G.; Hutchison, J. E.;: Ligand Exchange Reactions Yield Sudnanometer, Thiol-Stabilized Gold Particles with Defined Optical Transitions. *Journal of Physical Chemistry* **2002**, *106*, 9979-9981.

(168) Reyes, E. n.; Madueño, R.; Blázquez, M.; Pineda, T.: Facile Exchange of Ligands on the 6-Mercaptopurine-Monolayer Protected Gold Clusters Surface†. *The Journal of Physical Chemistry C* **2010**, *114*, 15955-15962.

(169) Sharma, R.; Holland, G. P.; Solomon, V. C.; Zimmermann, H.; Schiffenhaus, S.; Amin, S. A.; Buttry, D. A.; Yarger, J. L.: NMR Characterization of Ligand Binding and Exchange Dynamics in Triphenylphosphine-Capped Gold Nanoparticles. *The Journal of Physical Chemistry C* **2009**, *113*, 16387-16393.

(170) Miles, D. T. M., R. W.: *Analytical Chemistry* **2001**, *73*, 921-929.

(171) Ingram, R. S. H., M. J.; Murray, R. W.; : Poly-hetero-w-Functionalized Alkanethiolate-Stabilized Gold Cluster Compounds. *The Journal of the American Chemical Society* **1997**, *119*, 9175-9178.

(172) Wang, G.; Zhang, J.; Murray, R. W.: DNA Binding of an Ethidium Intercalator Attached to a Monolayer-Protected Gold Cluster. *Analytical Chemistry* **2002**, *74*, 4320-4327.

(173) Hicks, J. F.; Seok-Shon, Y.; Murray, R. W.: Layer-by-Layer Growth of Polymer/Nanoparticle Films Containing Monolayer-Protected Gold Clusters. *Langmuir* **2002**, *18*, 2288-2294.

(174) Song, Y.; Murray, R. W.: Dynamics and Extent of Ligand Exchange Depend on Electronic Charge of Metal Nanoparticles. *Journal of the American Chemical Society* **2002**, *124*, 7096-7102.

(175) Wojczykowski, K. M., D.; Jutzi, P.; Ennen, I.; Hutten, A.; Fricke, M.; Volkmer, D.;: Reliable stabilization and functionalization of nanoparticles through tridentate thilate ligands. *Chemcial Communications* **2006**, 3693-3695.

(176) Ansar, S. M. H., R.; Edmonds, B.; Liu, D.; Yu, L.; Sygula, A.; Zhang, D.;: Determination of the Binding Affinity, Packing, and Conformation of Thiolate and Thione Ligands on Gold Nanoparticles. *Journal of physical Chemistry C* **2011**, *115*, 653-660.

(177) Feng, Y. X., S.; Xu, J.; Wang, H.; Lim, J. W.; Chen, H.;: Probing the kinetics of ligand exchanges on colloidal gold nanoparticles by surface-enhanced Raman scattering. *Dalton Transactions* **2010**, *39*, 349-351.

(178) Joshi, H. S., P. S.; Bansal, V.; Ganesh, K. N., Sastry, M.; : Isothermal Titration Studies on the Binding of Amino Acids to Gold Nanoparticles. *Journal of Physical Chemistry B* **2004**, *108*, 11535-11540.

(179) Ohno, K.; Koh, K.-m.; Tsujii, Y.; Fukuda, T.: Synthesis of Gold Nanoparticles Coated with Well-Defined, High-Density Polymer Brushes by Surface-Initiated Living Radical Polymerization. *Macromolecules* **2002**, *35*, 8989-8993.

(180) D'Unger, D. W.: MEASURING LIGAND EXCHANGE ON THE SURFACE OF GOLD NANOPARTICLES: A STUDY OF COMPETITIVE BINDING OF LIGANDS UTILIZING FLUORESCENT RESONANCE ENERGY TRANSFER. *Masters Thesis* **2012**.

(181) Clegg, R. M.: Fluorescence resonance energy transfer. *Current Opinion in Biotechnology* **1995**, *6*, 103-110.

(182) Wu, P. G.; Brand, L.: Resonance Energy Transfer: Methods and Applications. *Analytical Biochemistry* **1994**, *218*, 1-13.

(183) Sarit S. Agasti, C.-C. Y., Palaniappan Arumugam, Vincent M. Rotello Structural control of the monolayer stability of water-soluble gold nanoparticlesElectronic supplementary information (ESI) available: Synthesis and characterization of the ligands, the preparation of nanoparticles, and experimental procedures. *Journal of Materials Chemistry* **2007**, *18*, 70-73.

(184) Jain, P. K.; Lee, K. S.; El-Sayed, I. H.; El-Sayed, M. A.: Calculated Absorption and Scattering Properties of Gold Nanoparticles of Different Size, Shape, and Composition: Applications in Biological Imaging and Biomedicine. *The Journal of Physical Chemistry B* **2006**, *110*, 7238-7248.

(185) Haiss, W.; Thanh, N. T. K.; Aveyard, J.; Fernig, D. G.: Determination of Size and Concentration of Gold Nanoparticles from UV−Vis Spectra. *Analytical Chemistry* **2007**, *79*, 4215-4221.

(186) Lee, K.-S. a. M. A. E.-S.: Gold and Silver Nanoparticles in Sensing and Imaging:‚Äâ Sensitivity of Plasmon Response to Size, Shape, and Metal Composition. *Journal of Physical Chemistry B* **2006**, *110*, 19220-19225.

(187) Ghosh, S. K.; Nath, S.; Kundu, S.; Esumi, K.; Pal, T.: Solvent and Ligand Effects on the Localized Surface Plasmon Resonance (LSPR) of Gold Colloids. *The Journal of Physical Chemistry B* **2004**, *108*, 13963-13971.

(188) McFarland, A. D.; Van Duyne, R. P.: Single Silver Nanoparticles as Real-Time Optical Sensors with Zeptomole Sensitivity. *Nano Letters* **2003**, *3*, 1057-1062.

(189) Adegboyega, N. F.; Sharma, V. K.; Siskova, K.; Zbořil, R.; Sohn, M.; Schultz, B. J.; Banerjee, S.: Interactions of Aqueous Ag+ with Fulvic Acids: Mechanisms of Silver Nanoparticle Formation and Investigation of Stability. *Environmental Science & Technology* **2012**.

(190) Lala, N., Lalbegi, Sachin P., Adyanthaya, S. D. Sastry, Murali: Phase Transfer of Aqueous Gold Colloidal Particles Capped with Inclusion Complexes of Cyclodextrin and Alkanethiol Molecules into Chloroform. *Langmuir* **2001**, *17*, 3766-3768.

(191) Ruiz, A.; Salas, G.; Calero, M.; Hernandez, Y.; Villanueva, A.; Herranz, F.; Veintemillas-Verdaguer, S.; Martinez, E.; Barber, D. F.; Morales, M. P.: Short-chain PEG molecules strongly bound to magnetic nanoparticle for MRI long circulating agents. *Acta Biomater* **2013**, *9*, 6421-30.

(192) Gonzales, M.; Krishnan, K. M.: Phase transfer of highly monodisperse iron oxide nanocrystals with Pluronic F127 for biomedical applications. *Journal of Magnetism and Magnetic Materials* **2007**, *311*, 59-62.

(193) He, X.; Wu, X.; Cai, X.; Lin, S.; Xie, M.; Zhu, X.; Yan, D.: Functionalization of magnetic nanoparticles with dendritic-linear-brush-like triblock copolymers and their drug release properties. *Langmuir : the ACS journal of surfaces and colloids* **2012**, *28*, 11929-38.

(194) Song, Y. H., T.; Murray, R. W.: Heterophase Ligand Exchange and Metal Transfer between Monolayer Protected Clusters. *The Journal of the American Chemical Society* **2003**, *124*, 11694-11701.

(195) Zachary, M.; Chechik, V.: Hopping of Thiolate Ligands between Au Nanoparticles Revealed by EPR Spectroscopy. *Angewandte Chemie International Edition* **2007**, *46*, 3304-3307.

(196) Matthew J. Banholzer, J. E. M., Lidong Qin, Chad A. Mirkin: Rationally designed nanostructures for surface-enhanced Raman spectroscopy. *Chemical Society Reviews* **2008**, *37*, 885-897.

(197) X.-M. Qian, S. M. N.: Single-molecule and single-nanoparticle SERS: from fundamental mechanisms to biomedical applications. *Chemical Society Reviews* **2008**, *37*, 912-920.

(198) Camden, J. P.; Dieringer, J. A.; Zhao, J.; Van Duyne, R. P.: Controlled Plasmonic Nanostructures for Surface-Enhanced Spectroscopy and Sensing. *Accounts of Chemical Research* **2008**, *41*, 1653-1661.

(199) Emory, S. N. a. S. R.: Probing Single Molecules and Single Nanoparticles by SERS. *Science* **1997**, *275*.

(200) Dieringer, J. A.; Wustholz, K. L.; Masiello, D. J.; Camden, J. P.; Kleinman, S. L.; Schatz, G. C.; Van Duyne, R. P.: Surface-Enhanced Raman Excitation Spectroscopy of a Single Rhodamine 6G Molecule. *Journal of the American Chemical Society* **2008**, *131*, 849-854.

(201) Xu, H.: Theoretical study of coated spherical metallic nanoparticles for single-molecule surface-enhanced spectroscopy. *Applied Physics Letters* **2004**, *85*, 5980-5982.

(202) Camden, J. P.; Dieringer, J. A.; Wang, Y.; Masiello, D. J.; Marks, L. D.; Schatz, G. C.; Van Duyne, R. P.: Probing the Structure of Single-Molecule Surface-Enhanced Raman Scattering Hot Spots. *Journal of the American Chemical Society* **2008**, *130*, 12616-12617.

(203) Weisbecker, C. S. M., M. V.; Whitesides, G. M.;: Molecular Self-Assembly of Aliphatic Thiols on Gold Colloids. *Langmuir* **1996**, *12*, 3763-3772.

(204) Lu, H. B.; Campbell, C. T.; Castner, D. G.: Attachment of Functionalized Poly(ethylene glycol) Films to Gold Surfaces. *Langmuir* **2000**, *16*, 1711-1718.

(205) Huang, T. M., R. W.: *Langmuir* **2002**, *18*, 7077-7081.

(206) Brown, L. O.; Hutchison, J. E.: Convenient Preparation of Stable, Narrow-Dispersity, Gold Nanocrystals by Ligand Exchange Reactions. *Journal of the American Chemical Society* **1997**, *119*, 12384-12385.

(207) Nuzzo, R. G.; Zegarski, B. R.; Dubois, L. H.: Fundamental studies of the chemisorption of organosulfur compounds on gold(111). Implications for molecular self-assembly on gold surfaces. *Journal of the American Chemical Society* **1987**, *109*, 733-740.

(208) Bain, C. D.; Biebuyck, H. A.; Whitesides, G. M.: Comparison of self-assembled monolayers on gold: coadsorption of thiols and disulfides. *Langmuir* **1989**, *5*, 723-727.

(209) Kumar, A., Mandal, Saikat, Pasricha, Renu, Mandale, A. B., Sastry, Murali: Investigation into the Interaction between Surface-Bound Alkylamines and Gold Nanoparticles. *Langmuir* **2003**, *19*, 6277-6282.

(210) Thompson, G.; Owen, D.; Chalk, P. A.; Lowe, P. N.: Delineation of the Cdc42/Rac-Binding Domain of p21-Activated Kinase. *Biochemistry* **1998**, *37*, 7885-7891.

(211) Künne, A. G. E.; Sieber, M.; Meierhans, D.; Allemann, R. K.: Thermodynamics of the DNA Binding Reaction of Transcription Factor MASH-1†. *Biochemistry* **1998**, *37*, 4217-4223.

(212) Wenk, M. R.; Seelig, J.: Magainin 2 Amide Interaction with Lipid Membranes: Calorimetric Detection of Peptide Binding and Pore Formation†. *Biochemistry* **1998**, *37*, 3909-3916.

(213) Bouchemal, K.: New challenges for pharmaceutical formulations and drug delivery systems characterization using isothermal titration calorimetry. *Drug Discovery Today* **2008**, *13*, 960-972.

(214) Gourishankar, A.; Shukla, S.; Ganesh, K. N.; Sastry, M.: Isothermal Titration Calorimetry Studies on the Binding of DNA Bases and PNA Base Monomers to Gold Nanoparticles. *Journal of the American Chemical Society* **2004**, *126*, 13186-13187.

(215) Phares, N.; White, R. J.; Plaxco, K. W.: Improving the Stability and Sensing of Electrochemical Biosensors by Employing Trithiol-Anchoring Groups in a Six-Carbon Self-Assembled Monolayer. *Analytical Chemistry* **2009**, *81*, 1095-1100.

(216) Li, Z.; Jin, R.; Mirkin, C. A.; Letsinger, R. L.: Multiple thiol-anchor capped DNA–gold nanoparticle conjugates. *Nucleic Acids Research* **2002**, *30*, 1558-1562.

(217) Fields-Zinna, C. A. P., Joseph F. Murray, Royce W.: Mass Spectrometry of Ligand Exchange Chelation of the Nanoparticle [Au25(SCH2CH2C6H5)18]1− by CH3C6H3(SH)2. *Journal of the American Chemical Society* **2010**, *132*, 17193-17198.

(218) Dass, A.; Stevenson, A.; Dubay, G. R.; Tracy, J. B.; Murray, R. W.: Nanoparticle MALDI-TOF Mass Spectrometry without Fragmentation: Au25(SCH2CH2Ph)18 and Mixed Monolayer Au25(SCH2CH2Ph)18−x(L)x. *Journal of the American Chemical Society* **2008**, *130*, 5940-5946.

(219) Kassam, A.; Bremner, G.; Clark, B.; Ulibarri, G.; Lennox, R. B.: Place Exchange Reactions of Alkyl Thiols on Gold Nanoparticles. *Journal of the American Chemical Society* **2006**, *128*, 3476-3477.

(220) Suguna Perumal, A. H., Norman Scholz, Eckart Ruhl, and Christina Graf: Kinetics Study of the Binding of Multivalent Ligands on Size-Selected Gold Nanoparticles. *Langmuir* **2011**, *27*, 4456–4464.

(221) Templeton, A. C., Wuelfing, W. P., Murray, R. W. : *Acc. Chem. Res.* **2000**, *33*, 27.

(222) Hakkinen, H. B., R. N.; Landman, U.: *Phys. Rev. Lett.* **1999**, *82*, 3264.

(223) Haberlen, O. D. C., S.-C.; Stener, M.; Ro¨sch, N.: *Journal of Chemical Physics* **1997**, *106*, 5189.

(224) Murphy, C. J.; Gole, A. M.; Hunyadi, S. E.; Orendorff, C. J.: One-Dimensional Colloidal Gold and Silver Nanostructures. *Inorganic Chemistry* **2006**, *45*, 7544-7554.

(225) Keul, H. A.; Moller, M.; Bockstaller, M. R.: Selective exposition of high and low density crystal facets of gold nanocrystals using the seeded-growth technique. *CrystEngComm* **2011**, *13*, 850-856.

(226) Sun, Y.; Mayers, B.; Herricks, T.; Xia, Y.: Polyol Synthesis of Uniform Silver Nanowires: A Plausible Growth Mechanism and the Supporting Evidence. *Nano Letters* **2003**, *3*, 955-960.

(227) Rapino, S.; Zerbetto, F.: Dynamics of Thiolate Chains on a Gold Nanoparticle. *Small* **2007**, *3*, 386-388.

(228) Myung, N.; Bae, Y.; Bard, A. J.: Enhancement of the Photoluminescence of CdSe Nanocrystals Dispersed in CHCl3 by Oxygen Passivation of Surface States. *Nano Letters* **2003**, *3*, 747-749.

(229) Pietron, J. J.; Hicks, J. F.; Murray, R. W.: Using Electrons Stored on Quantized Capacitors in Electron Transfer Reactions. *Journal of the American Chemical Society* **1999**, *121*, 5565-5570.

(230) Walczak, M. M.; Popenoe, D. D.; Deinhammer, R. S.; Lamp, B. D.; Chung, C.; Porter, M. D.: Reductive desorption of alkanethiolate monolayers at gold: a measure of surface coverage. *Langmuir* **1991**, *7*, 2687-2693.

(231) Chen, S., Templeton, A. C., Murray, R. W. : *Langmuir* **2000**, *16*, 3543.

(232) Wilcoxon, J. P. P., P.; : Etching and Aging Effects in Nanosize Au Cluster: Investigated Using High-Resolution-Size-Exclusion Chromatography. *Journal of Physical Chemistry B* **2003**, *107*, 12949-12957.

(233) McDermott, C. A. M., M. T.; Green, J.; Porter, M. D.;: Structural Origins of the Surface Depressions at Alkanethiolate Monolayers on Au(111): A Scanning Tunneling and Atomic Force Microscope Investigation. *Journal of Physical Chemistry* **1995**, *99*, 13257-13267.

(234) Alvarez, M. M.; Khoury, J. T.; Schaaff, T. G.; Shafigullin, M. N.; Vezmar, I.; Whetten, R. L.: Optical Absorption Spectra of Nanocrystal Gold Molecules. *The Journal of Physical Chemistry B* **1997**, *101*, 7885.

(235) Chaijapukui, O. S., L.; Xu, C.; Crooks, R. M.: *Journal of the American Chemical Society* **1993**, *115*, 12459.

(236) Woerhrle, G. H. B., L. O.; Hutchison, J. E.;: Thiol-Functionalized, 1.5-nm Gold Nanoparticles through Ligand Exchange Reactions: Scope and Mechanism of Ligand Exchange. *The Journal of the American Chemical Society* **2004**, *127*, 2172-2183.

(237) Park, J. N. V., A.; Barriet, D.; Shon, Y.; Lee, T. R.;: Systematic Control of the Packing Density of Self-Assembled Monolayers Using Bidentate and Tridentate Chelating Alkanethiols. *Langmuir* **2005**, *21*, 2902-2911.

(238) Eck, W.; Craig, G.; Sigdel, A.; Ritter, G.; Old, L. J.; Tang, L.; Brennan, M. F.; Allen, P. J.; Mason, M. D.: PEGylated Gold Nanoparticles Conjugated to Monoclonal F19 Antibodies as Targeted Labeling Agents for Human Pancreatic Carcinoma Tissue. *ACS Nano* **2008**, *2*, 2263-2272.

(239) McCash, E.: *Surface Chemistry*; Oxford University Press: UK, 2001.

(240) Petosa, A. R., Jaisi, D. P., Quevedo, I. R., Elimelech, m., Tufenkji, N.: Aggregation and Deposition of Engineered Nanomaterials in Aquatic Environments: Role of Physicochemical Interactions. *Environmental Science and Technology* **2010**, *44*, 6532–6549.

(241) Bain, C. D.; Evall, J.; Whitesides, G. M.: Formation of monolayers by the coadsorption of thiols on gold: variation in the head group, tail group, and solvent. *Journal of the American Chemical Society* **1989**, *111*, 7155-7164.

(242) Ulman, A.: *An Introduction to Ultrathin Organic Films: From Langmuir-Blodgett to Self-Assembly*; Academic Press: New York, 1991.

(243) Bryant, M. A.; Pemberton, J. E.: Surface Raman scattering of self-assembled monolayers formed from 1-alkanethiols: behavior of films at gold and comparison to films at silver. *Journal of the American Chemical Society* **1991**, *113*, 8284-8293.

(244) Grönbeck, H.; Curioni, A.; Andreoni, W.: Thiols and Disulfides on the Au(111) Surface: The Headgroup−Gold Interaction. *Journal of the American Chemical Society* **2000**, *122*, 3839-3842.

(245) Wan, L.-J.; Hara, Y.; Noda, H.; Osawa, M.: Dimerization of Sulfur Headgroups in 4-Mercaptopyridine Self-Assembled Monolayers on Au(111) Studied by Scanning Tunneling Microscopy. *The Journal of Physical Chemistry B* **1998**, *102*, 5943-5946.

(246) Fenter, P.; Schreiber, F.; Berman, L.; Scoles, G.; Eisenberger, P.; Bedzyk, M. J.: On the structure and evolution of the buried S/Au interface in self-assembled monolayers: X-ray standing wave results. *Surface Science* **1998**, *412–413*, 213-235.

(247) Biebuyck, H. A.; Bain, C. D.; Whitesides, G. M.: Comparison of Organic Monolayers on Polycrystalline Gold Spontaneously Assembled from Solutions Containing Dialkyl Disulfides or Alkanethiols. *Langmuir* **1994**, *10*, 1825-1831.

(248) Leff, D. V.; Brandt, L.; Heath, J. R.: Synthesis and Characterization of Hydrophobic, Organically-Soluble Gold Nanocrystals Functionalized with Primary Amines. *Langmuir* **1996**, *12*, 4723-4730.

(249) Xu, C.; Sun, L.; Kepley, L. J.; Crooks, R. M.; Ricco, A. J.: Molecular interactions between organized, surface-confined monolayers and vapor-phase probe molecules. 6. In-situ FT-IR external reflectance spectroscopy of monolayer adsorption and reaction chemistry. *Analytical Chemistry* **1993**, *65*, 2102-2107.

(250) Majzik, A. P., R.; Hornok, V.; Dekany, I.;: Growing and stability of gold nanoparticles and their functionalization by cysteine. *Gold Bulletin* **2009**, *42*, 113-123.

(251) Patrick M Shem, R. S., Jennifer S Shumaker-Parry: One-Step Synthesis of Phosphine-Stabilized Gold Nanoparticles Using the Mild Reducing Agent 9-BBN. *Langmuir*.

(252) OSSI HOROVITZ, A. M., GHEORGHE TOMOAIA, LIVIU BOBOS, DIANA DUBERT, IULIA DAIAN, TRAIANOS YUSANIS AND MARIA TOMOAIA-COTISEL: LYSINE MEDIATED ASSEMBLY OF GOLD NANOPARTICLES *STUDIA UNIVERSITATIS BABEŞ-BOLYAI, CHEMIA* **2007**, *1*.

CHAPTER THREE

INVESITGATION OF LIGAND BINDING AND EXCHANGE ON GOLD NANOPARTICLES WITH ISOTHERMAL TITRATION CALORIMETRY

Abstract

Isothermal titration calorimetry is a highly sensitive tool for measuring thermodynamic and kinetic aspects of molecular interactions and is a powerful tool to probe ligand-nanoparticle interactions. Knowledge of ligand binding is essential in the design of and prediction of the function and end fate of nanomaterials. In this study, isothermal titration calorimetry was used to measure the binding strengths of 1kDa polyethylene glycol end functionalized with thiol, amine, and carboxylic acid functional groups to the surface of freshly synthesized bare, citrate stabilized gold nanoparticles, and polyethylene glycol-amine stabilized gold nanoparticles. The effect of particle age on the heat of binding was also studied with bare and citrate stabilized gold nanoparticles. In the report, we demonstrate that thiols have higher heats (>100 kJ/mol) of binding than what has been reported for 2-dimensional gold surfaces. Polyethylene glycol-thiol exhibited a heat of binding to bare gold nanoparticles of -304kJ/mol. We also demonstrate that age affects the heat and extent of binding of thiols to gold nanoparticle surfaces. Aged bare gold nanoparticles exhibited a heat of binding of with polyethylene glycol-thiol of -205 kJ/mol. Citrate and polyethylene glycol-amine stabilized gold nanoparticles were also investigated and exhibited a heats of binding with polyethylene glycol-thiol of 252

kJ/mol and -200kJ/mol, respectively. These results also provide evidence of an associative, S_N2 mechanism of binding and exchange.

Introduction

Gold nanoparticles (GNPs) have been of increased interest due to their stability, optical properties and low toxicity. GNPs are small enough including individual cells and organelles; which makes them attractive for biomedical applications in targeting and drug delivery. GNPs can be functionalized with a variety of ligands; therefore it is important to be able to predict how GNPs will interact with a variety of functional groups. Many studies on the interaction of thiols [1-6] and amines [7-9] with GNPs have been conducted, but few provide real-time, quantitative information on ligand binding. Numerous studies have been conducted on the exchange of thiol-functionalized ligands on GNPs, which provide insight into the GNP-ligand interactions but do not provide quantitative information on the binding strengths to GNP surfaces. [10-16] Studies on the bond strength of sulfur groups to 2D surfaces of gold [17,18] provide data that is not completely analogous to the sulfur-gold bond strength on a GNP. This is due to the fact that gold is an inherently crystalline material and therefore, GNPs will not be perfectly spherical and have a high surface curvature. Gold nanoparticles are comprised of a combination of crystalline faces, whereas most studies of 2D gold measure isolate a specific crystalline face to study. Different crystalline faces exhibit different interatomic spacing and there for have difference steric accessibilities to functional groups of different sizes.[19] Due to the inherent crystallinity and high surface curvature of GNPs, their surfaces will contain

defect sites, such as edges and vertices, along with smooth terrace sites. Defect sites are more electron-dense and sterically accessible and therefore more reactive than terrace sites.[20-22] Density functional theory calculations have been used to calculate the 4*f* binding energies of surface atoms relative to bulk atoms in GNPs of various sizes. The simulations concluded that lower coordinated gold atoms, such as corners and edges, have lower Au-Au 4*f* binding energies and therefore will be more susceptible to ligand binding and exchange in order to complete their valence shell. [23] As GNPs age, surface atoms will rearrange causing a change in surface morphology, and the number of reactive defect sites decreases. Chechik investigated this surface reconstruction, or annealing, and found that the reactivity of GNPs is reduced as they age. [24] In this study, the effect of GNP age on polyethylene glycol-thiol, PEG-SH, binding is investigated with isothermal titration calorimetry, ITC. ITC is a temperature sensitive technique that can detect nanoWatts of heat change evolved from a reaction of one molecule titrated against another. ITC has been very useful in studying the thermodynamics of binding in biological systems such as protein-protein interactions,[25] protein-DNA interactions, [26] and protein-lipid interactions.[27] Recently, this method had been used to study ligand binding to the surface of gold nanoparticles, but few have investigated the effect age or competitive binding with ITC.[8,28] The objective of this study was to use ITC to determine the effect of age and surface chemistry on PEG-SH binging to gold nanoparticles. UV-Vis spectroscopy and dynamic light scattering were also used to characterize binding.

Experimental

Nanoparticle Synthesis

Bare gold nanoparticles, BGNPs, were synthesized by adapting Turkevich's method described previously.[29] In short, 0.165 mL of an iced aqueous solution of 0.1M sodium borohydride, $NaBH_4$ (Alfa Aeser, 99.9%) was added drop wise to a 5 mL solution of 0.25mM $HAuCl_3$, (Alfa Aeser, 99.0%), while rapidly stirring. It is important to note that while these nanoparticles are described as "bare" it is likely that boron is adsorbed to the surface and provides stabilization. Citrate stabilized gold nanoparticles were synthesized in a similar fashion by first preparing a 20 mL solution of 0.25 mM trisodium citrate dihydrate, (Alfa Aeser, 99.0%) and 0.25 mM $HAuCl_3$. Then, 0.1 mL of a 0.1M solution of iced, aqueous $NaBH_4$ was added drop wise while rapidly stirring. Polyethylene glycol-amine, PEG-NH_2, (Laysan Bio) stabilized GNPs were similarly synthesized by reduction with $NaBH_4$, however the pH needed to be adjusted above the pKa of PEG-NH_2. Studies have shown that amines need to be unprotonated in order to bind to GNPs.[7,8,30] The 10mL, 0.25mM PEG-NH_2 and $HAuCl_3$ solutions were pH adjusted to 10 with nitric acid. Then, while stirring rapidly, 50µL of 0.1M $NaBH_4$ was added drop-wise.

Nanoparticle Characterization

All nanoparticle samples were filtered with 0.2 µm PFTE syringe filters (VWR), and then degassed with a vacuum pump and characterized via a Hitachi 7600 transmission electron microscope, TEM, and images were analyzed with ImageJ

software. Further characterizations performed were UV-Vis spectroscopy on a Varian Cary 50 Bio UV-Vis spectrophotometer and dynamic light scattering and zeta potential measurements with a Malvern Zetasizer. Characterization was performed before and after titration experiments.

Isothermal Titration Calorimetry

A TA instruments TAM III microcalorimeter was used to perform titrations with various ligands into solutions of GNPs. In short, 0.8mL of gold nanoparticle (GNP) solution was loaded into the sample cell to be placed into the calorimeter. 10 µL of 0.25mM ligand solution was injected into the reaction cell every 20 minutes a total of 20 times while the nanoparticle solution was stirred at 120 rpm at 25 °C. Hastelloy samples cells and a gold propeller were used. Each experiment was performed in triplicate and dilution titrations were performed to correct each titration for heat of mixing and dilution affects.

Calculation of Binding Sites

In a study recently conducted by Hinterwirth et al. GNPs stabilized with various thiol ligands were synthesized then analyzed via inductively coupled plasma-mass spectroscopy to determine the surface coverage of thiols. [2] The surface coverage was determined by the gold to sulfur ratio, (Au/S) and size-independent but ligand chain length-dependent ligand densities were reported. The ligand density used in this study is 4.29 S/nm^{-2} as this value was reported in Hinterwirth's study for GNPs stabilized with 500 MW PEG-SH, which is similar to the ligand used in this study. Hinterwirth also

reported that ligand density decreases linearly with an increase in chain length;[2] therefore it is important to note that a ligand density of 4.29 S/nm^{-2} represents the maximum possible surface coverage.

The concentration of binding sites (μmol/L) was calculated using the average surface area of the GNP distribution obtained by TEM and a surface coverage of 4.29 sulfur atoms per nm^2.[2] First, the number of sites per GNP was calculated by multiplying the average GNP surface area by the expected surface coverage of sulfur;

$$Sites_{GNP} = \frac{\sum 4\pi \frac{{d_{GNP}}^2}{2}}{n_{GNPs}} * 4.29 \quad (1)$$

The concentration of binding sites (μmol/L) was calculated by multiplying the number of sites per GNP by the concentration of GNPs in solution;

$$[Binding\ Sites] = \frac{Sites_{GNP} * \frac{[Au]}{V_{GNP} * \frac{\rho_{Au}}{MW_{Au}}}}{N_A} * 10^5 \quad (2)$$

Table 3.1 summarizes information about the size and surface area determined by TEM, and concentration of binding sites in each GNP solution.

Table 3-1: Nanoparticle diameter and surface are determined by TEM and calculated concetrations of binding sites

GNP	Trial #	Average Diameter, nm	Average Surface Area, nm^2	Binding Sites, (umole/L)
Bare	1	6.7 ± 1.9	152.3	13.9
	2	6.4 ± 3.34	148.5	11.0
	3	7.0 ± 1.9	165.4	13.4
Aged Bare	1	9.7 ± 2.7	316.7	10.0
	2	11.3 ± 1.8	366.2	10.1
	3	11.8 ± 3.1	390.3	9.2
Citrate	1	5.9 ± 4.1	224.0	9.5
	2	5.7 ± 2.0	113.8	15.3
	3	5.5 ± 2.6	114.2	13.7
Aged Citrate	1	5.1 ± 1.4	89.7	17.9
	2	5.2 ± 1.4	83.6	21.1
	3	5.1 ± 1.3	89.7	17.9
PEG-NH_2	1	6.84 ± 1.7	156.2	13.9
	2	6.84 ± 1.7	156.2	13.9
	3	6.84 ± 1.7	156.2	13.9

Modeling

Each peak, Figure 3.1, in raw heat flow data from each titration was integrated and plotted to create a binding isotherm and then modelled with Protonic HypΔH software. This software performs up to 1000 iterations of a non-linear least squares fit of a system of equations described below. [31]The heat evolved in each reaction step is calculated using equation 3;

$$Q = -\sum \delta n \Delta H \qquad (3)$$

Where Q is the heat evolved, δn in the change in the number of moles of a particular reactant, and ΔH is the enthalpy of binding. Each cumulative equilibrium constant may be defined by Eq 4;

$$xA + yB \leftrightarrow A_xB_y \qquad \beta = \frac{[A_xB_y]}{[A]^x[B]^y} \qquad (4)$$

Where A is the component in the reaction cell, B is the titrant and β is the equilibrium constant. This software models ITC data as though a titration step takes place in 3 stages. In stage (1), an aliquot of titrant volume, ν_B, is added to the reaction solution of ν_A without mixing, and is considered athermic. In stage (2) the solutions of A and B are mixed without chemical reaction, the volume changes and the equilibrium concentrations of A and B change, and heat is evolved from mixing, Eq 5. Finally, in stage (3) a chemical reaction takes place without a change in volume and the heat evolved is calculated using Eq 6;[31]

$$Q_{(2)} = -\sum(v_{A+B}[A_xB_y]_{(2)} - v_A[A_xB_y]_{(1)})\Delta H \qquad (5)$$

$$Q_{(3)} = -v_{A+B}\sum([A_xB_y]_{(3)} - [A_xB_y]_{(2)})\Delta H \qquad (6)$$

A mass balance is then conducted to solve for [A] and [B] by solving Eq 4-6 simultaneously, and the enthalpies of formation are calculated by minimizing the objective function, U, Eq 7, with a linear least-squares fit because the calculated heat in each stage is a linear function of enthalpy.[31]

$$U = \sum(Q^{corr} - Q_2 - Q_3)^2 \qquad (7)$$

Where, Q^{corr} is the observed reaction heat that has been corrected for non-chemical heat contributions such as stirring, dilution and friction. This software determines formation enthalpies, binding constants and surface coverage from the calorimetric data and allows for simultaneous fitting of multiple curves. Inputs required to model the binding isotherms include raw integrated heat data, volume of GNP solution, concentration and volume of ligand solution for each injection and the total number of GNP binding sites.

Results and Discussion

Polyethylene glycol-thiol Titrations:

Bare GNPs

The heat of binding of PEGSH to bare gold nanoparticles, BGNPs, was investigated with ITC, raw heat signal curves for freshly synthesized BGNPs is show in Figure 1. Titrations were performed in triplicate to ensure reproducibility of the data. Each positive peak shown in the heat signal curves indicates an exothermic process, which represents the heat released in one injection of aqueous PEG-SH into the GNP solution as a function of time. The exothermicity of these peaks is to be due to the strong interaction between thiols and GNPs. Ligand binding and exchange is generally considered to follow an associative S_N2 pathway in which binding and exchange is initiated and occurs rapidly at reactive defect sites, then reaction rates slow as bound ligand migrates from defect sites to terrace sites to allow further binding onto defect sites.[32-35] Evidence of this type of mechanism is seen in this study from the raw heat flow diagrams resulting from the titration of PEG-SH into BGNPs, Figure 3.1 A-C.

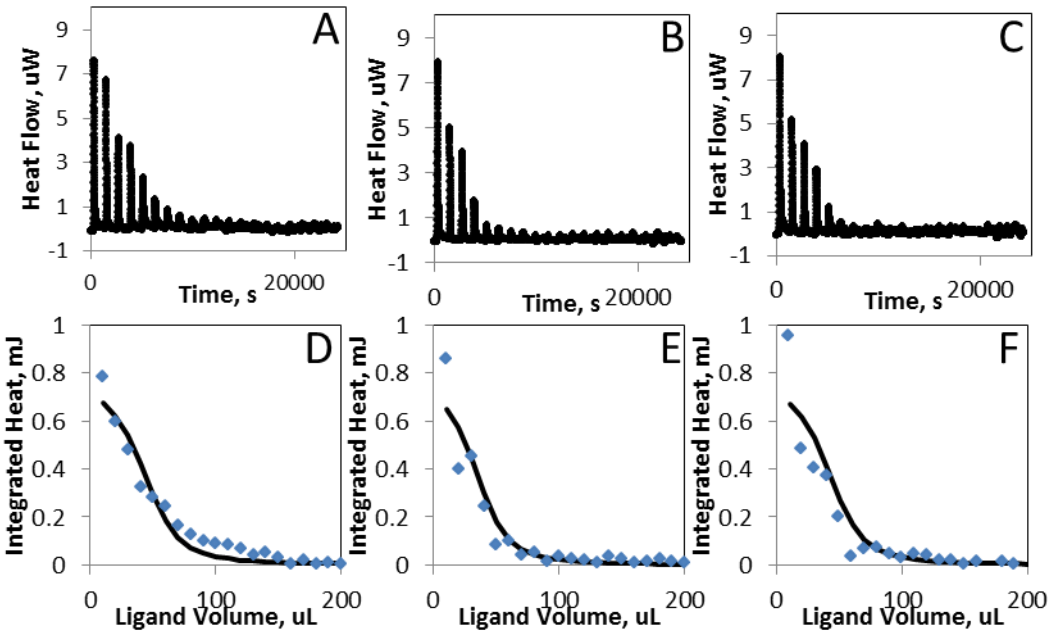

Figure 3-1: Raw heat flow data for 3 replicates of PEG-SH titrated into freshly synthesized BGNPs, (A-C) and their corresponding dilution corrected binding isotherms (D-F). Dots represent observed integrated heats and lines represent calculated heats

The heat signal is initially high and decreases rapidly as the number of defect sites is consumed and saturated and binding eventually reaches equilibrium. Plots of dilution corrected integrated heat values vs. accumulated ligand volume correspond to binding isotherms of PEG-SH to a GNP surface, Figure 1D-F. Control experiments were conducted to in order to subtract heat from non-chemical reactions such as mixing, dilution and friction from the integrated heats from titrations with GNPs. Thermodynamic modeling of the binding isotherms for freshly synthesized BGNPs resulted in an enthalpy of -304 ± 7 kJ/mol, and a binding constant of $7.0*10^5$. This enthalpy value is slightly higher than what is reported in literature for 2D SAMs (-130 -230kJ/mol) [36-38] and this is due to the fact that nanoparticles have reactive defect sites such as corners and vertices

whereas 2D surfaces do not. Because of the enhanced reactivity of these sites due to incomplete valance shells, binding reactions may be more exothermic at these sites. UV-vis characterization fresh BGNPs before and after PEG-SH titrations, resulted in a 7nm blue shift in the localized surface plasmon resonance, LSPR, peak indicating a change in surface chemistry. GNPs are plasmonic and their characteristic LSPR will shift depending on size, shape and surface chemistry.[39-41] The zeta potential of BGNPs decreased in magnitude from -40.6 to -27.2 mV after titration with PEG-SH. Since PEG-SH is uncharged, when it binds to the surface of BGNPs the zeta potential should decrease in magnitude. The surface coverage of PEG-SH on BGNPs was estimated by the HypDeltaH software to be 93.4 %, indicating near complete binding. This reaction exhibited an entropy value of -0.908 kJ/K mol which is calculated using the relationship between enthalpy and Gibbs free energy, Eq 8.

$$\Delta G = -RTLn(K) = \Delta H - T\Delta S \qquad (8)$$

Table 3-2: Thermodynamic and kinetic parameters of PEG-SH titrations as determined by HypDeltaH software

GNP	ΔH, kJ/mol	Logβ	K	ΔS, kJ/K·mol	ΔG, kJ/mol	NPSH, %
Bare	-304.11	5.845	7.00E+05	-0.908	-33.526	93.5
Aged Bare	-205.33	5.559	3.63E+05	-0.582	-31.894	88.7
Citrate	-252.9	5.712	5.15E+05	-0.73	-35.36	90.5
Aged Citrate	-244.2	5.929	8.49E+05	-0.7	-35.6	92.7
$PEGNH_2$	-204.6	5.826	6.70E+05	-0.58	-31.76	92.0

Table 3.2 summarizes the modeling results for each ligand/GNP pair investigated. From Figure 3.1, we show that the data obtained from these titrations is reproducible, as a

new batch of BGNPs was synthesized for each replicate and the 3 binding isotherms were modeled simultaneously.

After performing titrations with freshly synthesized BGNPs, the remaining nanoparticle solutions were aged in a dark, room temperature environment for 3 months. The solutions remained bright red in color and no precipitates were formed. Characterization with UV-vis spectroscopy, DLS and Zeta potential measurements verified that the aged particles were still stable, Table 3.3. The raw heat flow data and corresponding binding isotherms of PEG-SH titrated into aged BGNPs are shown in Figures 3.2 A-C and 3.2 D-E, respectfully. The resulting enthalpy for aged BGNPs was significantly lower than freshly synthesized particle, -205 ± 5 kJ/mol. This value is closer to what is reported in literature for 2D gold surfaces and indicates a change in GNP surface morphology. As stated previously, GNPs undergo surface annealing over time, and the number of reactive defect sites decreases[24] and this is evidenced by the rapid decrease and saturation of enthalpy. TEM analysis after titration revealed that aggregates present before titration were broken apart upon the addition of PEG-SH, Figure 3.4, which provides evidence that PEG-SH interacts strongly with aged BGNPs. The surface coverage was estimated at 88.75 %, which is similar to the surface coverage of PEG-SH on fresh BGNPs. The entropy of this system was calculated to be -0.582 kJ/K mol, which is lower in magnitude than the entropy of PEG-SH binding to fresh GNPs. Table 3 summarizes the heats of binding, binding constants and surface coverage for each system investigated in the study.

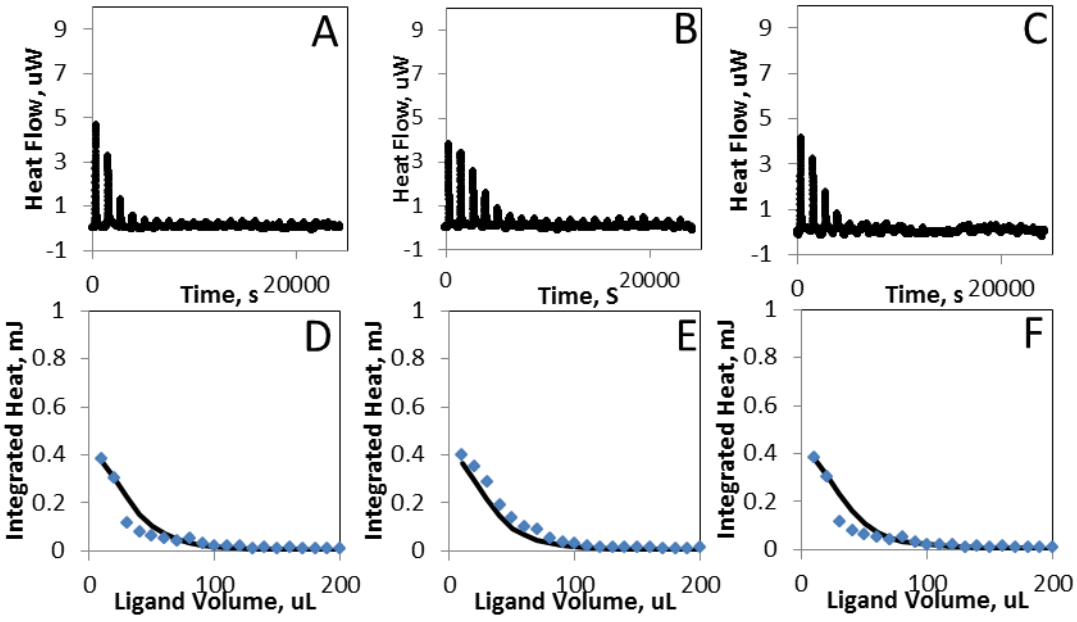

Figure 3-2: Raw heat flow data for 3 replicates of PEG-SH titrated into aged BGNPs, (A-C) and their corresponding dilution corrected binding isotherms (D-F). Dots represent observed integrated heats and lines represent calculated heats

Citrate-stabilized GNPs

Figure 5 depicts the heat flow data, A-C and binding isotherms, D-E, for freshly synthesized citrate GNPs. The enthalpy of PEG-SH binding to freshly synthesized citrate GNPs was calculated to be -252.9 kJ/mol, and the surface coverage was determined to be 90.5%. Carboxylic acid groups in citrate bind to GNPs weakly though an electrostatic interaction; therefore citrate should not have a large effect on the binding of thiols to the surface of GNPs. While citrate molecules are easily displace by thiols, some amount of heat is taken up by the desorption of citrate, which explains the ~50 kJ/mol difference between the heat of binding of PEG-SH BGNP and citrate stabilized GNPs. The energy

of a physical bond typically has a magnitude of 10-40 kJ/mol, and because citrate can potentially bind to GNPs through 3 COOH groups a bond energy of 50 kJ/mol is a reasonable value. A 26.9 nm blue shift was seen for citrate GNPs after titration with PEG-SH also indicating PEG-SH binding. The zeta potential measured for citrate GNPs decreased from -41.7 mV to -9.7 mV after titration which indicated

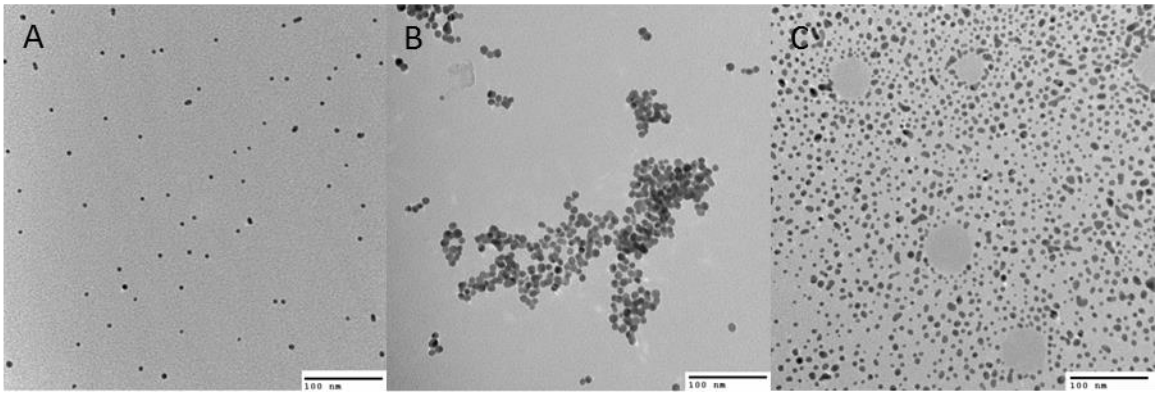

Figure 3-3: TEM images of A) freshly synthesized BGNPs, B) aged GNPs and C) aged BGNPs after titration with PEG-SH

that the GNP surface chemistry was now PEG-SH with a surface coverage of 90.5%. Surprisingly, the effect of age was not seen in citrate stabilized GNPs. Heat flow data and binding isotherms for these titrations are shown in Figure 6. An explanation for this could be that citrate preserves the reactivity of GNP surfaces as they age. The surface coverage of these particles after titration with PEG-SH was calculated to be 92.67 %, which is similar to the surface coverage of fresh citrate stabilized GNP. The entropy for freshly synthesized and aged citrate stabilized GNPs were very similar, with values of -0.73 and -0.7 kJ/k mol. These values are only slightly lower in magnitude than that of fresh BGNPs, indicating that citrate does not contribute entropic effects to the binding of

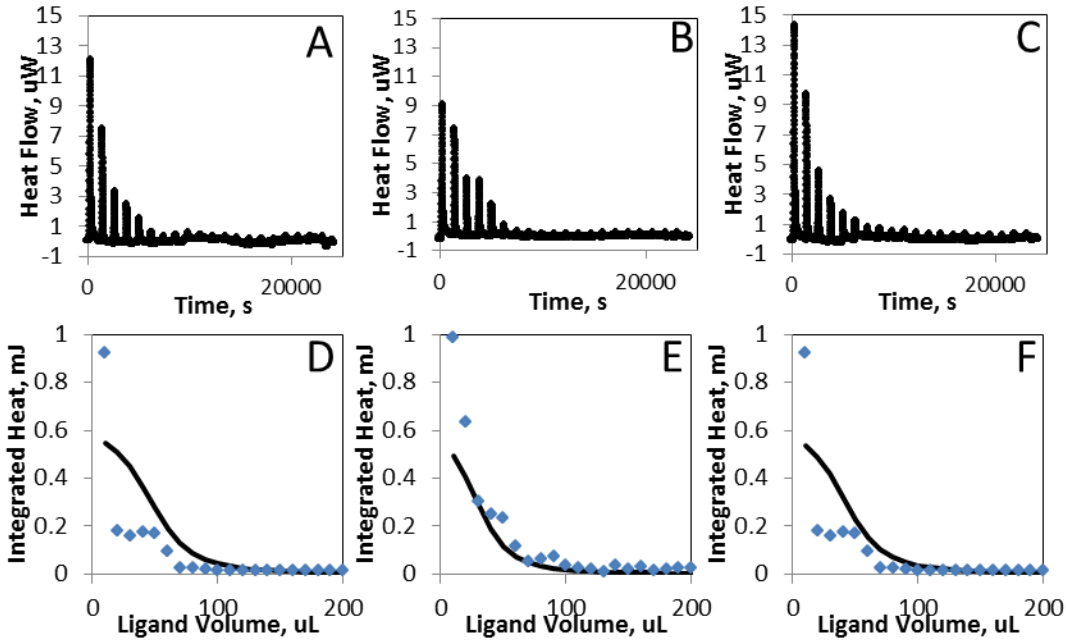

Figure 3-4: Raw heat flow data for 3 replicates of PEG-SH titrated into freshly synthesized citrate stabilized GNPs, (A-C) and their corresponding dilution corrected binding isotherms (D-F). Dots represent observed integrated heats and lines represent calculated heats

PEG-SH to the surface of GNPs. The reproducibility of ITC data with citrate stabilized GNPs, freshly synthesized and aged, is lower than that of BGNPs. This may be due to differences in surface coverage between batches of citrate GNPs.

Table 3-3: Summary of characterization by UV-Vis spectroscopy and Zeta potential measurements

GNP	LSPR (λ) nm		Zeta Potential (ζ) mV	
	As Synthesized	After titration	As Synthesized	After titration
Bare	506.9	513.9	-40.6	-27.2
Aged Bare	506.9	513.9	-45	-19.1
Citrate	529.9	519.9	-41.7	-9.7
Aged Citrate	529.9	519.9	-39.7	-11.2
$PEGNH_2$	506.9	519.9	-18.7	-0.05

PEG-NH_2 stabilized GNPs

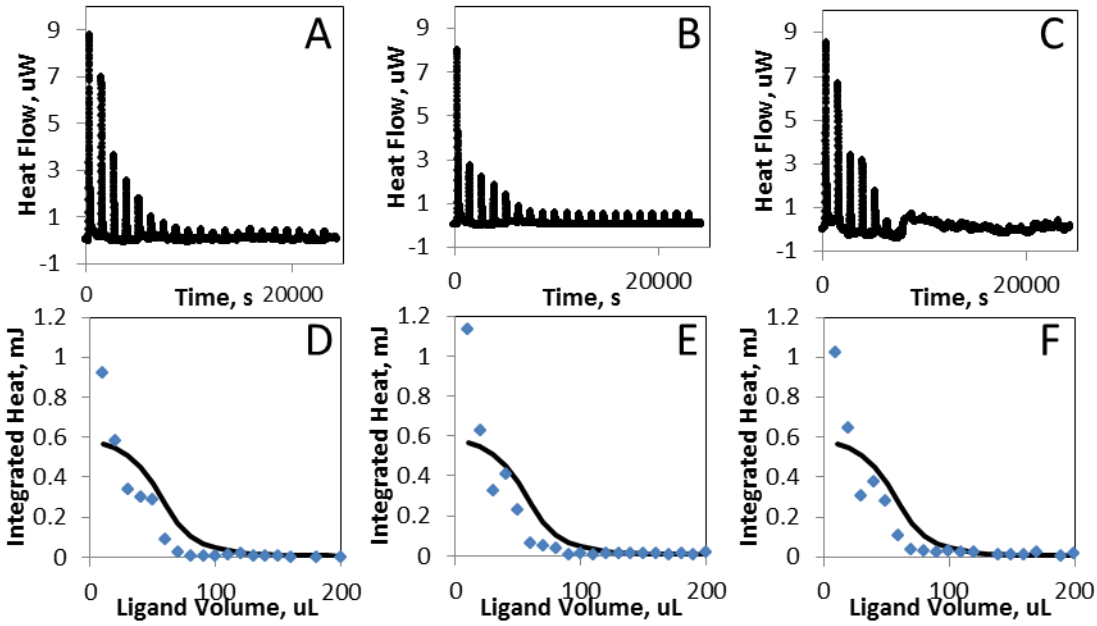

Figure 3-5: Raw heat flow data for 3 replicates of PEG-SH titrated into aged citrate stabilized GNPs, (A-C) and their corresponding dilution corrected binding isotherms (D-F). Dots represent observed integrated heats and lines represent calculated heats

Raw heat flow data and corresponding binding isotherms of this system are shown in Figure 7. The resulting heat of binding of PEG-SH to PEG-NH_2 stabilized GNPs was -204.6 kJ/mol. In order to bind to the GNP, PEG-SH has to overcome the steric hindrance of PEG-NH_2, which may decrease the heat of binding. PEG-NH_2 must desorb from the surface, and this is an endothermic process, in order for PEG-SH molecules to bind; therefore the heat of binding will be the combination of energy taken up by the desorption process and given off during the binding process. We can then infer that the heat of binding for PEG-NH_2 is equal to the difference in the heat of binding of PEG-SH to BGNPs and to PEG-NH_2 stabilized GNPs, which is 100.5 kJ/mol, which is indicative

of a chemical bond.[42] The heat flow diagrams for these titrations also provide evidence of an associative, S_N2 mechanism due to the high initial value and rapid decrease of heat signal. These particles underwent a 7nm blue shift of the SPR peak after titration with PEG-SH and the zeta potential of these particles remained about the same before and after titration because both molecules have PEG chains. The surface coverage of PEG-SH on the surface of the particles was calculated to be 92 %, which suggested near complete exchange. These particles are relatively small, 5 – 10nm, thus high extents of exchange would be expected. As stated in Chapter 2 of this dissertation, small particles exhibit high extents of reaction.

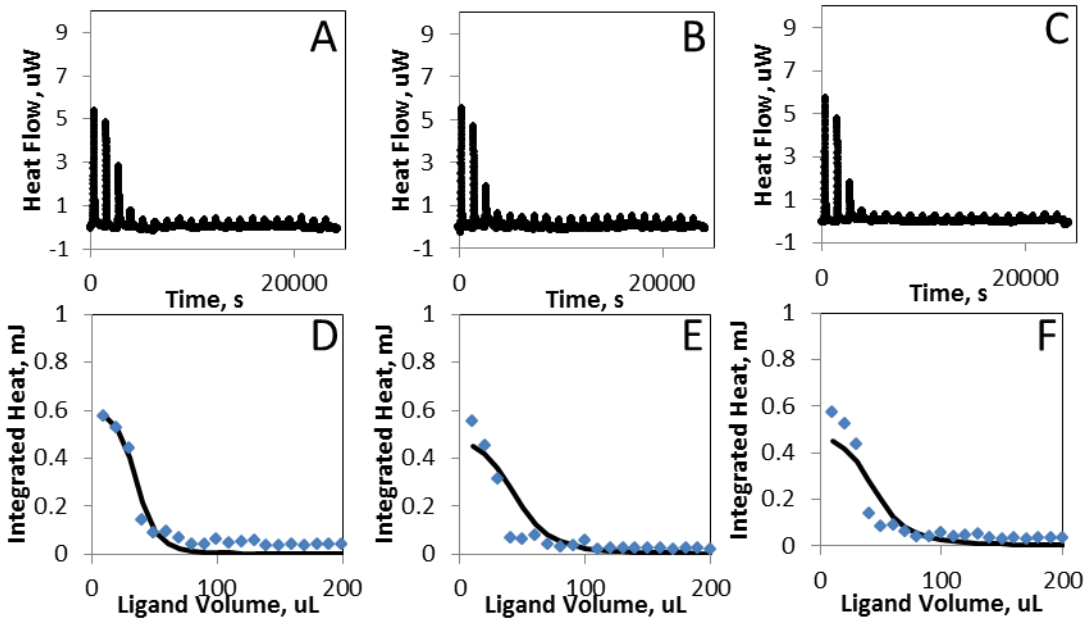

Figure 3-6: Raw heat flow data for 3 replicates of PEG-SH titrated into PEG-NH_2 stabilized GNPs, (A-C) and corresponding, dilution corrected binding isotherms (D-F). Dots represent observed integrated heats and lines represent calculated heats

PEG, PEG-NH_2, PEG-COOH and Citrate Titrations with GNP

Heat flow diagrams of titrations with unfunctionalized PEG, PEG-COOH, PEG-NH_2 and citrate into BGNPs do not indicate binding, as shown in Figure 8A, B, C, and D respectively. Unfunctionalized PEG was titrated into GNPs as a control to ensure that PEG chain was not contributing entropic effects to the heat of binding and that the OH groups were not interacting with GNPs. PEG-NH_2 solutions were adjusted to a pH of 10 to ensure that the amine was unprotonated in order to bind to the GNPs, which were also of pH 10. Very little heat is evolved during this titration and there is no decay in heat flow, which would indicate the consumption of binding sites. PEG-COOH titrations also lacked strong heat signals. While it is well established that carboxylic acids and amines bind to GNPs and gold surfaces, they do not bind covalently. This indicated that ITC may not be able to detect heats of electrostatic or physical binding since these mechanisms have binding strengths of only -10 to -40 kJ/mol.[43] On the other hand, a lack of ITC signal does not indicate a lack of ligands on the GNP surface. Joshi et al. were faced with this issue in their study of the binding of amino acids to GNPs and used XPS and gel electrophoresis to prove that while there was no ITC signal, amino acid were indeed bound weakly to the GNP surface.[8] Citrate was also titrated into BGNPs, Figure 8D, and exhibited very little heat signal, but a 23nm red shirt in the UV-Vis spectrum which indicated that citrate is bound to the surface.

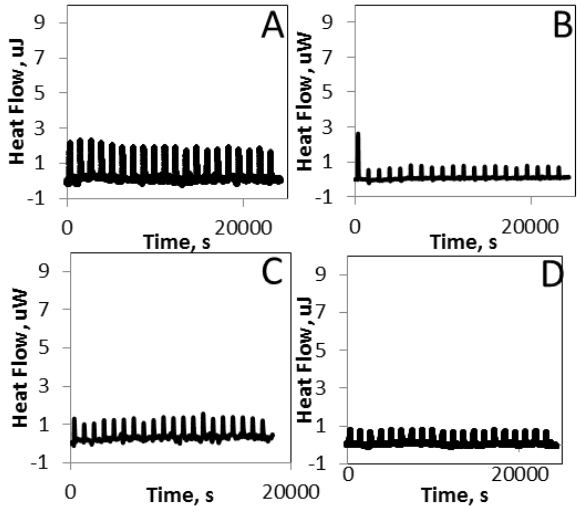

Figure 3-7: Heat flow data for A) PEG, B) PEG-COOH, C) PEG-NH2 and D) citrate titrated into BGNPs

Conclusions

We have demonstrated that isothermal titration calorimetry is a useful technique for studying ligand-nanoparticle interactions. We have demonstrated that thiols exhibited a heat of binding of 304kJ/mol which is >100kJ/mol higher than the heat of binding of thiols to 2D gold surfaces. We have shown that aging reduces the reactivity of bare gold nanoparticles, as the heat of binding of PEG-SH to aged BGNPs is 100 kJ/mol lower than the heat of binding to freshly synthesized BGNPs. On the other hand, a difference is surface coverage between fresh and aged BGNPs was not seen due to the small size of these GNPs. Our studies demonstrate that the presence of citrate on the surface of GNPs does not inhibit the binding of thiols. A 50kJ/mol decrease in the heat of binding of PEG-SH to citrate stabilized GNPs demonstrates that citrate interacts with GNPs through a physical bond. Surprisingly, citrate seems to preserve the reactivity of GNPs by possibly

preventing the reorganization of surface atoms. Titrations of PEG-SH into PEG-NH_2 stabilized GNPs resulted in a heat of binding of 204 kJ/mol, and from the difference in heats of binding of PEG-SH to BGNPs, we can infer that PEG-NH_2 bind to GNPs chemically with a bond strength of approximately 100kJ/mol. From the results in this study we can elucidate the following trend in binding affinities of the functional groups tested; SH >> NH_2 > COOH. Future work in this study includes the investigation of the effect of nanoparticle size and shape and ligand structure (chain length, multivalency) on ligand binding.

References

(1) Aiken, G. R.; Hsu-Kim, H.; Ryan, J. N.: Influence of Dissolved Organic Matter on the Environmental Fate of Metals, Nanoparticles, and Colloids. *Environmental Science & Technology* **2011**, *45*, 3196-3201.

(2) Hinterwirth, H.; Kappel, S.; Waitz, T.; Prohaska, T.; Lindner, W.; Lämmerhofer, M.: Quantifying Thiol Ligand Density of Self-Assembled Monolayers on Gold Nanoparticles by Inductively Coupled Plasma–Mass Spectrometry. *ACS Nano* **2013**, *7*, 1129-1136.

(3) Ansar, S. M. H., R.; Edmonds, B.; Liu, D.; Yu, L.; Sygula, A.; Zhang, D.;: Determination of the Binding Affinity, Packing, and Conformation of Thiolate and Thione Ligands on Gold Nanoparticles. *Journal of physical Chemistry C* **2011**, *115*, 653-660.

(4) Weisbecker, C. S. M., M. V.; Whitesides, G. M.;: Molecular Self-Assembly of Aliphatic Thiols on Gold Colloids. *Langmuir* **1996**, *12*, 3763-3772.

(5) Love, J. C.; Estroff, L. A.; Kriebel, J. K.; Nuzzo, R. G.; Whitesides, G. M.: Self-Assembled Monolayers of Thiolates on Metals as a Form of Nanotechnology. *Chemical Reviews* **2005**, *105*, 1103-1170.

(6) Badia, A.; Demers, L.; Dickinson, L.; Morin, F. G.; Lennox, R. B.; Reven, L.: Gold−Sulfur Interactions in Alkylthiol Self-Assembled Monolayers Formed on Gold Nanoparticles Studied by Solid-State NMR. *Journal of the American Chemical Society* **1997**, *119*, 11104-11105.

(7) Leff, D. V.; Brandt, L.; Heath, J. R.: Synthesis and Characterization of Hydrophobic, Organically-Soluble Gold Nanocrystals Functionalized with Primary Amines. *Langmuir* **1996**, *12*, 4723-4730.

(8) Joshi, H. S., P. S.; Bansal, V.; Ganesh, K. N., Sastry, M.; : Isothermal Titration Studies on the Binding of Amino Acids to Gold Nanoparticles. *Journal of Physical Chemistry B* **2004**, *108*, 11535-11540.

(9) Hotze, E. M.; Phenrat, T.; Lowry, G. V.: Nanoparticle aggregation: Challenges to understanding transport and reactivity in the environment. *Journal of environmental quality* **2010**, *39*, 1909-1924.

(10) M. J. Hostetler, A. C. T. a. R. W. M.: *Langmuir* **1999**, *15*, 3782.

(11) Templeton, A. C.; Wuelfing, W. P.; Murray, R. W.: Monolayer-Protected Cluster Molecules. *Accounts of Chemical Research* **1999**, *33*, 27-36.

(12) Guo, R. S., Y.; Wang, G.; Murray, R. W.;: Does Core Size Matter in the Kinetics of Ligand Exchanges of Monolayer-Protected Au Clusters? *The Journal of the American Chemical Society* **2005**, *128*, 2752-2757.

(13) Woerhrle, G. H. B., L. O.; Hutchison, J. E.;: Thiol-Functionalized, 1.5-nm Gold Nanoparticles through Ligand Exchange Reactions: Scope and Mechanism of Ligand Exchange. *The Journal of the American Chemical Society* **2004**, *127*, 2172-2183.

(14) Woerhrle, G. H. W., M. G.; Hutchison, J. E.;: Ligand Exchange Reactions Yield Sudnanometer, Thiol-Stabilized Gold Particles with Defined Optical Transitions. *Journal of Physical Chemistry* **2002**, *106*, 9979-9981.

(15) Ohno, K.; Koh, K.-m.; Tsujii, Y.; Fukuda, T.: Synthesis of Gold Nanoparticles Coated with Well-Defined, High-Density Polymer Brushes by Surface-Initiated Living Radical Polymerization. *Macromolecules* **2002**, *35*, 8989-8993.

(16) Kassam, A.; Bremner, G.; Clark, B.; Ulibarri, G.; Lennox, R. B.: Place Exchange Reactions of Alkyl Thiols on Gold Nanoparticles. *Journal of the American Chemical Society* **2006**, *128*, 3476-3477.

(17) Thio, B. J. R.; Montes, M. O.; Mahmoud, M. A.; Lee, D.-W.; Zhou, D.; Keller, A. A.: Mobility of Capped Silver Nanoparticles under Environmentally Relevant Conditions. *Environmental Science & Technology* **2011**, *46*, 6985-6991.

(18) Bourg, M.-C.; Badia, A.; Lennox, R. B.: Gold−Sulfur Bonding in 2D and 3D Self-Assembled Monolayers: XPS Characterization. *The Journal of Physical Chemistry B* **2000**, *104*, 6562-6567.

(19) Gai, P. L.; Harmer, M. A.: Surface Atomic Defect Structures and Growth of Gold Nanorods. *Nano Letters* **2002**, *2*, 771-774.

(20) Hostetler, M. J.; Murray, R. W.: Colloids and self-assembled monolayers. *Current Opinion in Colloid & Interface Science* **1997**, *2*, 42-50.

(21) A. Ivanisevic, K. V. M. a. C. A. M.: Site-Directed Exchange Studies with Combinatorial Libraries of Nanostructues. *Journal of the American Chemical Society* **2002**, *124*, 11997.

(22) Kell, K. J. D., R. L.; Workentin, M. S.;: Core Size Effects on the Reactivity of Organic Substrates as Monolayers on Gold Nanoparticles. *Langmuir* **2004**, *21*, 735-752.

(23) Fabrega, J.; Fawcett, S. R.; Renshaw, J. C.; Lead, J. R.: Silver Nanoparticle Impact on Bacterial Growth: Effect of pH, Concentration, and Organic Matter. *Environmental Science & Technology* **2009**, *43*, 7285-7290.

(24) Chechik, V.: Reduced Reactivity of Aged Au Nanoparticles in Ligand Exchange Reactions. *The Journal of the American Chemical Society* **2004**, *126*, 7780-7781.

(25) Thompson, G.; Owen, D.; Chalk, P. A.; Lowe, P. N.: Delineation of the Cdc42/Rac-Binding Domain of p21-Activated Kinase. *Biochemistry* **1998**, *37*, 7885-7891.

(26) Künne, A. G. E.; Sieber, M.; Meierhans, D.; Allemann, R. K.: Thermodynamics of the DNA Binding Reaction of Transcription Factor MASH-1†. *Biochemistry* **1998**, *37*, 4217-4223.

(27) Wenk, M. R.; Seelig, J.: Magainin 2 Amide Interaction with Lipid Membranes: Calorimetric Detection of Peptide Binding and Pore Formation†. *Biochemistry* **1998**, *37*, 3909-3916.

(28) Gourishankar, A.; Shukla, S.; Ganesh, K. N.; Sastry, M.: Isothermal Titration Calorimetry Studies on the Binding of DNA Bases and PNA Base Monomers to Gold Nanoparticles. *Journal of the American Chemical Society* **2004**, *126*, 13186-13187.

(29) J. Turkevich, P. C. S., J. Hillier: A study of the nucleation and growth processes in the synthesis of colloidal gold. *Discussions of the Faraday Society* **1951**, *11*, 55-75.

(30) Majzik, A. P., R.; Hornok, V.; Dekany, I.;: Growing and stability of gold nanoparticles and their functionalization by cysteine. *Gold Bulletin* **2009**, *42*, 113-123.

(31) Gans, P.; Sabatini, A.; Vacca, A.: Simultaneous Calculation of Equilibrium Constants and Standard Formation Enthalpies from Calorimetric Data for Systems with Multiple Equilibria in Solution. *J Solution Chem* **2008**, *37*, 467-476.

(32) Caragheorgheopol, A., Chechik, V.: Mechanistic aspects of ligand exchange in Au Nanoparticles. *Physical Chemistry Chemical Physics* **2008**, *10*, 5029-5041.

(33) Hostetler, M. J.; Templeton, A. C.; Murray, R. W.: Dynamics of Place-Exchange Reactions on Monolayer-Protected Gold Cluster Molecules. *Langmuir* **1999**, *15*, 3782-3789.

(34) Templeton, A. C. H., M. J.; Kraft, C. T.; Murray, R. W.;: Reactivity of Monolayer-Protected Gold Cluster Molecules: Steric Effects. *The Journal of the American Chemical Society* **1998**, *120*, 1906-1911.

(35) M. Hasan, D. B. a. M. B.: *Journal of the American Chemical Society* **2002**, *124*, 1132.

(36) Grönbeck, H.; Curioni, A.; Andreoni, W.: Thiols and Disulfides on the Au(111) Surface: The Headgroup−Gold Interaction. *Journal of the American Chemical Society* **2000**, *122*, 3839-3842.

(37) Hakkinen, H. B., R. N.; Landman, U.: *Phys. Rev. Lett.* **1999**, *82*, 3264.

(38) Nuzzo, R. G.; Zegarski, B. R.; Dubois, L. H.: Fundamental studies of the chemisorption of organosulfur compounds on gold(111). Implications for molecular self-assembly on gold surfaces. *Journal of the American Chemical Society* **1987**, *109*, 733-740.

(39) Jain, P. K.; Lee, K. S.; El-Sayed, I. H.; El-Sayed, M. A.: Calculated Absorption and Scattering Properties of Gold Nanoparticles of Different Size, Shape, and Composition: Applications in Biological Imaging and Biomedicine. *The Journal of Physical Chemistry B* **2006**, *110*, 7238-7248.

(40) Haiss, W.; Thanh, N. T. K.; Aveyard, J.; Fernig, D. G.: Determination of Size and Concentration of Gold Nanoparticles from UV−Vis Spectra. *Analytical Chemistry* **2007**, *79*, 4215-4221.

(41) Lee, K.-S. a. M. A. E.-S.: Gold and Silver Nanoparticles in Sensing and Imaging:‚Äâ Sensitivity of Plasmon Response to Size, Shape, and Metal Composition. *Journal of Physical Chemistry B* **2006**, *110*, 19220-19225.

(42) Weast, R. C.: *Handbook of Chemistry and Physics*; 57 ed.; CRC Press: Cleveland, 1976.

(43) McCash, E.: *Surface Chemistry*; Oxford University Press: UK, 2001.

CHAPTER FOUR

NATURAL ORGANIC MATTER AND ELECTROLYTE EFFECTS ON THE MOBILITY, DISSOLUTION AND SORPTION OF SILVER NANOPARTICLES

Abstract

The growing development and application of nanomaterials will inevitably lead to engineered nanoparticles in the environment. As a result, concern of the environmental fate and implications of these materials becomes imperative. In this study, the transport of silver nanoparticles was monitored through IOTA standard high purity quartz powder using miscible displacement column and batch nanoparticle dissolution experiments. Suspensions of nanoparticles stabilized with citrate or Suwanee River natural organic matter were introduced as a finite step of one column volume, followed by electrolyte solutions of 0.001M NaCl, $(CH_3)_4NClO_4$, or $NaClO_4$ at pH 6. The concentration of silver in the column effluent was monitored via inductively couple plasma mass spectroscopy. Results for citrate-stabilized silver nanoparticles with the NaCl electrolyte solution exhibited an initial breakthrough curve followed by a second breakthrough, which is attributed to enhanced nanoparticle dissolution by chloride ions. Similar experiments with citrate-stabilized silver nanoparticles in $(CH_3)_4NClO_4$, or $NaClO_4$ did not display a second breakthrough curve. No second break through curve was seen in the results of columns spiked with natural organic matter passivated silver nanoparticles in NaCl or $(CH_3)_4NClO_4$. Batch studies revealed that the studied concentrations, 20 % of citrate-stabilized silver nanoparticles in the absence of electrolytes is in the form of silver ions. In the presence of NaCl, 75% of these free ions form insoluble AgCl. Batch studies also

indicated that the release of ions from natural organic matter stabilized silver nanoparticles (2% Ag^+) was significantly lower than that of citrate stabilized silver nanoparticles, (20% Ag^+). Results from this study suggest that nanoparticle dissolution occurs for citrate stabilized silver nanoparticles in NaCl and the presence natural organic matter inhibits dissolution enhancement and the formation of free silver ions.

Introduction

The Project on Emerging Nanotechnologies at the Woodrow Wilson Center for Scholars reported, as of October 2013, 1628 consumer products containing nanomaterials, with 410 containing silver nanomaterials.[1] These products include textiles, cosmetics, paints, cleaners and plastics.[2, 3] Piccino reported that 55 tons of silver nanomaterials are produced worldwide each year.[4] Several reviews have called for a better understanding of the fate and transport properties of nano-materials in order to better assess the risk to human and environmental health.[5-10] Environmental systems are dynamic and heterogeneous, which greatly complicates the understanding of the risks associated with engineered nanoparticles (ENPs) released into the environment. ENPs have the potential to undergo many transformations in the environment such as reactions with biomacromolecules, redox reactions, aggregation, and dissolution depending on the exposure to environmental conditions.[7, 11] Furthermore, each of these occurrences can affect stability and aggregation potential of ENPs.[6, 7, 12-14] Organic macromolecules are commonly used to coat nanoparticles and provide enhanced colloidal stability over the metal core alone. Increased stability is achieved by

electrostatic, steric, or electrosteric stabilization (a combination of both) in which surface molecules provide enhanced colloidal stability and prevent irreversible aggregation for a diversity of applications.[15, 16]

Natural organic matter, NOM, is a class of natural organic macromolecules, ubiquitous in nature and typically present in concentrations that are orders of magnitude higher than the potential concentration of engineered nanoparticles in natural waters.[7] NOM has a complex molecular structure that contains many functional groups such as alcohols, hydroxyls, aldehydes, ketones, and thiols; all having the ability to serve as binding and reduction sites for nanoparticles and metal ions. NOM has the potential to substantially modify ENP toxicity[17-23] by blocking oxidation sites[24] and complexing with released metal ions.[25] NOM can also alter fate and transport of ENPs by enhancing the colloidal stability and reducing aggregation and deposition.[20, 26] Most nanoparticles are prone to NOM adsorption, including gold,[27] iron,[12, 28] titanium dioxide,[29, 30] aluminum oxide,[31, 32] carbon nanotubes,[33, 34] and boron nanoparticles.[35] Furman et al. reported that steric stabilization by NOM may play an important role in AgNP transformations and mobility because this mechanism of stabilization provides resistance against nanoparticle aggregation and dissolution when exposed to natural salts.[20] They demonstrated that higher molecular weight NOM had a higher affinity to AgNP surfaces than lower molecular weight NOM and was more effective at stabilizing AgNPs over a range of pH and ionic strength.[20] This increased stability leads to enhanced silver nanoparticle mobility in natural waters, making them more bioavailable to aquatic organisms.[2, 20] NOM can also reduce Ag^+ and form

AgNPs at room temperature over a period of days. [21, 36] Nanoparticle dissolution is a key component in determining the toxicity, transport properties, and ultimately the end fate of these materials. In recent years, there has been a large body of work focused on the impacts of nanoparticle dissolution on AgNP toxicity; however there is little work focused on how these factors impact nanoparticle transport. Furthermore, because of highly variability of environmental systems, a study that investigates the nanoparticle dissolution and fundamental transport properties under ideal conditions is needed in order to better design and predict the outcome of environmentally relevant experiments. This study investigates the dissolution and transport and of silver nanoparticles stabilized with citrate or NOM in the presence of variable electrolyte solutions in ultrapure quartz columns. This study also outlines an experimental procedure that can be used for various types of nanomaterials and environmental settings. This work is significant due to the length of the column experiments performed, over 100 pore volumes, which a provided insight on the long term effects of silver nanoparticles

Experimental

Nanoparticle Synthesis

Silver nanoparticles stabilized by citrate, (citrate AgNPs), were synthesized using methods described previously.[37, 38] In short, a 50 mL solution of 0.25mM silver nitrate (99.95% purity, Alfa Aesar) and 0.25mM trisodium citrate dihydrate (99% purity, Alfa Aesar) was prepared in DDI water. While mixing, 0.5 mL of 0.05M aqueous sodium borohydride (EMD chemicals) was added drop wise to the silver salt/citrate solution. The

resulting bright yellow solution and was mixed for 15 minutes, then dialyzed in DDI H_2O, with 3000 MW cellulose acetate dialysis tubing for 24 hours to remove excess reactants. Suwanee River NOM stabilized particles, (NOM AgNPs), were synthesized by the same method with the addition of NOM to the nanoparticle solution after dialysis in a ratio of 3g of NOM per gram of silver. The nanoparticles were characterized by transmission electron microscopy, Figure 4-1, using a Hitachi 7600 TEM, and by UV-Vis spectroscopy on a Varian Cary 50 spectrophotometer.

Column Experiments

An 8.3 cm long, 0.5 cm inner diameter, polycarbonate column was assembled and packed with ultra-pure quartz powder (IOTA-STD, Unimin Corp, Spruce Pine, NC) 1 cm at a time, tapping the column to ensure tight packing. The powder was chosen because of its minimal

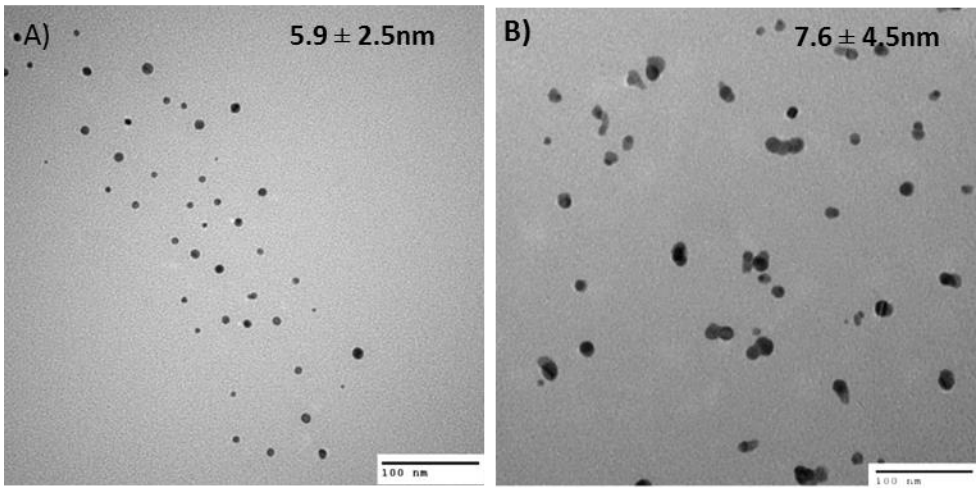

Figure 4 -1: TEM imaged of A) citrate stabilized AgNPs and B) NOM capped AgNPs

interaction with most substances and high purity. Type 13 Masterflex C-type tubing was used to introduce the flush solution into the column. The pore volumes of each experiment were determined by weighing the dry packed column then weighing the column after being saturated with nanoparticle free electrolyte solution for 12 hours. A flow rate of 0.1 mL/min (Masterflex digital pump) was used to obtain a residence time of approximately one hour. Effluent samples were analyzed by inductively coupled plasma mass spectroscopy (ICP-MS, Thermo Scientific X Series II) to determine Ag concentration. Pore volumes for each column were 6.5 to 7mL depending on the porosity of the column and spike volumes were approximately 7 mL. Each AgNP spike solution was prepared to be 3500 to 4500ppb Ag then ionic strength adjusted to 0.001M electrolyte. The pH of each spike solution was adjusted to 6 with dilute HNO_3 to ensure a negative surface charge on the silver nanoparticles. This was done in order to decrease NP-NP and NP-packing interactions. Each spike solution also contained 10ppb of rhenium as a tracer to characterize residence time and flow. Exact pore volumes and spike concentrations can be found in Table 1.After saturating each column with nanoparticle free electrolyte solution, the tubing leading into the column was flushed with the AgNP spike solution in order to achieve equilibrium adsorption of silver on the tube walls. This was done in order to achieve a high recovery of silver from each experiment. One pore volume of spike at the same ionic strength as the electrolyte solution was then introduced onto the column as a finite step followed by at least 125pore volumes of nanoparticle free electrolyte solution. Electrolytes used to adjust ionic strength were 0.001M NaCl, tetramethylammonium perchlorate, TMAP, or $NaClO_4$. The columns will

be referred to with the following notation; (A) citrate AgNPs in NaCl, (B) citrate AgNPs in TMAP, (C) citrate AgNPs in $NaClO_4$, (D) NOM AgNPs in NaCl and (E) NOM AgNPs in TMAP. After approximately 120 pore volumes, each column was flushed with one pore volume of DDI water, followed by 3 pore volumes of electrolyte solution, then with a high ionic strength solution, 0.1M NaCl, for columns A and D, or a change in electrolyte, 0.001M NaCl in the case of columns B, C and E. Ionic strength flushes were performed to study the effect of ionic strength and electrolyte type on nanoparticle solubilization. Following nearly 125 pore volumes, each column was segmented into 1 cm portions. Each portion was digested in 2% nitric acid (BDH Falcon Aristar Plus) over night and the liquid phase was analyzed for silver content three times on the ICP-MS.

Table 4-1: Spike volumes and concentrations

NP	Electrolyte, 0.001M, pH 6	$[Ag]_{Spike,}$ (ppb)	Pore Volume, PV	Spike Volume, V_s
Ag-Citrate	NaCl	3440	6.55	6.7
	TMAP	4277	7.25	7.9
	$NaClO_4$	4640	7.03	7.07
Ag-NOM	NaCl	3190	6.84	6.8
	TMAP	4655	6.96	7.4

Batch Dissolution

Batch dissolution experiments were performed on model spike solutions to determine the chemical state of silver in each spike solution. Citrate and NOM coated AgNPs in the absence of electrolytes were used as a control. Each NP solution was prepared at approximately 3500 ppb Ag, and then adjusted to 0.001M ionic strength for

the electrolytes used in the column experiments. After 24 hours of mixing, 4mL of each solution was immediately centrifuged at 8000 rpm in 3kDa MW cut off polysulfone centrifuge filters (Millipore Corp) to separate soluble Ag ions/species from AgNPs. Each sample was first centrifuged for 3 minutes, to let 1mL pass through and saturate the filter. The filtrate was discarded and the remaining 3 mL of solution were centrifuged at 8000rpm for 45 minutes until all of the liquid passed through the filter. The silver concentration in the filtrate was measured on ICP-MS.

Results and Discussion

Citrate-stabilized Silver Nanoparticles

There are four distinct transport regions in column A, which was spiked with citrate-stabilized AgNPs in a 0.001M NaCl electrolyte solution, Figure 4-2a. The first region is the initial peak, which is the nearly unretarded transport of NPs through the column during the first 3 pore volumes. We know that the silver eluting from the column is in the form of nanoparticles because the effluent is yellow in color. This peak accounted for 32 % of the silver in the spike, with a retardation factor of 1.23. This retardation factor indicated that the nanoparticles were relatively mobile, but it is important to note that it applies to only the 32% of the total silver that eluted off the column in the initial peak. This region is followed by a diffusion tail, which is the second transport region and accounts for 7 % of the total silver. Ag^0 has a tendency to oxidize and complex with Cl^- ions and form AgCl precipitates that have a significantly lower solubility than Ag^+ ions.[39] AgCl has a K_{sp} of $1.8*10^{-10}$ at 25 °C, which results in AgCl

precipitation when the Ag concentration is greater than 19.4 ppm in the presence of 0.001M Cl. [39] Speciation calculations indicate that insoluble silver chloride is present in the spike solution prior to introduction to the column. The silver concentration in the spike was measured at 3438 ppb, and with a Cl^- concentration of 0.001M, solid AgCl may form, since the solubility limit of AgCl at 25 ºC is 475.7ppb.[39] These precipitates would likely follow a more tortuous pathway through the column packing and thus elute from the column more slowly than dispersed AgNPs, as dissolved AgCl. Therefore it is likely that both AgNPs and AgCl are eluting from the column in the diffusion tail. The third transport region is a second breakthrough, starting at the 20th pore volume. There are two possible explanations of the second breakthrough curve; speciation calculations indicate that solid AgCl may have been present in the spike solution before this solution

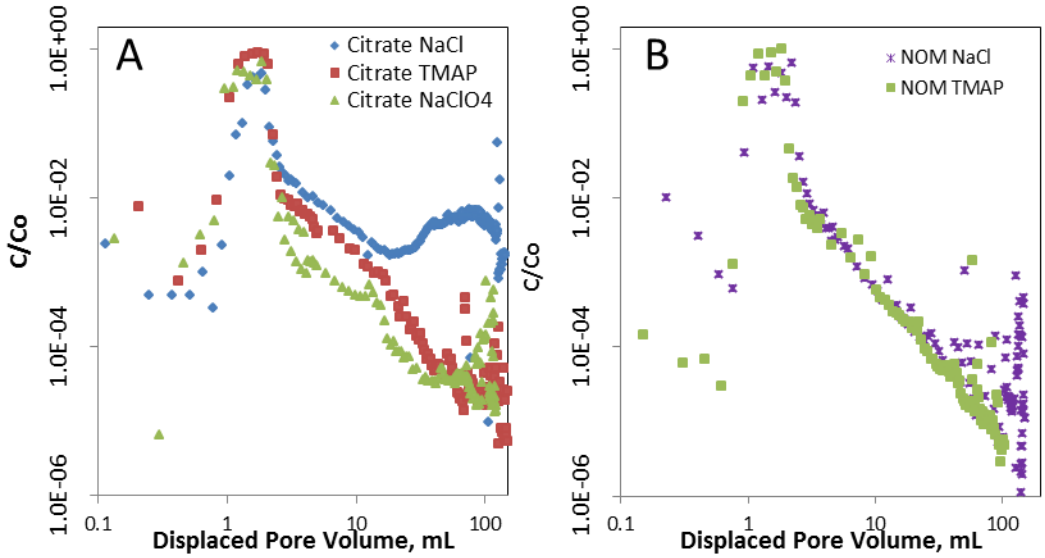

Figure 4-2: The Concentration of silver in column effluent was normalized to spike silver concentrations and plotted vs displaced pore volume on a log-log scale; A) Ag-Citrate and B) Ag-NOM NPs

was introduced to the column, and these particles may have taken a more torturous pathway through the quartz powder and thus eluted after the nanoparticles. When the solid precipitates exit the column, they encounter a concentration gradient and solubilize. This region accounted for 55 % of the silver in the spike, a significant amount. Li et al. showed that a layer of AgCl can from on the surface of AgNPs that will inhibit NP dissolution at low $[Cl^-]/[Ag^+]$ ratios.[40] The second breakthrough of silver in column A may also be due to the kinetics of the formation and dissolution of an AgCl layer on AgNPs adsorbed to the quartz powder, since higher $[Cl^-]/[Ag^+]$ would be necessary for dissolution of the AgCl layer. This region accounted for 55 % of the silver in the spike, a significant amount. Figure 3 depicts a plot of $[Cl^-]/[Ag^+]$ as a function of pore volume for column A. Brown *et al.* investigated the effect of Cl^- on AgNP dissolution rates and demonstrated that as the $[Cl^-]/[Ag^+]$ increases, the formation of soluble $AgCl_x^{(x-1)-}$ is thermodynamically favorable.[40] A $[Cl^-]/[Ag^+]$ of 2383 represents the solubility limit of AgCl for the conditions in column A, which is indicated by the red line in Figure 4-4. Ratios above this limit result in the formation of soluble $AgCl_x^{(x-1)-}$ species. Ratios below this limit result in the formation of zero-valent silver, which may be in the form of nanoparticles or solid AgCl. Figure 5 depicts a speciation diagram of silver as a function of chloride ion concentration with data points from column A. Many points from the initial spike fall in the zero-valent silver phase, supporting that silver was in nanoparticle or solid AgCl form, while the other points fall in the soluble AgCl phase, the red line in this plot also represents the solubility limit of AgCl, while black lines represent phase boundaries. Similar speciation diagrams have been used by other research groups as

well.[40] Data points from the diffusion tail and second breakthrough curve fall in the soluble AgCl phase, which is consistent with the column results. In the fourth transport region the column was flushed with one pore volume of DDI water, 3 pore volumes of electrolyte solution, and then one pore volume of 0.1M NaCl, Figure 4-5.

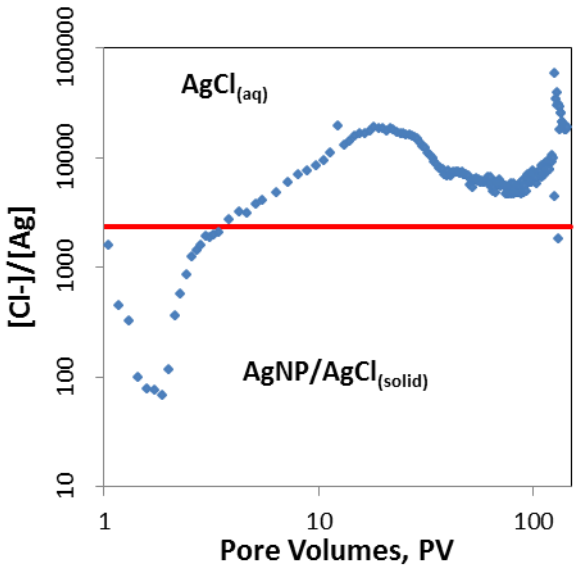

Figure 4-3: Plot of the ratio of chloride ions to silver ions as a function of pore volume in column A.

In the fourth transport region the column was flushed with one pore volume of DDI water, 3 pore volumes of electrolyte solution, and then one pore volume of 0.1M NaCl, Figure 4-5. When DDI water is passed through column A, the silver concentration decreased slightly; Figure 5a, section 1. Had these concentrations of silver been in the form of NPs, lowering the ionic strength should increase the double layer thickness and this would theoretically enhance NP transport; thus increasing the silver concentration in

the effluent. This suggests that the silver at this point in the column was in the form of AgCl and not nanoparticles. An observed 2 orders of magnitude increase in silver concentration in the effluent with increased NaCl concentration,

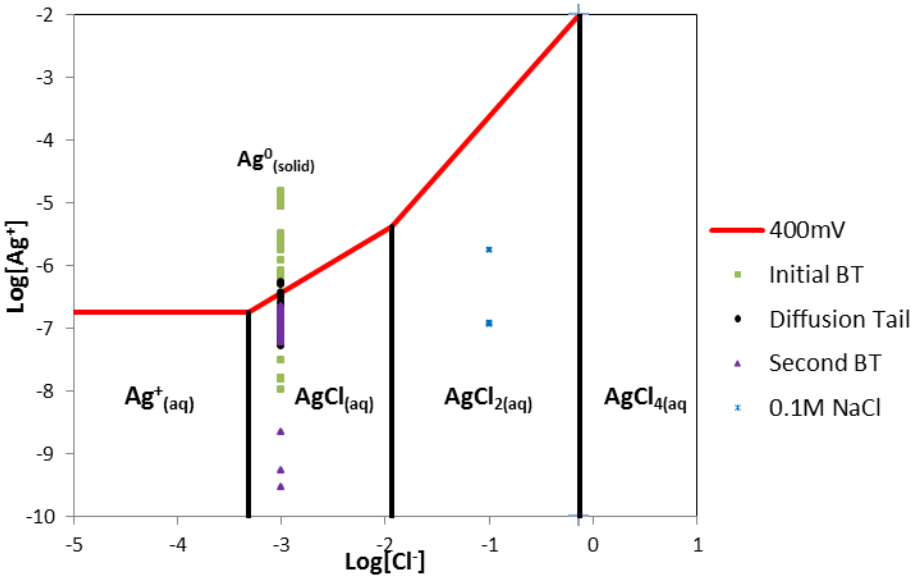

Figure 4-4: Speciation diagram of AgCl as a function of ionic silver and ionic chloride concentration

Figure 5a, section 2, supports the argument that soluble $AgCl_x^{(x-1)-}$ species are present. The data points from the ionic strength swing with 0.1M NaCl, fall in the $AgCl_2$ phase providing evidence that soluble $AgCl_x^{(x-1)-}$ species are indeed forming.

Tetramethyl ammonium perchlorate, $(CH_3)_4NClO_4$, or TMAP, was chosen as a second electrolyte due to perchlorate's (ClO_4^-) weak oxidation potential. The central chlorine in a perchlorate anion is a closed shell atom and is well protected by the four oxygen atoms. Hence, perchlorates do not react with silver ions as chloride anions do. The results from column B, Figure 4-2a, display an initial breakthrough curve that is

broader than the initial breakthrough curve in column A accounting for 94 % of the recovered, and a diffusion tail, accounting for only 4.4 % of the recovered silver. The retardation factor for column B was calculated to be 1.39, which is slightly higher than

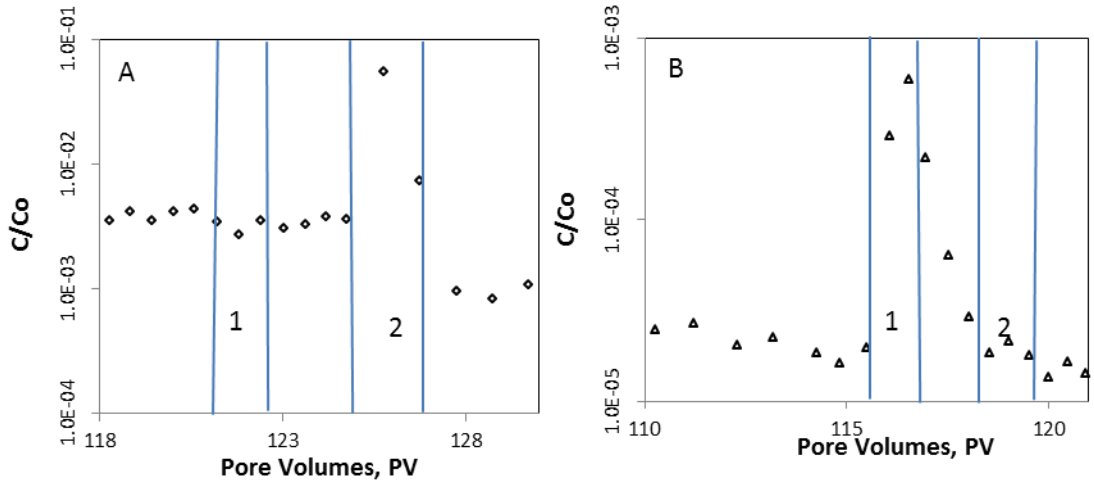

Figure 4-5: Plots of normalized concentration of silver in effluent vs. displaced pore volumes in the regions of ionic strength flushes: A) Ag-Citrate in 0.001M NaCl, B) Ag-Citrate in 0.001M $NaClO_4$

the retardation factor for column A, but this retardation factor is skewed by the higher percentage of silver in the first break though curve. A higher recovery of silver in the initial breakthrough curve is expected since no Cl^- is present to form AgCl precipitates. The results do not show a second breakthrough curve, which confirms the conclusions from column A. Since there are no Cl^- ions to complex with silver from the AgNPs, and the lack of reactivity of perchlorate, AgNP dissolution and AgCl dispersion or solubilization do not occur, which explains the lower recovery of silver in the diffusion tail. Table 4-2 summarizes the mass balances and retardation factors for each column, with recoveries of silver from each transport region. Per cent recoveries were calculated

with respect to total concentration of silver in the spike solution, and per cent of total recoveries were calculated with respect to the amount of silver recovered from each column. Column B was also subjected to ionic strength flushes; however there was no change in the effluent silver concentration with either flush.

Table 4-2: Mass balances of each column. Recoveries were also normalized to the total recovery of Ag in each column to column to column comparison

		Initial Break through		Diffusion Tail		Second Break through		Quartz Powder		Total Recovery
Column	**R**	**%**	**% of total**	**%**	**% of total**	**%**	**% of total**	**%**	**% of total**	**%**
A	1.23	32	32.3	7	7.1	55	55.9	4.9	4.9	98.9
B	1.39	81	94.2	3.8	4.4	-	-	0.48	0.56	86.0
C	1.49	61.9	97.5	1.73	3.1	-	-	0.41	0.65	63.5
D	1.08	59	95.5	2.7	4.4	-	-	0.85	1.4	61.9
E	1.36	70	86.2	2.3	2.8	-	-	0.48	0.59	81.2

Sodium perchlorate, $NaClO_4$, was also used as an electrolyte with citrate-stabilized AgNPs, column C. The effluent concentrations of this column are shown in Figure 4-2a. This column also exhibits an initial breakthrough curve that accounted for 98 % of the total silver recovered, and diffusion tail, accounting for 3.1 % of the total silver recovered. Similar to column B, no second breakthrough curve was observed due to the lack of Cl^-. Column C was also subjected to ionic strength flushes; DDI H_2O and 0.001M NaCl. 0.001M NaCl was used instead of 0.1M to limit the changes to the experiment. The concentration of silver increased by 2 orders of magnitude during the flush with DDI water, suggesting that this silver is in the form of NPs. Flushing the column with DDI water may have increased the double layer thickness of the nanoparticles, facilitating the

desorption of AgNPs from the quartz powder and enhancing mobility through the column. A change in Ag concentration was not seen when column C was flushed with 0.001 M NaCl.

NOM-Passivated Silver Nanoparticles

The transport of AgNPs passivated with Suwanee River natural organic matter, NOM, was investigated in 0.001M NaCl (column D), and TMAP (column E). The results from column D, Figure 4-2b, portray a large initial peak, and long diffusion tail, but do not display a second breakthrough curve. NOM is a large multifunctional molecule that adheres to most surfaces; including nanoparticles where it provides enhanced electrostatic and steric stabilization to AgNPs. 95.5 % of the total recovery of silver is accounted for in the initial breakthrough, with a retardation factor of 1.08, and 4.4 % of the recovered silver is accounted for in the diffusion tail. This column resulted in the smallest retardation factor, indicating that these particles were the most mobile relative to the other columns, and that NOM is enhancing AgNP mobility. The lack of a second breakthrough curve indicates that NOM is shielding the AgNPs from dissolution caused by NaCl that was seen in column A. NOM prevents dissolution by blocking the oxidation sites on the AgNP surface. [24] The total recovery of silver that eluted from the column was 61.9%. The decrease in total recovery for this column relative to the other columns is likely due to incomplete equilibrium adsorption of silver to the tubing leading to the column. If this tubing was not flushed with nanoparticle solution long enough prior to the experiment, some of the silver in the spike would adsorb to the tubing and subsequently not enter the column.

The results for column E, NOM-AgNPs with TMAP are also shown in Figure 4-2b. 86.2 % of the recovered silver eluted from the column in the initial breakthrough and exhibited a retardation factor of 1.36. TMAP may be interfering with the NOM coated AgNPs and causing them to elute more slowly from the column. 2.8 % of the recovered silver eluted from the column in the diffusion tail. There was also no second breakthrough of silver in column E, which was expected since there was no free chloride in solution to interact with the nanoparticles. After at least 120 pore volumes, columns D and E were both flushed with one pore volume of DDI water, 3 pore volumes of background solution, then with 0.1M NaCl in column D and 0.001M NaCl in column E. Neither column displayed a trend with these flushes. This suggests that the presence of NOM is effectively screening the ionic interactions. There are few points that are higher concentrations of silver above 100 pore volumes in column D and E that can be explained by small concentrated pockets of silver nanoparticles in the column packing that were released towards the end of the experiment.

Column Segmentation

The electrolyte solutions were stopped in each column after the ionic strength flushes and 125 pore volumes. Each column was segmented into 1cm sections of quartz powder, washed with 2% HNO3 for 24 hours, and analyzed for silver content on ICP-MS to determine the total remaining concentration and concentration profile of silver in each column. Figure 5 displays the mass of silver in each column as a function of column height. The recovery of silver in column A, citrate-stabilized AgNPs in 0.001M NaCl, was 4.9%. The silver left in column A is likely due to residual insoluble AgCl

precipitates on the quartz powder. The residual silver in the other columns was significantly lower at 0.48% in column B and 0.41 % in column C.

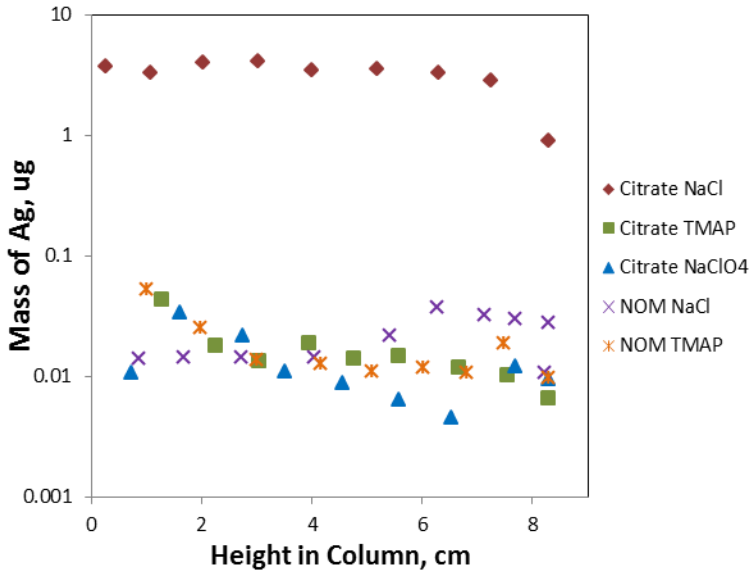

Figure 4-6: Plot of the concentration of silver recovered from column packing as a function of height

The absence of free chloride in columns B and C, reinforces the conclusion that the remaining silver is in the form of AgCl precipitates. Columns D and E, NOM-AgNPs in 0.001M NaCl and 0.001M TMAP, respectively, contained 0.73% and 0.46% of the spike silver in the quartz powder, respectively. This provides evidence that NOM inhibits AgNP adsorption to quartz powder.

Batch Dissolution

Batch dissolution experiments were conducted on each spike solution to determine the extent of ionization in each 0.001M electrolyte solution, as well as an electrolyte free

control, after 24 hours. Results from this study, Figure 6, revealed that electrolyte free citrate AgNP contained about 20 % of silver in ionic form, and citrate AgNPs in NaCl

Table 4-3: Characterization of AgNPs via UV-Vis and DLS

NP	Electrolyte Solution, pH 6, 0.001M	Maximum Wavelength, (nm)	Z-Avg R_h, (nm)	Zeta Potential, ζ, (mV)
Ag-Citrate	Control	406.1	35.2	-34.3
	NaCl	404.1	45.09	-25.2
	TMAP	405.0	58.68	-26.7
	$NaClO_4$	408.9	53.33	-21.5
Ag-NOM	Control	408.0	30.3	-31.7
	NaCl	405.0	70.55	-30.8
	TMAP	403.0	52.64	-29.7
	$NaClO_4$	418.2	61.93	-22.6

contained less than 5 % ionic silver. Speciation calculations indicated, at the concentrations of Ag^+ and Cl^- in the solution, the formation of insoluble AgCl. As stated previously the K_{sp} of AgCl in water at 25 C is $1.8*10^{-10}$,[39] and the molar solubility at these conditions is 475.7 ppb. Therefore at 0.001M Cl^-, concentrations of silver above 19.4 ppb Ag^+ would result in the formation of AgCl. The concentration of Ag^+ in the Citrate AgNP/NaCl batch solution was 1200 ppb, therefore AgCl would form at concentration above the solubility limit. Filtration experiments indicated that insoluble AgCl would pass through the filters. Citrate AgNP in 0.001 M TMAP or $NaClO_4$ both contained a higher percentage of ionic silver than electrolyte free citrate AgNPs. Citrate AgNPs in 0.001M TMAP contained about 33% silver in the form of ions and about 27% in 0.001M $NaClO_4$. While perchlorate ions are unlikely to complex with silver ions in solution, they could potentially destabilize the nanoparticle–ligand shells allowing for a

higher degree of AgNP dissolution compared to electrolyte free AgNPs. These ions would not form insoluble precipitates, therefore a second breakthrough of silver would

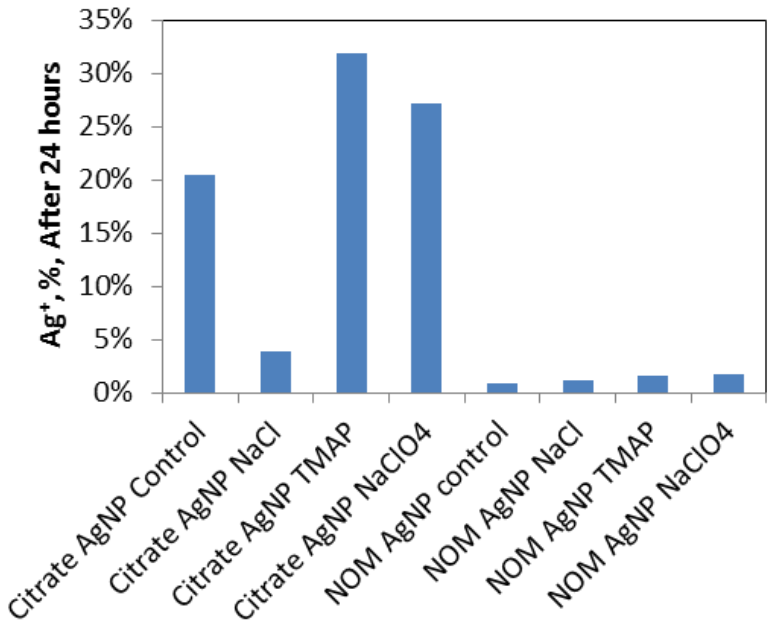

Figure 4-7: Plot of the extent of AgNP ionization after 24 hours

not occur in the column study. The zeta potential of citrate AgNPs decreased from -34.3 mV in the control to -25.2 mV, Table 3, when TMAP was present, indicating that TMAP is indeed destabilizing the AgNPs. NOM AgNP were not as effected by electrolyte solutions and exhibited lower extents of dissolution than the citrate AgNP electrolyte solution. This indicated that NOM is inhibiting AgNP dissolution by provide greater stabilization than citrate and screening ionic interactions. NOM can also chelate any free silver ions in solution; therefore these ions would not pass through the filter because of the molecular weight of NOM.

Conclusions

We have investigated the influence of NOM and electrolyte type and concentration on the mobility of silver nanoparticles through ultrapure quartz powder. We established that even under ideal conditions, AgNPs will interact with a solid phase. In the presence of NaCl, AgNPs will dissolve and from AgCl. Column A, citrate AgNPs in 0.001 M NaCl, exhibited a narrow initial breakthrough curve with a low recovery of silver, then a second breakthrough curve due to the slower elution of AgCl. Our results indicated that when exposed to high ionic strengths (0.1M) of NaCl, soluble $AgCl_x^{(x-1)-}$ formed. Further evidence of the formation of AgCl precipitates is provided when this column was segmented and 4.5% of the initial silver was recover from the packing. Perchlorate electrolytes do not interact with AgNPs to the extent of chloride electrolytes due to its weak oxidation potential. This was demonstrated in columns B and C, which had higher recoveries of silver their initial breakthroughs and neither column had a second breakthrough curve. We have also demonstrated that NOM plays an important role in the fate and transport of AgNPs. NOM effectively shields AgNPs from ionic interactions and inhibits the deposition of AgNPs onto quartz powder, as seen in column D. This column had a high recovery of silver in its initial breakthrough and no second breakthrough curve, providing evidence that NOM is shielding AgNPs from chloride ion attack and only 0.7% of the initial silver was recovered from the column packing. Our batch dissolution experiments also demonstrate that NOM inhibits the dissolution of AgNPs. After 24 hours of exposure to electrolytes, NOM-passivated AgNPs released less than 5% of the total silver concentration in ionic form. These findings are import in determining the environmental implications of silver nanoparticles. Every body of water

will have a significant amount of sodium chloride, whether natural or sea water. Natural organic matter is an abundant material in natural waters and has the potential for being carried to sea water, especially when bound to mobile particulate matter. Studying the effects of NaCl, as well as other electrolytes, and NOM on nanoparticle transport is quintessential in determining the environmental fate of these materials. Future work for this study would include investigating other environmental conditions such as the effect of nanoparticle age, and futher investigation of the effect of NOM by incorporating NOM into the column packing before spiking the column with nanoparticles.

References

1. Scholars, W.W.I.C.f. *Consumer Products Inventory*. The Project on Emerging Nanotechnologies 2014; Available from: http://www.nanotechproject.org/cpi/.

2. Mueller, N.C. and B. Nowack, *Exposure Modeling of Engineered Nanoparticles in the Environment.* Environmental Science & Technology, 2008. **42**(12): p. 4447-4453.

3. Benn, T.M. and P. Westerhoff, *Nanoparticle Silver Released into Water from Commercially Available Sock Fabrics.* Environmental Science & Technology, 2008. **42**(11): p. 4133-4139.

4. Fabiano Piccinno, F.G., Stefan Seeger, Bernd Nowack, *Industrial production quantities and uses of ten engineered nanomaterials in Europe and the world.* Journal of Nanoparticle Research, 2012. **14**.

5. Nel, A., et al., *Toxic Potential of Materials at the Nanolevel.* science, 2006. **311**(5761): p. 622-627.

6. Levard, C., et al., *Environmental Transformations of Silver Nanoparticles: Impact on Stability and Toxicity.* Environmental Science & Technology, 2012. **46**(13): p. 6900-6914.

7. Lowry, G.V., et al., *Transformations of Nanomaterials in the Environment.* Environmental Science & Technology, 2012. **46**(13): p. 6893-6899.

8. Yu, S.-j., Y.-g. Yin, and J.-f. Liu, *Silver nanoparticles in the environment.* Environmental Science: Processes & Impacts, 2013. **15**(1): p. 78-92.

9. Wiesner, M.R., et al., *Assessing the Risks of Manufactured Nanomaterials.* Environmental Science & Technology, 2006. **40**(14): p. 4336-4345.

10. Andrew D. Maynard, R.J.A., Tilman Butz, Vicki Colvin, Ken Donaldson, Günter Oberdörster, Martin A. Philbert, John Ryan, Anthony Seaton, Vicki Stone, Sally S. Tinkle, Lang Tran, Nigel J. Walker & David B. Warheit, *Safe handling of nanotechnology.* Nature materials, 2006. **444**: p. 267-269.

11. Liu, J., et al., *Chemical Transformations of Nanosilver in Biological Environments.* ACS Nano, 2012. **6**(11): p. 9887-9899.

12. Baalousha, M., *Aggregation and disaggregation of iron oxide nanoparticles: Influence of particle concentration, pH and natural organic matter.* Science of The Total Environment, 2009. **407**(6): p. 2093-2101.

13. Dobias, J. and R. Bernier-Latmani, *Silver Release from Silver Nanoparticles in Natural Waters.* Environmental Science & Technology, 2013. **47**(9): p. 4140-4146.

14. Dunphy Guzman, K.A., M.P. Finnegan, and J.F. Banfield, *Influence of Surface Potential on Aggregation and Transport of Titania Nanoparticles.* Environmental Science & Technology, 2006. **40**(24): p. 7688-7693.

15. Badawy, A.M.E., et al., *Impact of Environmental Conditions (pH, Ionic Strength, and Electrolyte Type) on the Surface Charge and Aggregation of Silver Nanoparticles Suspensions.* Environmental Science & Technology, 2010. **44**(4): p. 1260-1266.

16. Hotze, E.M., T. Phenrat, and G.V. Lowry, *Nanoparticle aggregation: Challenges to understanding transport and reactivity in the environment.* Journal of environmental quality, 2010. **39**(6): p. 1909-1924.

17. Fabrega, J., et al., *Silver nanoparticles: Behaviour and effects in the aquatic environment.* Environment International, 2011. **37**(2): p. 517-531.

18. Fabrega, J., et al., *Silver Nanoparticle Impact on Bacterial Growth: Effect of pH, Concentration, and Organic Matter.* Environmental Science & Technology, 2009. **43**(19): p. 7285-7290.

19. Wang, J., C.P. Huang, and D. Pirestani, *Interactions of silver with wastewater constituents.* Water Research, 2003. **37**(18): p. 4444-4452.

20. Furman, O., S. Usenko, and B.L.T. Lau, *Relative Importance of the Humic and Fulvic Fractions of Natural Organic Matter in the Aggregation and Deposition of Silver Nanoparticles.* Environmental Science & Technology, 2013. **47**(3): p. 1349-1356.

21. Adegboyega, N.F., et al., *Interactions of Aqueous Ag+ with Fulvic Acids: Mechanisms of Silver Nanoparticle Formation and Investigation of Stability.* Environmental Science & Technology, 2012.

22. Aiken, G.R., H. Hsu-Kim, and J.N. Ryan, *Influence of Dissolved Organic Matter on the Environmental Fate of Metals, Nanoparticles, and Colloids.* Environmental Science & Technology, 2011. **45**(8): p. 3196-3201.

23. Sotiriou, G.A., et al., *Quantifying the Origin of Released Ag+ Ions from Nanosilver.* Langmuir, 2012. **28**(45): p. 15929-15936.

24. Liu, J. and R.H. Hurt, *Ion Release Kinetics and Particle Persistence in Aqueous Nano-Silver Colloids.* Environmental Science & Technology, 2010. **44**(6): p. 2169-2175.

25. Mansoori, G.A., K.S. Brandenburg, and A. Shakeri-Zadeh, *A Comparative Study of Two Folate-Conjugated Gold Nanoparticles for Cancer Nanotechnology Applications.* Cancers, 2010. **2**(4): p. 1911-1928.

26. Sagee, O., I. Dror, and B. Berkowitz, *Transport of silver nanoparticles (AgNPs) in soil.* Chemosphere, 2012. **88**(5): p. 670-675.

27. Stankus, D.P., et al., *Interactions between Natural Organic Matter and Gold Nanoparticles Stabilized with Different Organic Capping Agents.* Environmental Science & Technology, 2010. **45**(8): p. 3238-3244.

28. Johnson, R.L., et al., *Natural Organic Matter Enhanced Mobility of Nano Zerovalent Iron.* Environmental Science & Technology, 2009. **43**(14): p. 5455-5460.

29. Thio, B.J.R., D. Zhou, and A.A. Keller, *Influence of natural organic matter on the aggregation and deposition of titanium dioxide nanoparticles.* Journal of Hazardous Materials, 2011. **189**(1–2): p. 556-563.

30. Domingos, R.F., N. Tufenkji, and K.J. Wilkinson, *Aggregation of Titanium Dioxide Nanoparticles: Role of a Fulvic Acid.* Environmental Science & Technology, 2009. **43**(5): p. 1282-1286.

31. Wang, C., et al., *Retention and Transport of Silica Nanoparticles in Saturated Porous Media: Effect of Concentration and Particle Size.* Environmental Science & Technology, 2012. **46**(13): p. 7151-7158.

32. Huynh, K.A. and K.L. Chen, *Aggregation Kinetics of Citrate and Polyvinylpyrrolidone Coated Silver Nanoparticles in Monovalent and Divalent Electrolyte Solutions.* Environmental Science & Technology, 2011. **45**(13): p. 5564-5571.

33. Mukherjee, B. and J.W. Weaver, *Aggregation and Charge Behavior of Metallic and Nonmetallic Nanoparticles in the Presence of Competing Similarly-Charged Inorganic Ions.* Environmental Science & Technology, 2010. **44**(9): p. 3332-3338.

34. Lecoanet, H.F., J.-Y. Bottero, and M.R. Wiesner, *Laboratory Assessment of the Mobility of Nanomaterials in Porous Media.* Environmental Science & Technology, 2004. **38**(19): p. 5164-5169.

35. Dixit, V., et al., *Synthesis and grafting of thioctic acid-PEG-folate conjugates onto Au nanoparticles for selective targeting of folate receptor-positive tumor cells.* Bioconjugate Chemistry, 2006. **17**(3): p. 603-609.

36. Akaighe, N., et al., *Humic Acid-Induced Silver Nanoparticle Formation Under Environmentally Relevant Conditions.* Environmental Science & Technology, 2011. **45**(9): p. 3895-3901.

37. Brown, K.R., Walter, D. G., Natan, M. J., *Seeding of Colloidal Au Nanoparticle Solutions. 2. Improved Control of Particle Size and Shape.* Chemical Materials, 2000. **12**: p. 306-313.

38. Jana, N.R., Gearheart, L., Murphy, C. J. , *Seeding Growth for Size Control of 5-40 nm Diameter Gold Nanoparticles.* Langmuir, 2001. **17**: p. 6782-6786.

39. Weast, R.C., *Handbook of Chemistry and Physics*. 57 ed1976, Cleveland: CRC Press.

40. Levard, C., et al., *Effect of Chloride on the Dissolution Rate of Silver Nanoparticles and Toxicity to E. coli.* Environmental Science & Technology, 2013. **47**(11): p. 5738-5745.

CHAPTER FIVE

REVERSE MICELLE SYNTHESIS OF SILVER NANOPARTICLES IN GAS EXPANDED LIQUIDS

Abstract

The tunable solvent properties of gas expanded liquids (GXLs) have been previously used for the fractionation and separation of polydispersed ligand-stabilized metal nanoparticles into distinct monodispersed fractions. This work employs CO_2 expanded hexane for silver nanoparticle synthesis within an AOT reverse micelle system where the tunable GXL solvent properties are used to control the nanoparticle size and polydispersity. The objective of this project is to answer two questions: (1) can nanoparticles with narrow and well-defined size distributions be synthesized in GXLs? and (2) how do the solvent properties impact the resulting nanoparticle size? In the reverse micelle synthesis, the AOT surfactant provides a nano-scale aqueous micelle core for nanoparticle nucleation, as well as, acts as a nanoparticle stabilizing ligand. Increasing the CO_2 partial pressure in a GXL impacts the surfactant–solvent interaction and results in the synthesis of different sized nanoparticles. At ambient pressures, the mean particle diameter synthesized was 6.1 ± 2.1 nm with W = 40 and 5.4 ± 2.0 nm with W = 20, where W is the molar ratio of water to AOT. At CO_2 partial pressures of 6.9 and 13.8 bar, there was no significant change in particle size, but decreases in the size distributions were observed. At CO_2 partial pressures ranging from 20.7 to 41.4 bar, steady decreases in the mean particle diameter and size distribution were observed with values of 4.0 ± 0.8 for W = 40 and 4.1 ± 1.0 for W = 20 at 41.4 bar. This demonstrates

some degree of nanoparticle size tunability within the GXL solvent, where smaller particle diameters and size distributions are achieved at higher CO_2 compositions.

Introduction

Nanotechnology is based on materials built from particles less than a critical length. In the case of metallic nanoparticles, the unique chemical, optical, and physical properties depend heavily on size, shape, and polydispersity. [1,2] Preparation of monodispersed populations is often required to employ size-dependent properties, and many methodologies require post synthesis processing to obtain the desired size monodispersity. The objective of this work is to use tunable solvents to synthesize monodispersed popu-lations of silver nanoparticles of a controllable size. Traditional silver nanoparticle synthesis methods can produce nanoparticles with wide size distributions or are limited in the tunability on the synthesized particle size. Since size greatly impacts nanoparticle properties, it is imperative to (1) control the synthesized nanoparticle size or (2) fractionate the synthesized nanoparticles into monodispersed populations. There are several post-synthesis methods to narrow size polydispersity and obtain a specific particle size fraction including liquid anti-solvent precipitation, [3–5] chromatography techniques, [6] and isoelectric focusing [7] Sigman et al. used an ethanol/chloroform anti-solvent/solvent pair and centrifugation to size selectively precipitate and separate a polydispersed population of silver nanoparticles capped with dodecanethiol ligands into monodispersed particle fractions. [5] The addition of anti-solvent results in poorer solvent conditions and reduces the favorable solvent–ligand interactions and leads to nanoparticle precipitation. The reduced ability of the

solvent/anti-solvent mixture to disperse the particles is due to the decreased steric repulsion of the ligands and inability to overcome the van der Waals attraction between particles. Larger particles have greater van der Waals attractive forces, and as a result, precipitate first upon increasing anti-solvent concentration. [8,9] Further additions of anti-solvent and subsequent centrifugation to provide an external force to accelerate precipitation leads to smaller particles precipitating out of solution. Successive incremental additions of anti-solvent can lead to narrow size fractions with standard deviations less than 5%. Although the use of liquid anti-solvents for size fractionation will produce very narrow size distributions, copious amounts of anti-solvents are used, and the required centrifugation is time and energy intensive and not easily scalable. This leads to a large amount of waste and energy usage. [3–5] There is motivation then to develop greener techniques to obtain nanoparticle populations with narrow size distributions. Previous work using compressed and supercritical fluid solvents has shown that pressure and temperature tunable solvent properties can be used to control the size of dispersed nanoparticles during synthesis and post synthesis processing. [10] Shah et al. utilized the tunable density of supercritical ethane to obtain a size-selective dispersion of dodecanethiol coated nanoparticles. [10,11] This work illustrated that by changing solvent density, the dispersible particle size could be controlled where the largest particles were dispersed at the highest pressure. Ethane, for example, requires high pressures above 500 bar to synthesize and disperse copper nanoparticles of 3.4 nm in diameter. [9] Roberts et al. used the tunable solvent properties of GXLs to fractionate a polydispersed solution of silver Brust particles. [12,13] CO_2 partial pressure was used to

tune the solvent strength of solution for nanoparticles, and narrow size distributions were obtained at different CO_2 pressures. CO_2 is used as an anti-solvent because it dissolves easily into organic solvents and expands their volume; therefore changing the solvent mixture properties. [12,14] For example, the composition of CO_2 in gas-expanded n-hexane can be adjusted from zero mole percent at ambient conditions to 81 mol% at 49.4 bar. CO_2 is a good choice for GXLs because it is a weak solvent, even at high pressures [15] and has no dipole moment and a very low refractive index. [10] GXLs provide a wide range of tunability with adjustments in pressure, which affords control over the size of nanoparticles achieved in post synthesis processing. [9–12,16–19] Nanoparticle size control can also be achieved using surfactant-mediated reverse microemulsion techniques, in particularly the surfactant sodium bis(2-ethylhexyl) sulfosuccinate (AOT) in pro-portions such a reverse micelle water-in-oil microemulsion is formed. [2,20–23] The AOT reverse micelle system has been used widely for the synthesis of metallic nanoparticles including silver. Synthesis variables in the system that have been investigated include the type and concentration of surfactant, metal precursor, and reducing agent, as well as the temperature, pH, bulk sol-vent and water-to-surfactant molar ratio (W-value). [2,20,22] CO_2 has been used as an effective anti-solvent to recover nanoparticles synthesized via a reverse micelle method. [18,19,24,25] This work explores the use of GXLs as a tunable fluid medium for the reverse micelle synthesis of silver nanoparticles. It was our hypothesis that the nanoparticle–surfactant–solvent interactions can be adjusted by tuning the solvent strength with GXLs in order to control nanoparticle size and polydispersity. We were able to synthesize particles of controlled sizes using the

pressure-tunable solvent properties of GXLs where the particle size decreases with increasing CO_2 partial pressure. As a result, GXLs provide a greener alternative to control the size of synthesized nanoparticles.

Experimental

Materials

The surfactant sodium bis(2-ethylhexyl) sulfosuccinate (AOT) was obtained from Fisher Scientific and used without further purifi-cation. 98% n-hexane was purchased from Sigma Aldrich, sodium borohydride from EMD Chemicals, and 99.995% silver nitrate from Alfa Aesar. Industrial grade CO2 was purchased from National Welders Supply.

Particle synthesis

The method for the synthesis silver nanoparticles via the AOT reverse micelle synthesis has been discussed previously. [13,26] In short, 4.80 ml of 0.1 M AOT in n-hexane was combined with 0.10 ml of 0.01 M aqueous silver nitrate (W = [H2O]/[AOT] = 40) in a custom pressure cell. For a W-value of 20, 5.55 ml of 0.1 M AOT in hexane was combined with 0.10 ml of 0.01 M silver nitrate in water. The cell was sealed and pressurized. The CO_2 partial pressures used in this study were 6.9, 13.8, 20.7, 27.6, 34.5 and 41.1 bar and ambient conditions as a control. The pressure was controlled using a Teledyne ISCO D-Series Model 500HP syringe pump. 0.25 ml of 0.10 M (W = 40) or 0.10 ml of 0.25 M (W = 20) of aqueous sodium borohydride was then injected at constant

pressure through a Valco VICI W type injection loop. The pressure cell was vented to create laminar flow to ensure that all of the NaBH4 solution entered the cell. Following the reaction and nanoparticle synthesis, 0.10 ml of dodecanethiol was injected in the same fashion through an additional injection loop after 15 min of stirring via magnetic stir bar. The system was then depressurized, and a cloudy brown solution was removed from the pressure cell. The nanoparticles were crashed out of solution with ethanol, centrifuged, redispersed in 10 mL of fresh n-hexane containing 0.1 ml of dodecanethiol.

Characterization

Nanoparticle samples were deposited on copper grids (Ted Pella), and TEM images were obtained on a Hitachi 7600 TEM. The particle diameters were determined using ImageJ software and reported as the Max Feret and Min Feret (the maximum and minimum diameters of a given particle). Histograms were created using Origin 7, and statistical analysis was performed using Minitab 16.

Results

Nanoparticle Synthesis with W = 40

A mean particle size of 6.1 ± 2.1 nm was synthesized with a W-value of 40 and ambient pressure, while particles with diameters of 5.9 ± 2.0 nm, 6.1 ± 1.4 nm, 5.3 ± 1.4 nm, 4.7 ± 1.2 nm, 4.6 ± 1.4, and 4.0 ± 0.8 nm were obtained with CO2 partial pressures of 6.9 bar, 13.8 bar, 20.7 bar, 27.6 bar, 34.5 bar, and 41.4 bar respectively. Table 5-1 summarizes the results for both W-values with the mean particle size and the standard

deviation for both the Max Feret (maximum diameter) and Min Feret (minimum diameter) for each particle, as determined by ImageJ. Differences between the Max Feret and Min Feret are indicative of the particle sphericity. The reported particle diameter error is representative of the distribution of measured particle diameters within the population and is determined from the standard deviation with a 90% confidence integral. Fig. 1 shows representative TEM images and particle diameter histograms for the seven different reaction pressures at W = 40. From the results it can be seen that the AOT reverse micelle synthesis in gas expanded hexane does indeed produce particles of lower polydispersity and smaller diameters with increasing CO_2 partial pressure at a W-value of 40. ANOVA with the Tukey's method was performed to determine if the mean particle size measured for each CO_2 pressure demonstrated statistical independence. It should be noted that the Tukey's method tests the hypothesis that the mean particle diameters being tested for each sample within the population are independent, thus determining if statistically significant differences exist between samples. This is opposed to inferring if statistical differences exist from overlap of the particle size distribution standard deviation, which is indicative of the distribution of sizes and not error in the particle size measurement. Tukey's test demonstrated that within a 95% confidence interval, the mean particle diameters for the ambient, 6.9 bar and 13.8 bar samples were not significantly different. Nanoparticle samples synthesized at 20.7 bar and 27.6 bar were significantly different from the lower pressures but not from one another. The nanoparticle samples synthesized at 34.5 bar and 41.4 bar were significantly different from each other as well as all other samples synthesized with W = 40.

Table 5-1: Summary of results for TEM size results

Pressure (bar)	W-Value	Max Diameter (nm)	Min Diameter (nm)	Particle Counted
Ambient	20	5.4 ± 2.0	4.3 ± 1.7	675
6.9	20	5.6 ± 1.5	4.2 ± 1.1	665
13.8	20	5.4 ± 1.4	4.1 ± 1.1	384
20.7	20	5.1 ± 1.3	3.9 ± 1.1	383
27.6	20	5.0 ± 1.3	3.8 ± 1.0	463
34.5	20	4.6 ± 1.0	3.4 ± 0.8	425
41.4	20	4.1 ± 1.0	2.0 ± 0.9	502
Ambient	40	6.1 ± 2.1	4.8 ± 1.8	544
6.9	40	5.9 ± 2.0	4.7 ± 2.1	290
13.8	40	6.1 ± 1.4	4.4 ± 1.3	574
20.7	40	5.3 ± 1.4	3.8 ± 1.1	396
27.6	40	4.7 ± 1.2	3.7 ± 1.1	529
34.5	40	4.6 ± 1.4	3.4 ± 1.0	584
41.4	40	4.0 ± 0.8	3.1 ± 0.7	445

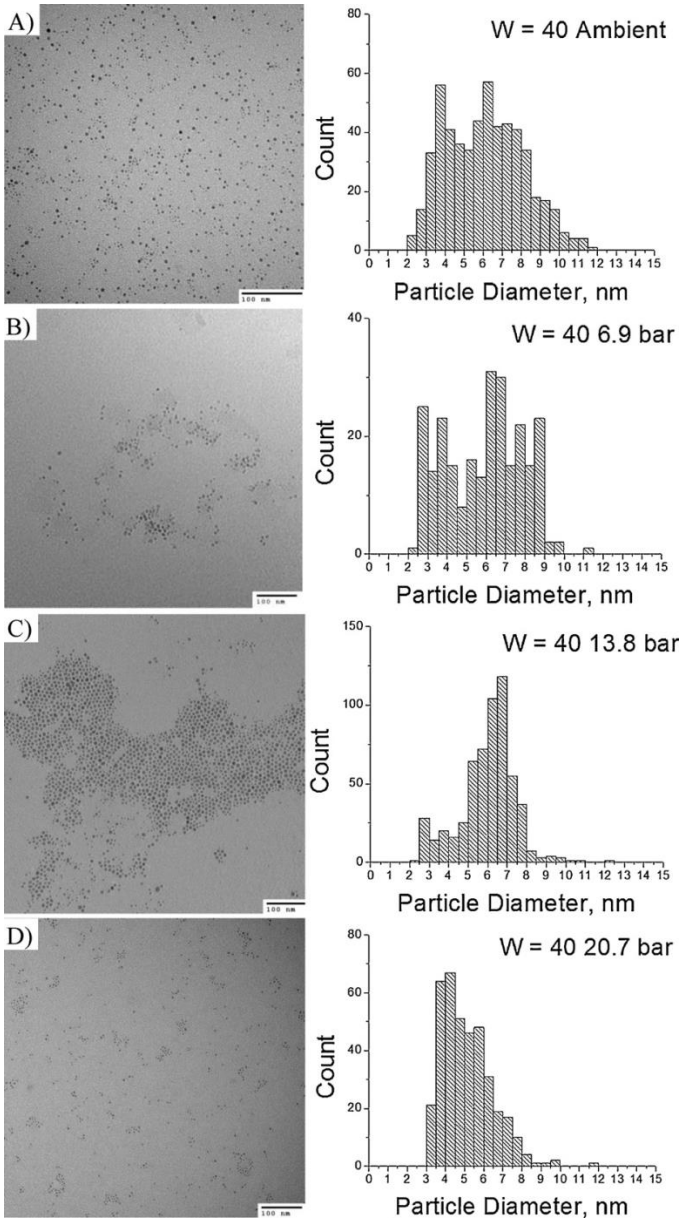

Figure 5-1: TEM images and particle size distribution histograms for silver nanoparticles synthesized with W = 40 at (A) ambient pressure, (B) 6.9 bar, (C) 13.8 bar, (D) 20.7 bar, (E) 27.6 bar, (F) 34.5 bar and (G) 41.4 bar.

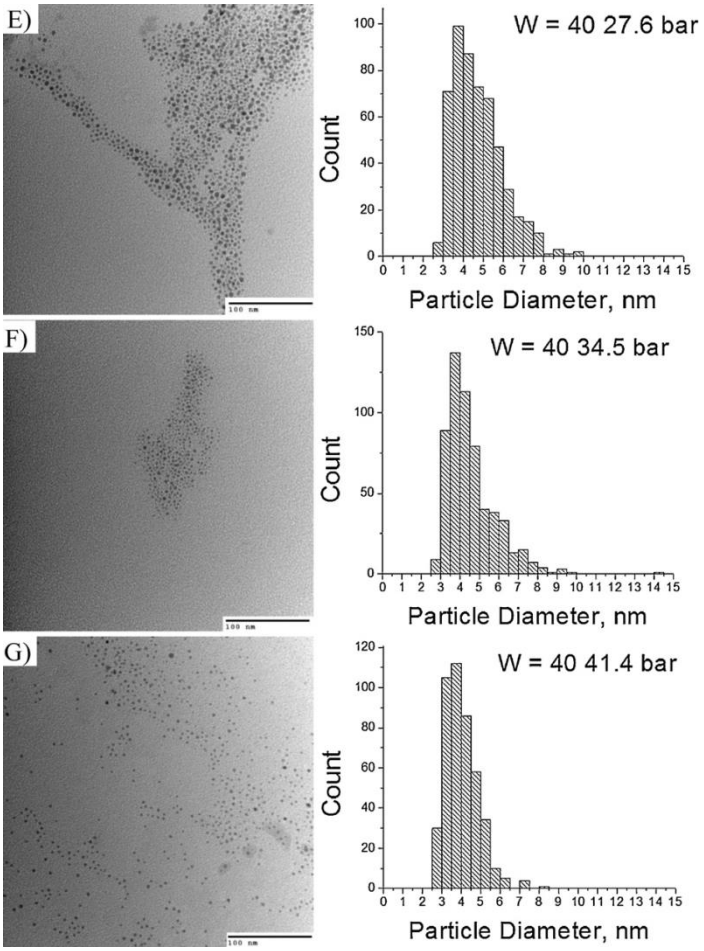

Figure 5-1. *(Continued)*

Nanoparticle synthesis with W = 20

The decreasing trend in synthesized mean particle size and size distribution with increasing CO_2 partial pressure is also seen with particles synthesized with a W-value of 20. The mean particle size synthesized with a W-value of 20 at ambient pressure was 5.4 ± 2.0 nm and 5.6 ± 1.5 nm, 5.4 ± 1.4 nm, 5.1 ± 1.3 nm, 5.0 ± 1.3 nm, 4.6 ± 1.0, and 4.1 ± 0.7 nm at pressures of 6.9 bar, 13.8 bar, 20.7 bar, 27.6 bar, 34.5 bar, and 41.4 bar respectively. Fig. 2 shows representative TEM images of these particles and the size

distribution histograms for each of the pressures investigated with W = 20. ANOVA with Tukey's test demonstrated that within 95% confidence interval that the mean particle diameters for the ambient, 6.9 bar and 13.8 bar samples were also not significantly different from one another but were significantly different from the same pressures with W = 40. Nanoparticles synthesized at 20.7 bar were significantly different from all other pressures at W = 20, nanoparticles synthesized at 27.6 bar and 35.4 bar were significantly different from other pressures but not from one another, and nanoparticles synthesized at 41.4 bar were significantly different from all other samples synthesized with W = 20. The nanoparticles synthesized at each of the pressures above 13.8 bar were not significantly different based on the W-value. It should be noted that all of the particle size distributions were skewed right but based on the large sample populations; it was assumed that the ANOVA results are relevant. Kruskal–Wallis test confirmed this assumption.

Discussion

In order to elucidate the governing factors that dictate nanoparticle size control, we must consider each of the influencing variables. The first and most obvious factor to consider is the W-value, which determines the size of the reverse micelles. Eastoe et al. used small angle neutron scattering (SANS) to determine the size of AOT reverse micelles and found that micelles with W-values of 20 and 40 have diameters of 6.58 nm and 11.64 nm, respectively. [27] When we consider the nanoparticle sizes synthesized at ambient pressure and W = 20, the micelle size correlates well with the synthesized nanoparticle diameter. This supports a theory of a micelle template governing the resulting particle

size, however this theory does not hold true for the W = 40 results, and it is not expected that the addition of CO_2 partial pressure will impact the micelle size, assuming an incompressible water core. It can be argued that the solvent property changes with the addition of CO_2 will impact properties such as the critical micelle concentration or relative solubility of water in the bulk or CO_2 in the micelle core; however, it is unlikely that any of these factors will significantly impact the micelle size. [25,28] The presence of CO_2 will make a significant effect on the pH of the micelle core [29]; however the most significant pH changes would likely occur between the ambient condition and the lowest pressure investigated. There is an effect of W-value and CO_2 pressure on the pH of the aqueous micelle core, but it is not that significant over the pressures investigated. [29]

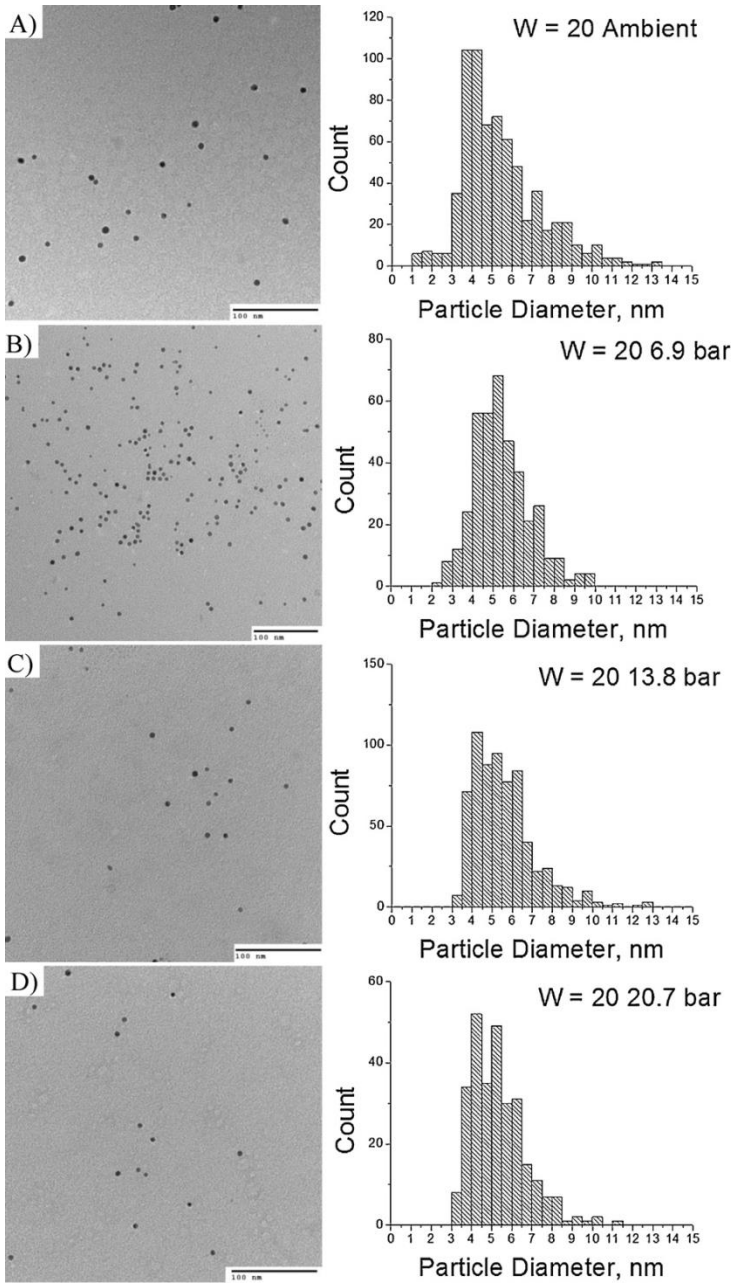
A)
W = 20 Ambient
Count
Particle Diameter, nm
B)
W = 20 6.9 bar
Count
Particle Diameter, nm
C)
W = 20 13.8 bar
Count
Particle Diameter, nm
D)
W = 20 20.7 bar
Count
Particle Diameter, nm

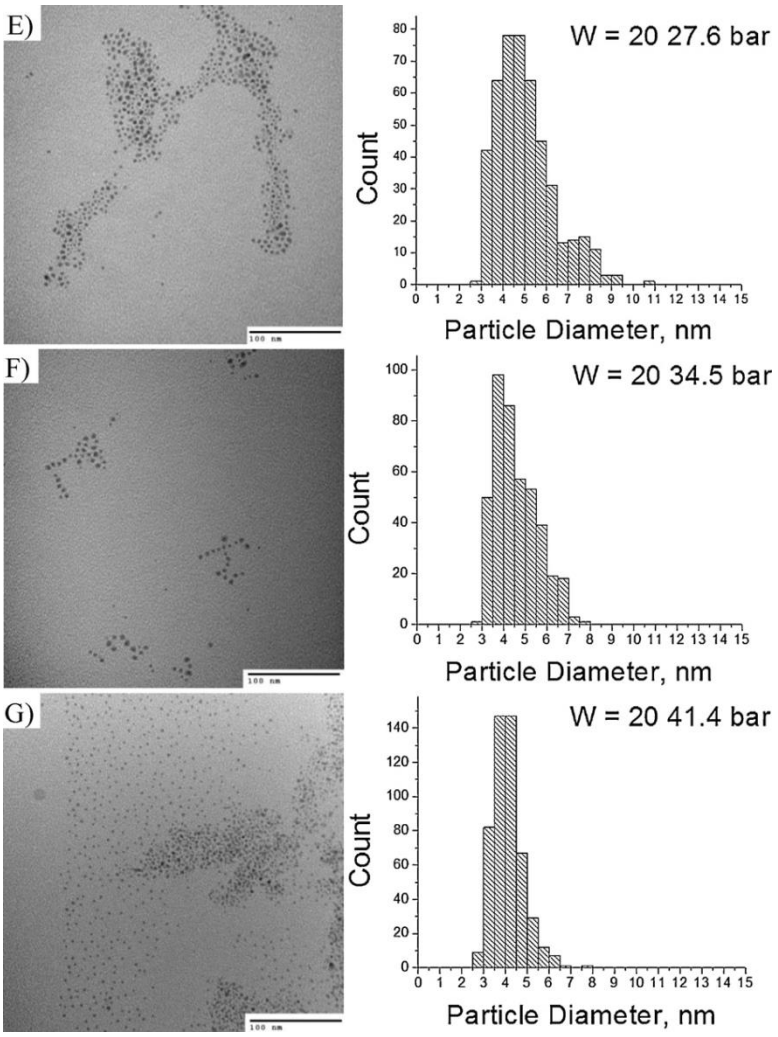

Figure 5-2: TEM images and particle size distribution histograms for silver nanoparticles synthesized with W = 20 at (A) ambient pressure, (B) 6.9 bar, (C) 13.8 bar, (D) 20.7 bar, (E) 27.6 bar, (F) 34.5 bar and (G) 41.4 bar.

An alternative theory is that particle size is governed by a directed assembly process where the colloidal phenomena of the AOT surfactant dictates the nanoparticle size. [8,9] The formation of this theory would be based on the AOT surfactant acting as a nanoparticle stabilizing ligand, and the surfactant–solvent interactions would be the

limiting factor that governs the synthesized particle size. Prior work by Han and co-workers has demonstrated that CO_2 can be used to size selectively precipitate metallic nanoparticles from an AOT reverse micelle system, where increasing pressure yields the recovery of smaller nanoparticles. [18,19,24] Furthermore, Roberts and co-workers found that 5.7 nm dodecanethiol-capped silver nanoparticles precipitated at 37.9 bar and 3.4 nm particles at 44.8 bar. [12] White et al. investigated nanoparticle dispersibility in GXLs with small angle neutron scattering (SANS) to determine solvation of ligand tails as a function of CO_2 pressure. [30] They showed that upon pressurization with CO_2, the ligand length and solvation of dodecane-capped silver nanoparticles decreases with increasing CO_2 pressure. As the CO_2 pressure increases, the molar composition of CO_2 dissolved in gas-expanded hexane increases, and a critical CO_2 composition exists where the dodecane ligand begins to collapse onto the nanoparticle surface. It is conceivable that a comparable CO_2 pressure exists for AOT and is impacted by the system W-value.

Table 5-2: Calculated solvent Properties for n-hexane/CO2 GXL by the PT-EOS

Bar	XCO2 %	Density, g/cm3	% Vol Expansion
0.0	0	0.767	0
8.0	8	0.768	1
14.3	16	0.77	6
20.4	24	0.773	11
28.1	36	0.775	21
31.3	42	0.776	27
40.3	60	0.774	63
45.5	72	0.766	113
49.4	81	0.75	190

Table 2 shows the composition of CO_2 and solvent density as a function of CO_2 pressure, calculated with the Patel–Teja equation of state (PT-EOS) [30–32]. The CO_2 mol-fraction compositions were estimated by the PT-EOS to be 5% at 6.9 bar, 17% at 13.8 bar, 28% at 20.7 bar, 40% at 27.6 bar, 51% at 34.5 bar, and 63% at 41.4 bar. As the CO_2 mole fraction increases in gas-expanded hexane, the local solvent environment around the ligand tails changes. With respect to density, small changes are predicted over the composition range indicating little effect on particle dispersibility. Each of these studies demonstrates that a critical CO_2 com-position exists for the dispersion of a nanoparticle with a given size, depending on the nanoparticle composition, ligand chemistry, and bulk solvent. Assuming that colloidal stabilization by the AOT surfactant is a controlling factor in the synthesized particle size, it is conceivable that at the lower pressures investigated, the solvent–surfactant interactions are not the primary factor governing the synthesized particle size. At pressures of 13.8 bar and below, there is no effect of pressure but there is a slight effect of W-value. This may be due to concentration differences. While the overall moles of Ag ions and NaBH4 are constant, the amount of water in the system does change, thus impacting the concentration within the micelle. Based on the theory of particle nucleation kinetics and growth, the concentration differences could result in the differences in particle size observed for the two W-values investigated at the low pressures. At pressures above 13.8 bar, the impact of W-value is not observed, but an effect of CO_2 partial pressure is observed. It is conceivable that under these conditions, the surfactant–solvent inter-actions become the limiting factor that dictates the synthesized nanoparticle size. In this scenario, it is possible that an

equilibrium particle size is reached or that the AOT-stabilized nanoparticles precipitate from solution once a critical size is reached. The fact that the GXL solution remains colored suggests the former.

Conclusions

Gas expand liquids provide a wide range of solvent tunability by simply adjusting CO_2 partial pressure. The tunability of CO_2 expanded n-hexane was implemented to control the size of silver nanoparticles synthesized within the AOT reverse micelle system with a W value of 20 and 40. Above a critical CO_2 pressure, a decrease in synthesized particle size and size distribution was observed. We propose a scenario by which a directed assembly mechanism is deterministic of the synthesized nanoparticle size where the surfactant–solvent interactions are the primary influencing factor. Future work in this area will include, thermodynamic modeling to gain a better understanding of the fundamental mechanisms that correlate bulk solvent properties with synthesized nanoparticle size and size distribution control. Furthermore, a wide range of system parameters are available to tune the particle size, which include the nanoparticle core material, surfactant, organic solvent, and temperature. In order to maintain the GXL system, the pressure is limited to pressures below the vapor pressure of CO_2, unless one wishes to explore the supercritical regime at higher temperatures and pressures. With this system, one could envision a wide range of tunable solvent properties that may be used to synthesize nanomaterials of a desired size and size distribution for a multitude of applications.

References

1. J.P. Wilcoxon, B.L. Abrams, Synthesis, structure and properties of metal nano-clusters, *Chemical Society Reviews* 35 (2006) 1162–1194.
2. W. Zhang, X. Qiao, J. Chen, Synthesis of silver nanoparticles - effects of concerned parameters in water/oil microemulsion, *Materials Science and Engineering B: Solid State Materials for Advanced Technology* 142 (2007) 1–15.
3. B.A. Korgel, S. Fullam, S. Connolly, D. Fitzmaurice, Assembly and self-organization of silver nanocrystal superlattices: ordered "soft spheres", *Journal of Physical Chemistry* B 102 (1998) 8379–8388.
4. C.B. Murray, D.J. Norris, M.G. Bawendi, Synthesis and characterization of nearly monodisperse CdE (E = S, Se, Te) semiconductor nanocrystallites, *Journal of the American Chemical Society* 115 (1993) 8706–8715.
5. M.B. Sigman, A.E. Saunders, B.A. Korgel, Metal nanocrystal superlattice nucleation and growth, *Langmuir* 20 (2004) 978–983.
6. T. Siebrands, M. Giersig, P. Mulvaney, C.H. Fischer, Steric exclusion chromatography of nanometer-sized gold particles, *Langmuir* 9 (1993) 2297–2300.
7. I. Arnaud, J.P. Abid, C. Roussel, H.H. Girault, Size-selective separation of gold nanoparticles using isoelectric focusing electrophoresis (IEF), *Chemical Communications* (2005) 787–788.
8. C.L. Kitchens, M.C. McLeod, C.B. Roberts, Solvent effects on the growth and steric stabilization of copper metallic nanoparticles in AOT reverse micelle systems, *Journal of Physical Chemistry B* 107 (2003) 11331–11338.
9. C.L. Kitchens, C.B. Roberts, Copper nanoparticle synthesis in compressed liquid and supercritical fluid reverse micelle systems, *Industrial & Engineering Chemistry Research* 43 (2004) 6070–6081.
10. P.S. Shah, T. Hanrath, K.P. Johnston, B.A. Korgel, Nanocrystal and nanowire synthesis and dispersibility in supercritical fluids, *Journal of Physical Chemistry B* 108 (2004) 9574–9587.
11. P.S. Shah, S. Husain, K.P. Johnston, B.A. Korgel, Role of steric stabilization on the arrested growth of silver nanocrystals in supercritical carbon dioxide, *Journal of Physical Chemistry B* 106 (2002) 12178–12185.
12. M. Anand, M.C. McLeod, P.W. Bell, C.B. Roberts, Tunable solvation effects on the size-selective fractionation of metal nanoparticles in CO2 gas-expanded solvents, *Journal of Physical Chemistry B* 109 (2005) 22852–22859.
13. M. Brust, M. Walker, D. Bethell, D.J. Schiffrin, R. Whyman, Synthesis of thiol-derivatized gold nanoparticles in a 2-phase liquid–liquid system, *Chemical Communications* (1994) 801–802.
14. J.P. Hallett, C.L. Kitchens, R. Hernandez, C.L. Liotta, C.A. Eckert, Probing the cybotactic region in gas-expanded liquids (GXLs), *Accounts of Chemical Research* 39 (2006) 531–538.

15. E.J. Beckman, Green chemical processing using CO2, *Industrial & Engineering Chemistry Research* 42 (2003) 1598–1602.
16. N.Z. Clarke, C. Waters, K.A. Johnson, J. Satherley, D.J. Schiffrin, Size-dependent solubility of thiol-derivatized gold nanoparticles in supercritical ethane, *Langmuir* 17 (2001) 6048–6050.
17. P.S. Shah, J.D. Holmes, K.P. Johnston, B.A. Korgel, Size-selective dispersion of dodecanethiol-coated nanocrystals in liquid and supercritical ethane by density tuning, *Journal of Physical Chemistry* B 106 (2002) 2545–2551.
18. H.L. Zhang, B.X. Han, J.C. Liu, X.G. Zhang, G.Y. Yang, H.Z. Zhao, Size tailoring of ZnS nanoparticles synthesized in reverse micelles and recovered by com-pressed CO2, *Journal of Supercritical Fluids* 30 (2004) 89–95.
19. J.L. Zhang, B.X. Han, J.C. Liu, X.G. Zhang, J. He, Z.M. Liu, T. Jiang, G.Y. Yang, Recovery of silver nanoparticles synthesized in AOT/C12E4 mixed reverse micelles by antisolvent CO2, Chemistry: *A European Journal* 8 (2002) 3879–3883.
20. I. Capek, Preparation of metal nanoparticles in water-in-oil (w/o) microemulsions, *Advances in Colloid and Interface Science* 110 (2004) 49–74.
21. J. Eastoe, M.J. Hollamby, L. Hudson, Recent advances in nanoparticle synthesis with reversed micelles, *Advances in Colloid and Interface Science* 128 (2006) 5–15.
22. J.N. Solanki, Z.V.P. Murthy, Controlled size silver nanoparticles synthesis with water-in-oil microemulsion method: a topical review, *Industrial & Engineering Chemistry Research* 50 (2011) 12311–12323.
23. C. Tojo, M. de Dios, F. Barroso, Surfactant effects on microemulsion-based nanoparticle synthesis, *Materials* 4 (2011) 55–72.
24. D.X. Liu, J.L. Zhang, B.X. Han, J. Chen, Z.H. Li, D. Shen, G.Y. Yang, Recovery of TiO2 nanoparticles synthesized in reverse micelles by antisolvent CO2, *Colloids and Surfaces A: Physicochemical and Engineering Aspects* 227 (2003) 45–48.
25. J.L. Zhang, B.X. Han, Supercritical CO2-continuous microemulsions and compressed CO2-expanded reverse microemulsions, *Journal of Supercritical Fluids* 47 (2009) 531–536.
26. K.R. Brown, D.G. Walter, M.J. Natan, Seeding of colloidal au nanoparticle solutions. 2. Improved control of particle size and shape, *Chemistry of Materials* 12 (1999) 306–313.
27. S. Nave, J. Eastoe, R.K. Heenan, D. Steytler, I. Grillo, What is so special about aerosol-OT? 2. Microemulsion systems, *Langmuir* 16 (2000) 8741–8748.
28. J. Chen, J.L. Zhang, B.X. Han, X.Y. Feng, M.Q. Hou, W.J. Li, Z.F. Zhang, Effect of compressed CO2 on the critical micelle concentration and aggregation number of AOT reverse micelles in isooctane, *Chemistry: A European Journal* 12 (2006) 8067–8074.
29. D.X. Liu, J.L. Zhang, B.X. Han, J.F. Fan, T.C. Mu, Z.M. Liu, W.Z. Wu, J. Chen, Effect of compressed CO2 on the properties of AOT reverse micelles studied by

spectroscopy and phase behavior, *Journal of Chemical Physics* 119 (2003) 4873–4878.
30. G. Von White, C.L. Kitchens, Small-angle neutron scattering of silver nanoparticles in gas-expanded hexane, Journal of *Physical Chemistry C* 114 (2010) 16285–16291.
31. N.C. Patel, A.S. Teja, New cubic equation of state for fluids and fluid mixtures, *Chemical Engineering Science* 37 (1982) 463–473.
32. K. Ohgaki, T. Katayama, Isothermal vapor–liquid equilibrium data for binary systems containing carbon dioxide at high pressures: methanol–carbon dioxide, n-hexane–carbon dioxide, and benzene–carbon dioxide systems, *Journal of Chemical & Engineering Data* 21 (1976) 53–55.

CHAPTER SIX

CONCLUSIONS AND RECOMMENDATIONS

Conclusions

In this dissertation, we have summarized applications, methods to perform and analyze, and effects on ligand exchange and binding. Ligand exchange has proved to be a versatile and robust method for modifying nanoparticle surfaces regardless of core material. Overall, a S_N2, associative mechanism in which an incoming ligand binds to a nanoparticle surface while an outgoing ligand desorbs from the surface in a simultaneous process; can be used to describe ligand exchange on gold nanoparticles with thiols and amines. We have concluded through review of recent literature that ligand binding and exchange is initiated and occurs rapidly at highly reactive defect sites and then slows as defect site-bound ligands migrate to less reactive terrace sites to allow more ligands to bind. We have discussed the many factors contribute to the strengths and kinetics of ligand binding and exchange. Nanoparticle properties that affect ligand binding and exchange include size, shape, crystalline structure, charge, oxidation state and age. Ligand properties that affect ligand exchange and binding include structure, i.e. multivalency, chain length, extent of branching and chirality, and chemistry; end group and perhaps most importantly head group, through which ligands bind to nanoparticle surfaces. We have also concluded from literature that thiols preferentially bind to GNPs followed by amines, phosphines and carboxylic acids.

We have demonstrated experimentally with isothermal titration calorimetry that thiols exhibit a heat of binding of 304kJ/mol which is >100kJ/mol higher than the heat of

binding of thiols to 2D gold surfaces. A significant conclusion of this work is that aging significantly reduces the reactivity of bare gold nanoparticles, as the heat of binding of PEG-SH to aged BGNPs decreased to 200 kJ/mol. Our studies demonstrate that the presence of citrate on the surface of GNPs does not inhibit the binding of PEG-SH, which was expected. A 50kJ/mol decrease in the heat of binding of PEG-SH to citrate stabilized GNPs demonstrates that citrate interacts with GNPs through a physical bond. Surprisingly, citrate seems to preserve the reactivity of GNPs by possibly preventing the reorganization of surface atoms. Titrations of PEG-SH into PEG-NH_2 stabilized GNPs resulted in a heat of binding of 204 kJ/mol. From the difference in the heats of binding of PEG-SH to BGNPs and PEG-NH_2 stabilized GNPs we can infer that PEG-NH_2 binds to GNPs chemically with a bond strength of approximately 100kJ/mol. From the results in this study we can elucidate the following trend in binding affinities of the functional groups tested; SH >> NH_2 > COOH.

We have investigated the influence of NOM and electrolyte type and concentration on the mobility of silver nanoparticles through ultrapure quartz powder. In the presence of NaCl, AgNPs will dissolve and from AgCl and we have demonstrated that this will largely affect the transport properties of silver nanoparticles. This study demonstrated that when AgNPs are in the presence of NaCl, they will exhibit 2 different breakthroughs when passed through a quartz column. This work is significant because of the length of the experiments, over 120 pore volumes, without which we would have not observed the second breakthrough of silver when silver nanoparticles are exposed to NaCl. We also demonstrated that when exposed silver nanoparticles are exposed to high

ionic strengths (0.1M) of NaCl, soluble $AgCl_x^{(x-1)-}$ will form. Perchlorate electrolytes do not interact with AgNPs to the extent of chloride electrolytes due to its weak oxidation potential. We have also demonstrated that NOM plays an important role in the fate and transport of AgNPs. NOM effectively shields AgNPs from ionic interactions and inhibits the deposition of AgNPs onto quartz powder, thereby enhancing AgNP mobility. NOM was also found to inhibit AgNP sorption as less than 1 % of the initial silver in the column studies was recovered from the column packing. Our batch dissolution experiments also demonstrate that NOM inhibits the dissolution of AgNPs. After 24 hours of exposure to electrolytes, NOM-passivated AgNPs released less than 5% of the total silver concentration in ionic form. These findings are import in determining the environmental implications of silver nanoparticles. Every body of water will have a significant amount of sodium chloride, whether natural or sea water. Natural organic matter is an abundant material in natural waters and has the potential for being carried to sea water, especially when bound to mobile particulate matter. This work has also raised a question on the long term impacts of AgNPs stabilized by NOM, as these particles will be more bioavailable to organisms in ecosystems.

Lastly we have presented a facile synthesis of AgNPs of controllable size. The tunability of CO_2 expanded n-hexane was implemented to control the size of silver nanoparticles synthesized within the AOT reverse micelle system with a W value of 20 and 40. We have proposed a scenario by which a directed assembly mechanism is deterministic of the synthesized nanoparticle size where the surfactant–solvent interactions are the primary influencing factor. We have demonstrated that a wide range

of system parameters are available to tune the particle size, which include the nanoparticle core material, surfactant, organic solvent, and temperature. With this system, one could envision a wide range of tunable solvent properties that may be used to synthesize nanomaterials of a desired size and size distribution for a multitude of applications. Since this method requires a simple change in pressure to change synthesis conditions we hope that this technique can be used to synthesis industrial quantities of nanomaterials of controllable size.

Recommendations

One of the questions that arose during the work in this dissertation was how to quantity the amount of ligand displaced during ligand exchange reactions. Quantifying the extent of ligand exchange will allow a more accurate estimation of binding strengths. While the use of various binding isotherms, such as the Langmuir isotherm can estimate the surface coverage of molecules they do not always provide accurate results. A proposed solution is to use radio-label ligands during the synthesis of GNPs, then exchange the radio-labeled (C^{14}) ligands with non-radio ligands. After isolating the ligand-exchanged nanoparticles with antisolvent and centrifugation, the supernatant could then be analyzed via inductively coupled plasma-mass spectroscopy (ICP-MS) to quantify the amount of radio-ligand that was displaced from the nanoparticle surface. ICP-MS is a sensitive technique that is capable of distinguishing between different isotopes of carbon. The difficulty of this method is that even after purification of nanoparticles, an equilibrium will exist between ligands on the nanoparticle surface

surface and in solution. Recursive washing with antisolvent addition and centrifugation has shown to strip ligands from the surface of nanoparticles. Chromatography is a possible solution to isolate radio-labeled nanoparticles from excess ligand. After washing particles with an antisolvent/centrifugation method and dispersing the particles in a "neat" solvent, the solution would be passed through a column packed with polystyrene beads. This would facilitate the separation of nanoparticles and excess ligand due to the fact that the nanoparticles and free ligand would elute from the column at different rates.

I also believe that further investigation of ligand binding and exchange with isothermal titration calorimetry would increase the understanding of binding and exchange mechanisms. This would include the investigation of ligand binding to nanoparticles of various sizes and the investigation of the effect of ligand structure, i.e. chain length and multivalency. By varying ligand chain length and multivalency, we could potentially determine if and what entropic affects contribute to or inhibit ligand binding and exchange. We were unable to measure the heat of binding of amine functionalized ligand to gold nanoparticle and it would be possible to measure the heat of binding of amine functionalized ligands by increasing the concentration of ligand titrated into a gold nanoparticle solution.

The work performed investigating the mobility, dissolution and sorption properties of silver nanoparticles as affected by natural organic matter and electrolytes provides a technique to study a wide range of environmental conditions. I would recommend studying the effect of age on nanoparticle transport in order to better access

long term impacts of nanoparticles on the environment. I would also recommend studying the effect of natural organic matter the transport properties of various hydrophobically stabilized nanoparticles under saturated flow conditions. I believe that with sufficient concentrations of natural organic matter, hydrophobically stabilized nanoparticle would be mobilized and become bioavailable in the environment.

Another fundamental question that arose after finishing this dissertation was how surfactant-solvent interactions in GXLs affect particle size during synthesis. A proposed solution is to determine the surfactant structure and solvation via small-angle neutron scattering and apply this data to thermodynamic interaction energy modelling to gain a better understanding of the fundamental mechanisms that correlate bulk solvent properties with synthesized nanoparticle size and size distribution control. Interaction energy modeling used to predict the dispersibility of hydrophobically stabilized metal nanoparticles often over predicts the mean particle size dispersed at a given solvent composition and these models require an accurate description of the nanoparticle ligand structure.[1,2] White et al. utilized small-angle neutron scattering (SANS) to obtain in-situ ligand solvation measurements in GXLs by contrasting hydrogenated nanoparticle ligands with deuterated solvents.[3] The same technique could be applied here by utilizing deuterated hexane, hydrogenated sodium 1,4-bis(2-ethylhexoxy)-1,4-dioxobutane-2-sulfonate (AOT) and D_2O for contrast matching to determine the solvation of AOT. The Flory-Huggins interaction energy model could then be applied to determine the surfactant-solvent interactions. I hypothesize that AOT surfactant tails collapse in gas expanded hexane as the partial pressure of CO_2 is increased and that this inhibits

intermicellar exchange, which is the mechanism of nanoparticle growth in surfactant-mediated microemulsion nanoparticle syntheses.[4] Another explanation of the change in particle size with increased CO_2 partial pressure is that the solvent strength is not sufficient enough to disperse particles with diameters greater than a critical length.

References

(1) Kitchens, C. L.; McLeod, M. C.; Roberts, C. B.: Solvent Effects on the Growth and Steric Stabilization of Copper Metallic Nanoparticles in AOT Reverse Micelle Systems. *The Journal of Physical Chemistry B* **2003**, *107*, 11331-11338.

(2) Shah, P. S.; Holmes, J. D.; Johnston, K. P.; Korgel, B. A.: Size-Selective Dispersion of Dodecanethiol-Coated Nanocrystals in Liquid and Supercritical Ethane by Density Tuning. *The Journal of Physical Chemistry B* **2002**, *106*, 2545-2551.

(3) Von White, G.; Kitchens, C. L.: Small-Angle Neutron Scattering of Silver Nanoparticles in Gas-Expanded Hexane. *The Journal of Physical Chemistry C* **2010**, *114*, 16285-16291.

(4) Wanzhong Zhang, X. Q., Jianguo Chen: Synthesis of silver nanoparticles—Effects of concerned parameters in water/oil microemulsion. *Materials Science and Engineering: B* **2007**, *142*, 1-15.

APPENDICES

APPENDIX A

ADDITIONAL ITC AND TEM DATA

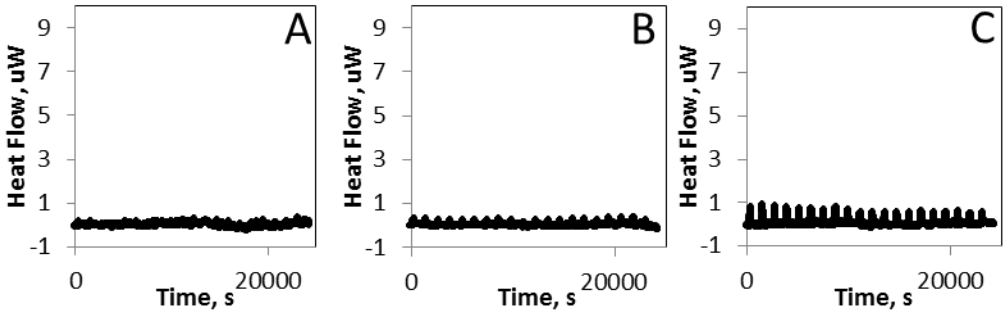

Figure A1: ITC heat signals of titrations performed for dilution corrections, of PEG-SH into; A. DDI H20, B. 0.25mM citrate, C. 0.25mM PEG-NH2, pH 10.

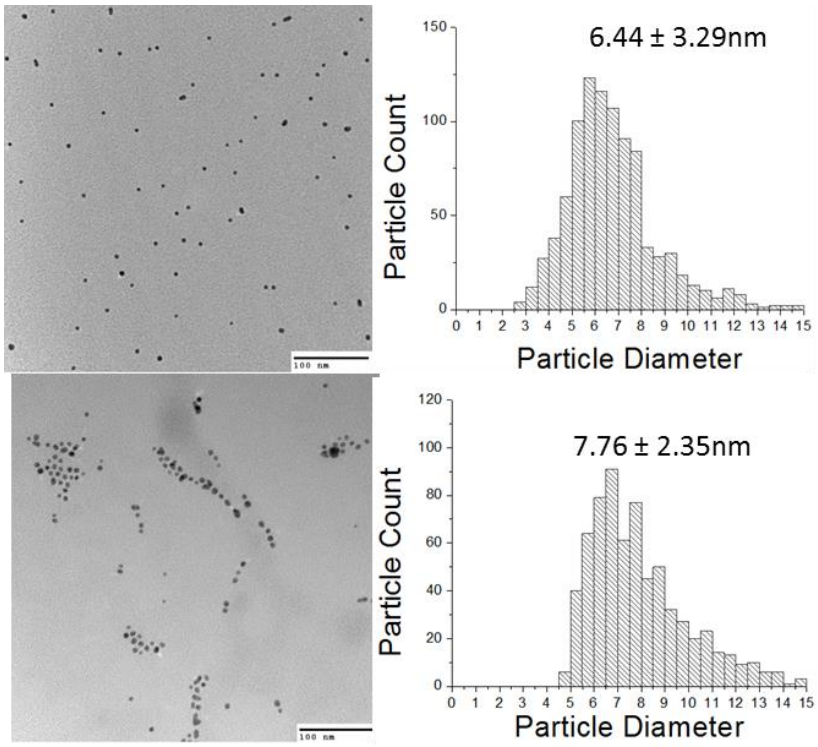

Figure A2: TEM Images and histograms for freshly synthesized BGNPs A) before titration and B) after titration with PEG-SH

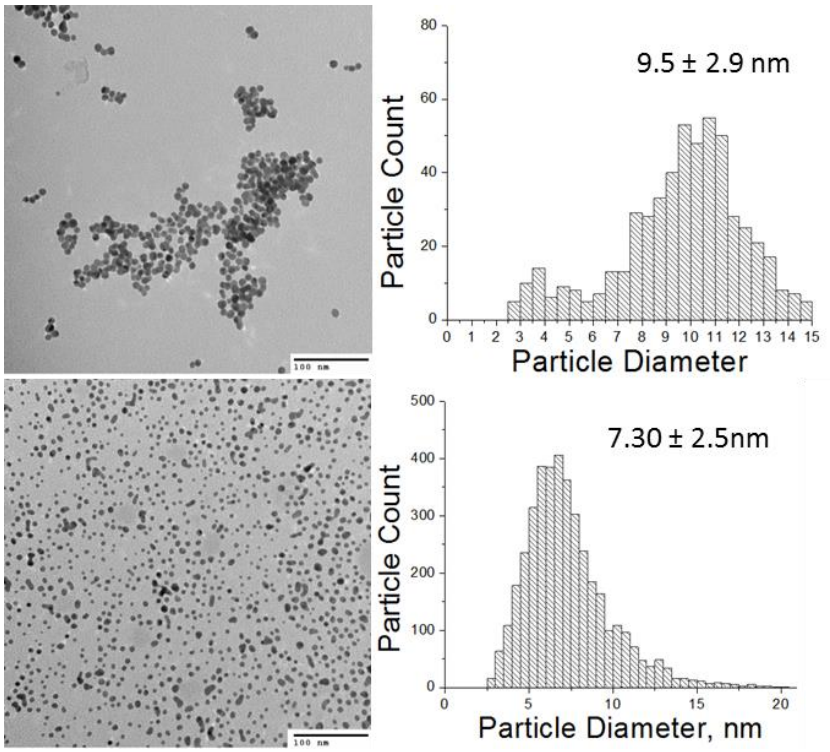

Figure A3:TEM Images and histograms for aged BGNPs A) before titration and B) after titration with PEG-SH

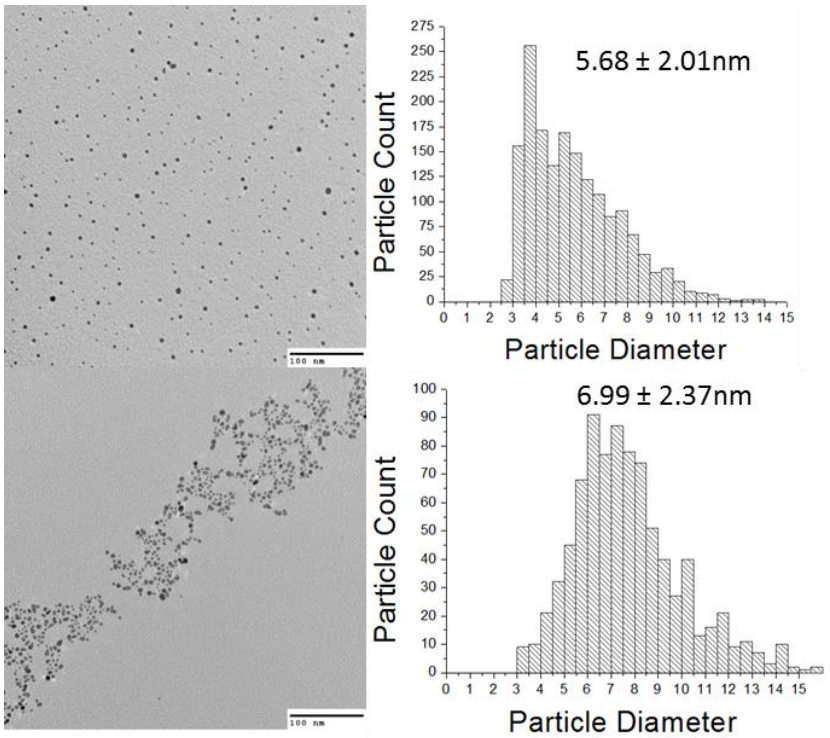

Figure A4: TEM Images and histograms for freshly synthesized citrate stabilized GNPs A) before titration and B) after titration with PEG-SH

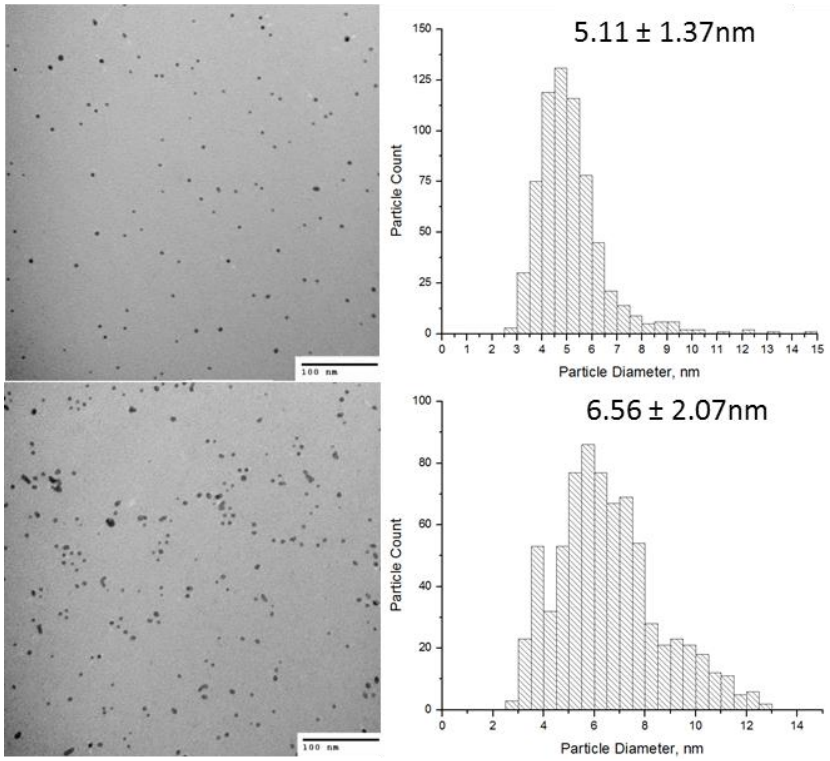

Figure A5: TEM Images and histograms for aged citrate stabilized GNPs A) before titration and B) after titration with PEG-SH

APPENDIX B

TRANSMISSION ELECTRON MICROSCOPY PROCEDURES

Initial Procedures

1. Verify that the liquid nitrogen traps near the condenser stage and on the rear of the instrument are full and refill if necessary. The trap levels should be checked at least every hour and topped off if need be.
2. Set the accelerating voltage to at least 100 kV, this voltage was used to the images obtained for this dissertation.
3. Turn on the filament, ensuring the filament bias is on.
4. Insert prepared TEM grid into the sample holder and load into the scope at the "standby" position.

TEM Alignment

1. Ensure that the beam is on.
2. Press the LENS PRESET button on the top of the left hand panel to ensure the instrument is at the lowest magnification setting
3. Verify that the objective and diffraction apertures are in the out position
4. Press the beam horizontal position, BH, then adjust brightness until you locate the beam and it is in a small focused spot.
5. Use the xy knobs to center the brightly focused beam, and adjust the beam to ensure that it is moving in a concentric fashion (in and out)
6. If the beam is not spherical, or does not move in a concentric fashion, use the condenser aperture knobs to center and make the beam symmetrical
7. Press CS above multifunction knobs, and use MF knobs to make beam perfectly round
    a. Adjust brightness to ensure rounded shape
8. Change to mid-magnification and repeat
9. Fully load the sample holder into the chamber and align the beam at high magnification with the digital camera by using the following functions;
    a. WOBL – adjust knob under sample holder until there is no movement in the picture
    b. MODL – use MF knobs so that the sample moves in and out on itself and does not move side to side
10. Put sample back in standby position with camera still on and press IN/OUT button to insert the aperture.
11. Click corrections and acquire a background by adjusting the brightness until the histogram is centered, click ok.
12. Click button for live image and being taking images with the AMT camera.

APPENDIX C

IMAGEJ ANALYSIS

1. Open ImageJ and select an image for analysis.
2. Set scale;
    a. Zoom in on the scale bar and draw a line along the length of it

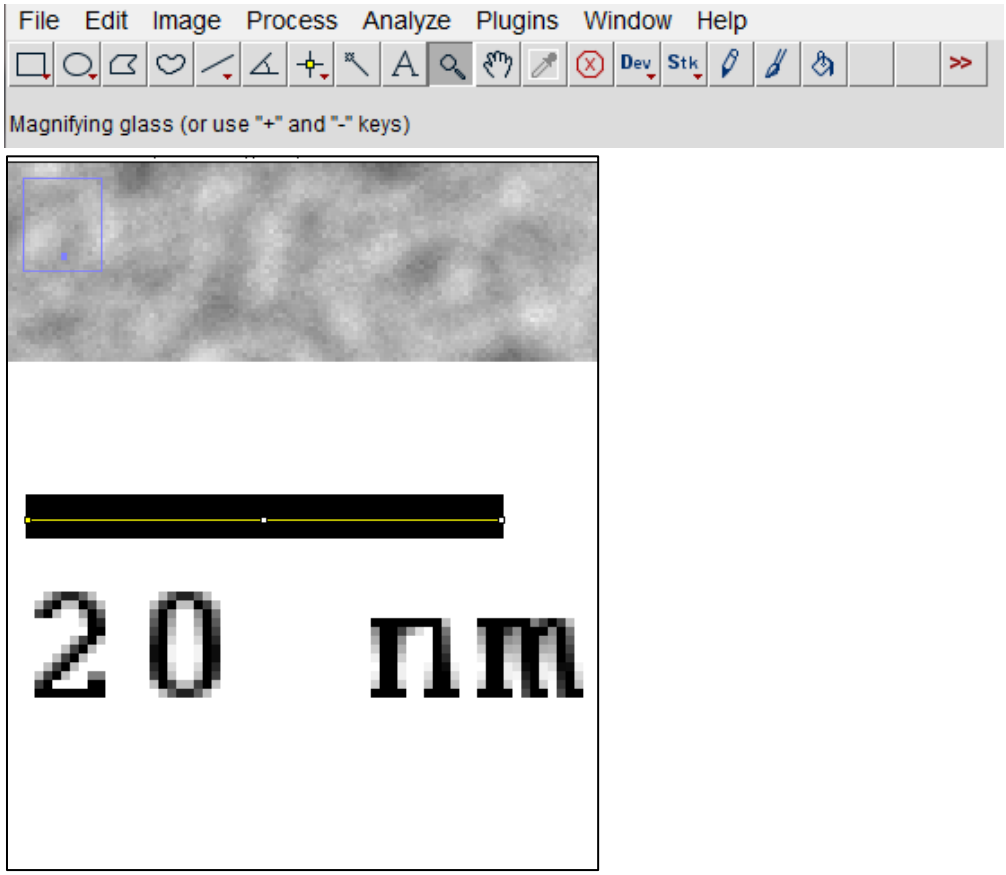

    b. Analyze - Set Scale -
        i. Input the length of the scale bar
        ii. Click “Global if all of your images are at the same magnification.
    c. Press OK

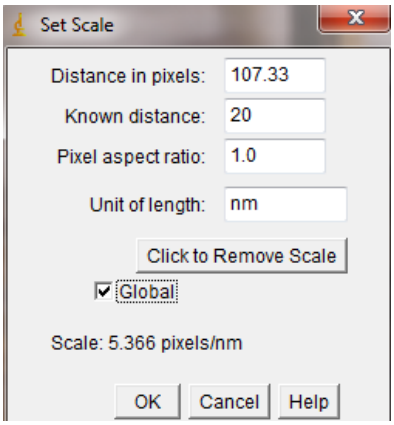

3. Crop your image so that just the nanoparticles show.
    a. Image – Crop
4. Maximize the Bright/Contrast;
    a. Image – Adjust - Brightness/Contrast
5. Adjust the Threshold of the image
    a. Zoom in on a good part of the image.
    b. Image – Adjust - Threshold

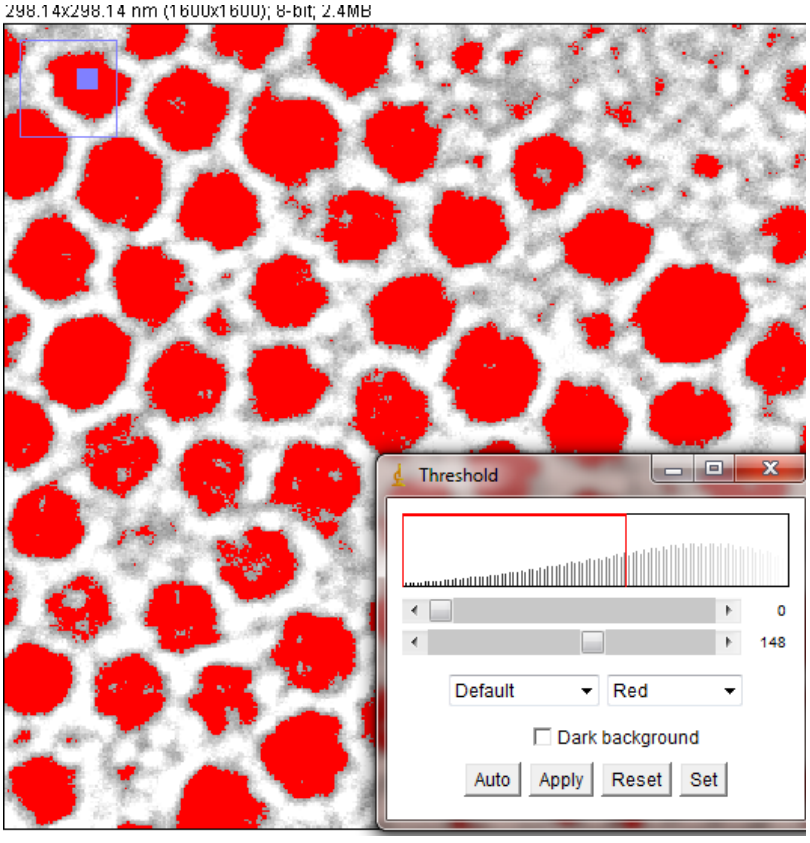

    c. Hit apply and the red spots will turn black.

6. Set measurements
    a. Analyze - Set Measurements

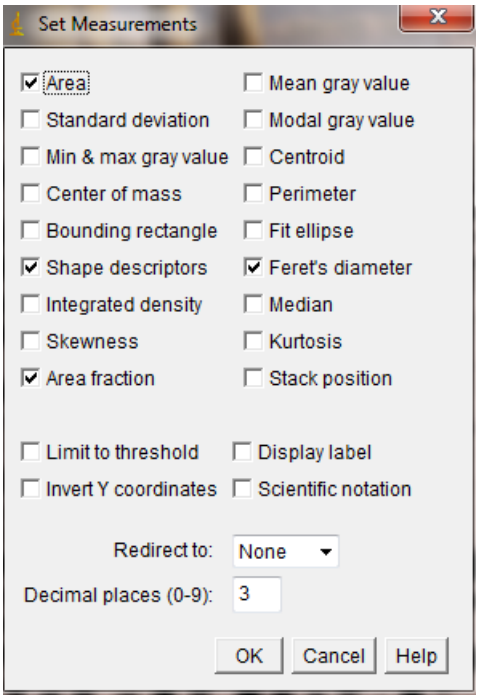

7. Analyze Partcles;
    a. Analyze - Analyze Particles

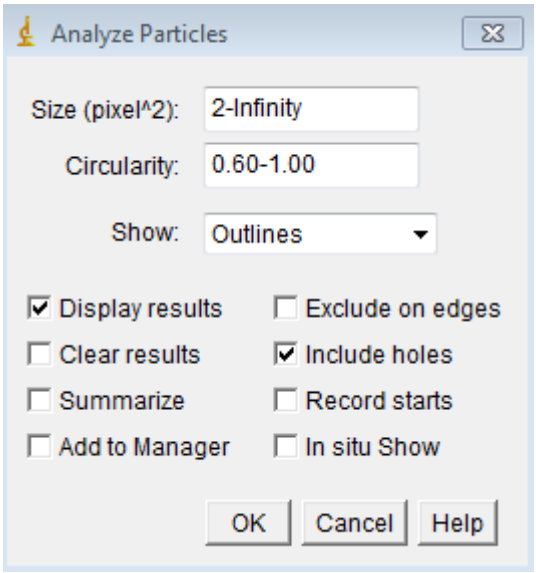

    b. Set the circularity limits to 0.6 to 1.0 and ensure that the "Show" Tab says outlines.

c. A list of measurements will then pop up and you can copy and paste the results into a statistical analysis program to obtain a histogram and average size.

APPENDIX D

ISOTHERMAL TITRATION CALORIMETRY

Ampule Preparation

- Ensure that the O-rings on the central shaft are lubricated with vacuum grease
- Wet the central shaft by slowly pushing 10 mL of DDI water into the plastic tube connected to the upper part of the ampule with a syringe, then push 20 mL of air through the ampule to remove excess water.
- Use a kim wipe to remove any water droplets from the stirring shaft and the bottom of the ampule
- Ensure that the propeller is clean and dry. This may require sonication and acid washing with 5 % HCl, then thoroughly rinsed with DDI water and dried with a kim wipe
- Install the propeller on the bottom end of the central stirring shaft, and ensure that its position is adjusted so that it is fully submerged in the liquid that is to be placed in the ampule.
- Insert the cannula into the ampule until the tip is seen above the propeller while submerged in liquid.

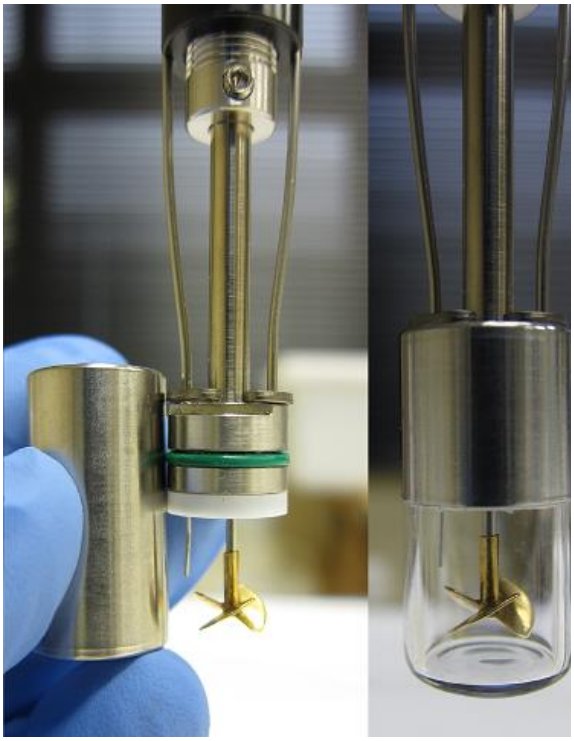

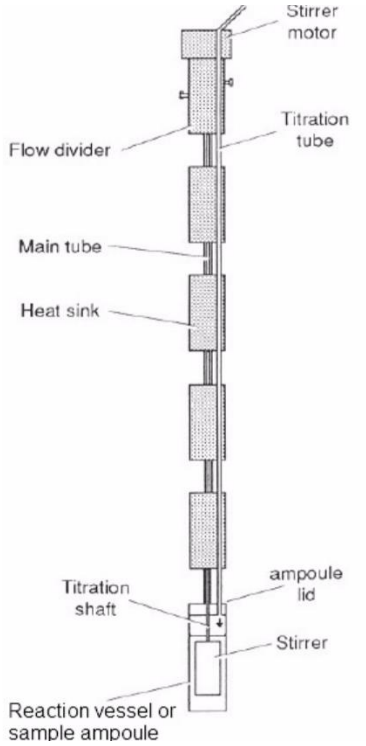

- Pipette 0.8 mL of nanoparticle sample into the ampoule; rinse it using sample liquid first if the ampoule is not dried.
    - The nanoparticle solution should be degassed for at least 30 minutes in advance

- Ensure the green O-ring is properly greased, then slide on the sample ampoule and click the cir-clip into place using the plier provided to secure the ampoule.

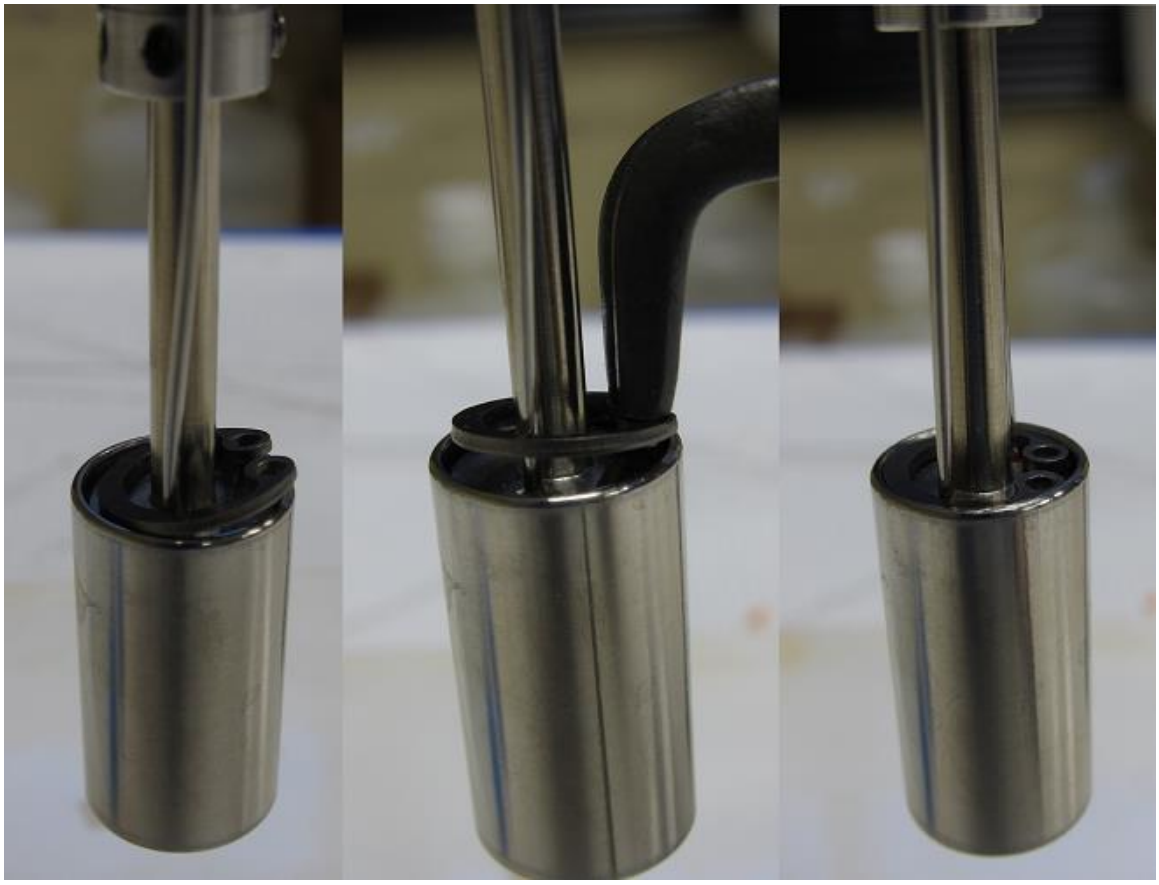

- The reference ampoule should also be prepared as stated above, but this ampoule does not contain a stirrer or cannula.
- The ampoules can now be inserted into the instrument by first installing the circular locking ring onto the calorimeter by screwing the lower part.
- Place the stirrer motor onto the top of the sample ampoule accessory, and rotate it until it locks in place.
- Insert the both of ampoule accessories into the calorimeter through the circular locking ring, until the second lowest heat sink is half way in then tighten the upper part of the circular locking ring to hold the ampoule accessories in position.
- Lower the ampoule accessories step by step at 10-15 min intervals
- When the ampoule is lowered to the second to last step, insert the cannula so that the tape is about 1 inch from the top of the ampoule
- After the ampoule accessories are both completely in the calorimeter, tighten both circular locking rings.
- Allow the instrument to equilibrate for 3-4 hours.

Preparing the syringe

- Ensure that the titrant solution has been degassed in advance and that the syringe and plunger are properly cleaned and dried in advance.
- Remove the plunger and load titrant into the glass syringe using a larger plastic syringe that is connected to a plastic tube.
- Ensure there are no bubbles inside the syringe once it is loaded and push the plunger to ensure that the cannula is completely filled. The syringe should be rinsed with titrant at least once and refilled.
- Place the syringe in the pump system so that the plunger and the flange of the syringe fit in the respective slots.
- Dispense liquid by pushing the feed button until air free droplets can be seen at the tip of the cannula, removing the droplets using kim wipe.

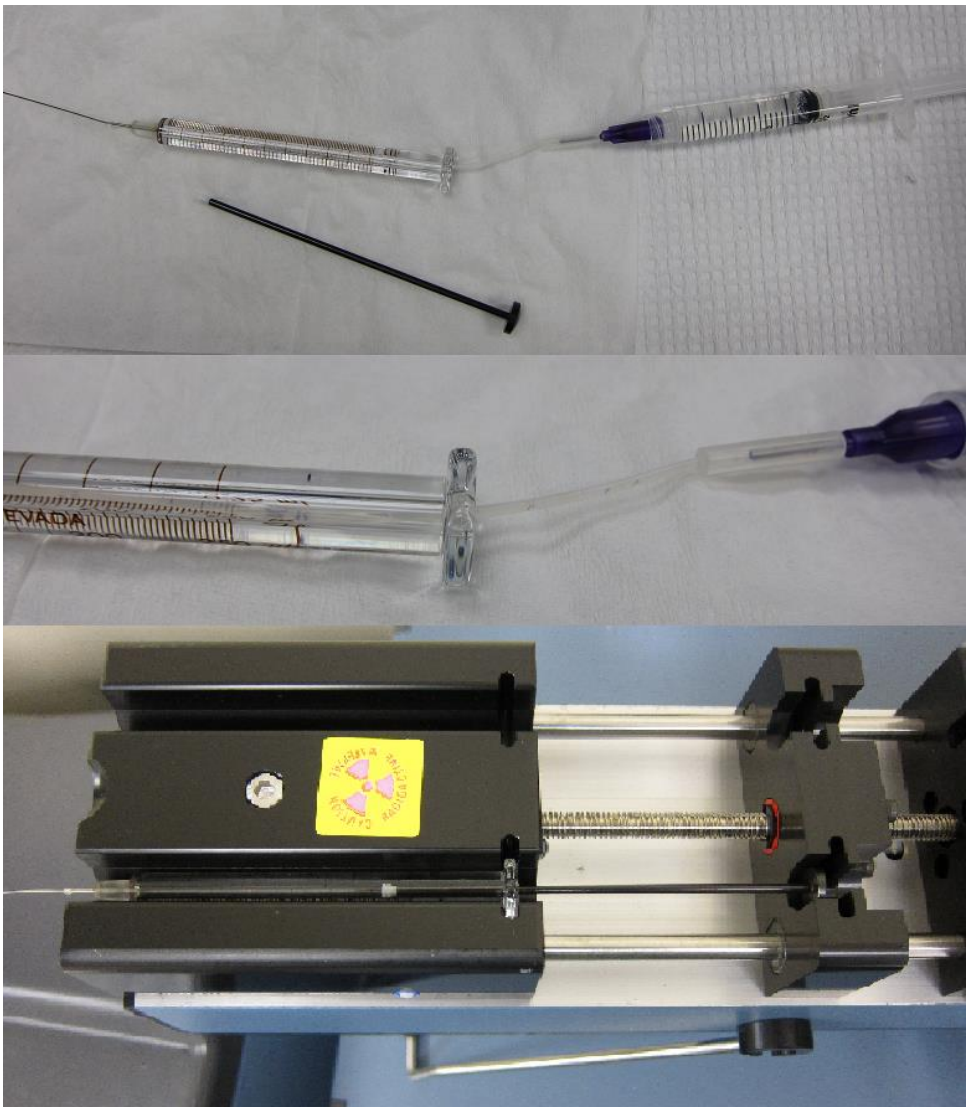

Dynamic Calibration

- Dynamic calibration should be performed before each titration once the calorimeter has reached equilibrium and the change in heat flow is less than 50 nW
- Within the calorimeter controller interface, choose the calorimeter you want to use:
    - CLICK – Control - Perform full dynamic calibration
- Record the parameters of calibration, including gain, $\tau_1+\tau_2$, $\tau_1\tau_2$, and experimental parameters

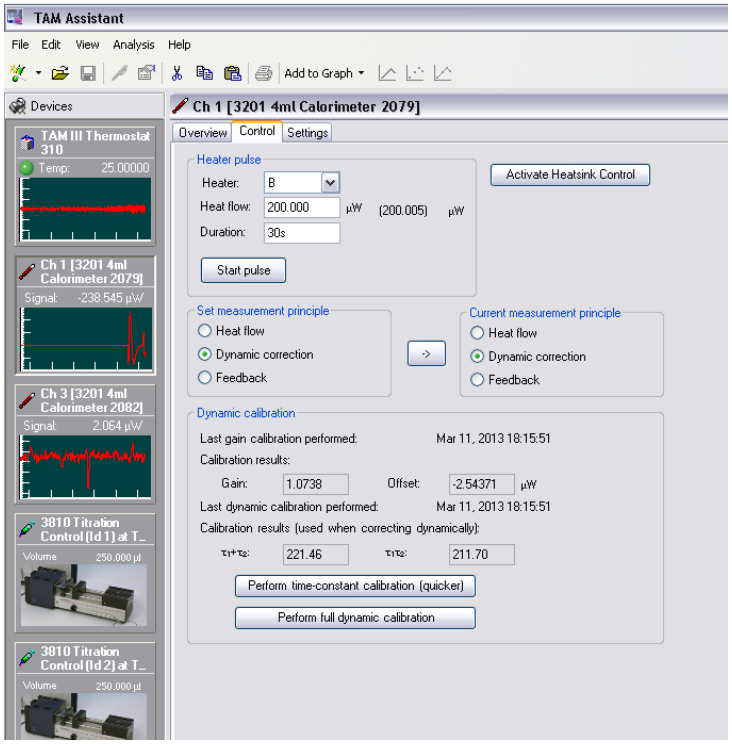

Running a titration experiment

- Within the calorimeter controller interface;
    - Click the wizard icon and choose “Experiments” to open new experiment wizard, then follow the instructions on the screen to set titration parameters, including calorimeter ID, pump ID, number of injections, injection volume, injection duration, interval between injections, etc.

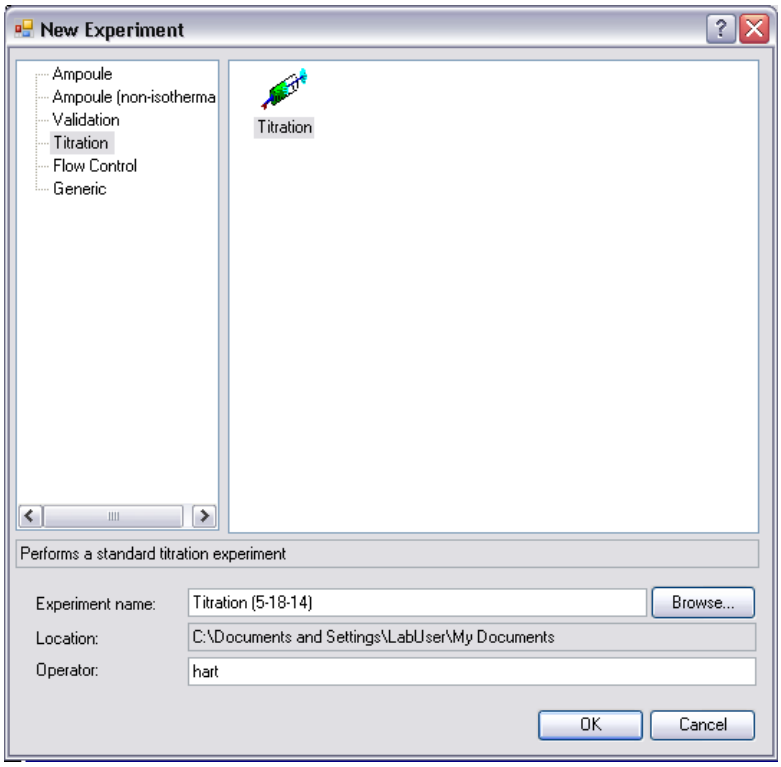

- Choose the calorimeter and pump ID being used in the experiment

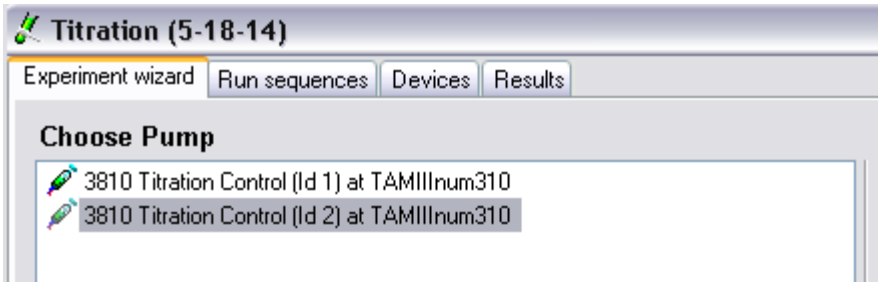

- Enter the solution IDs, concentrations and volumes;

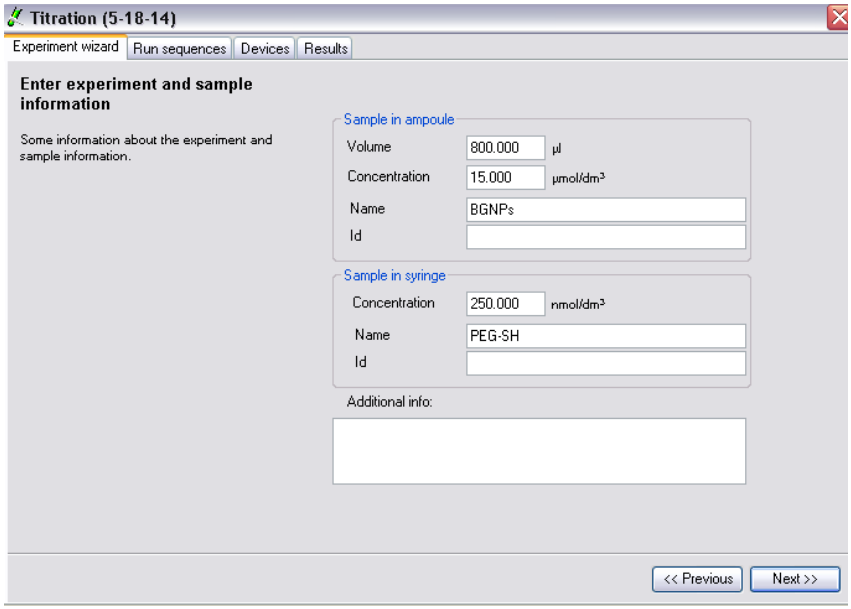

- Enter the number of injections desired, 20 injections were used for experiments in this dissertation and the injection duration was set to 10 seconds

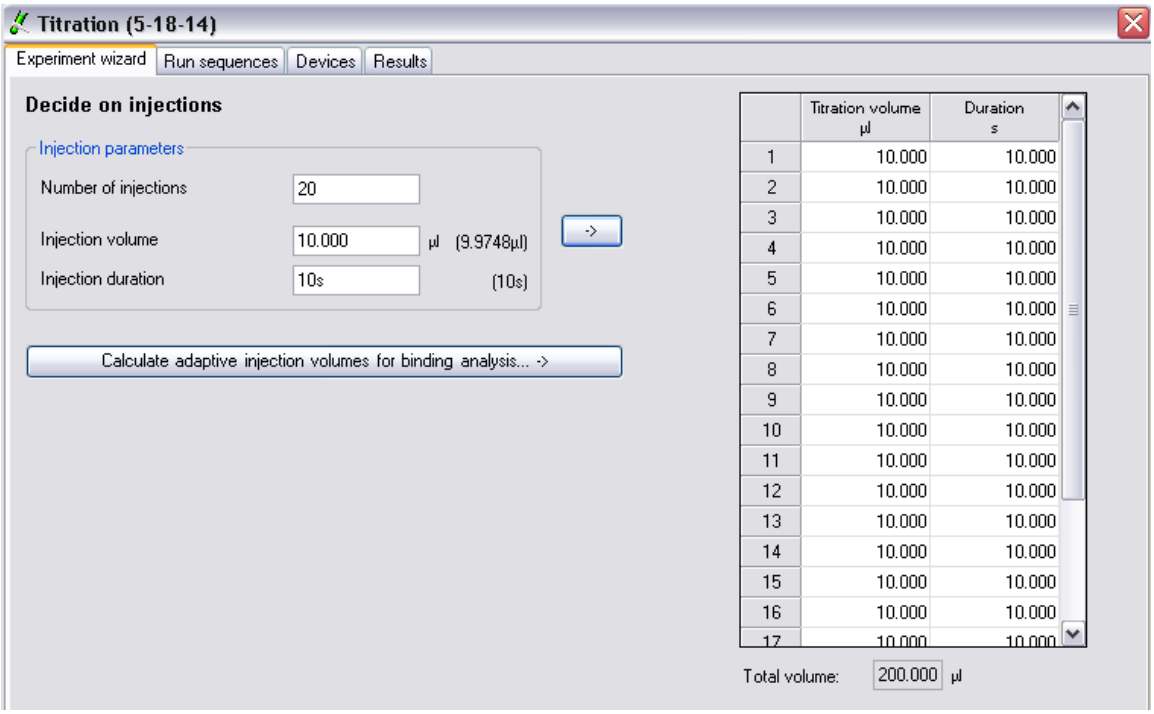

- Enter the time to reach baseline between injections, 20 minutes was selected for the experiments in this dissertation, and ensure that "Dynamic correction" is check

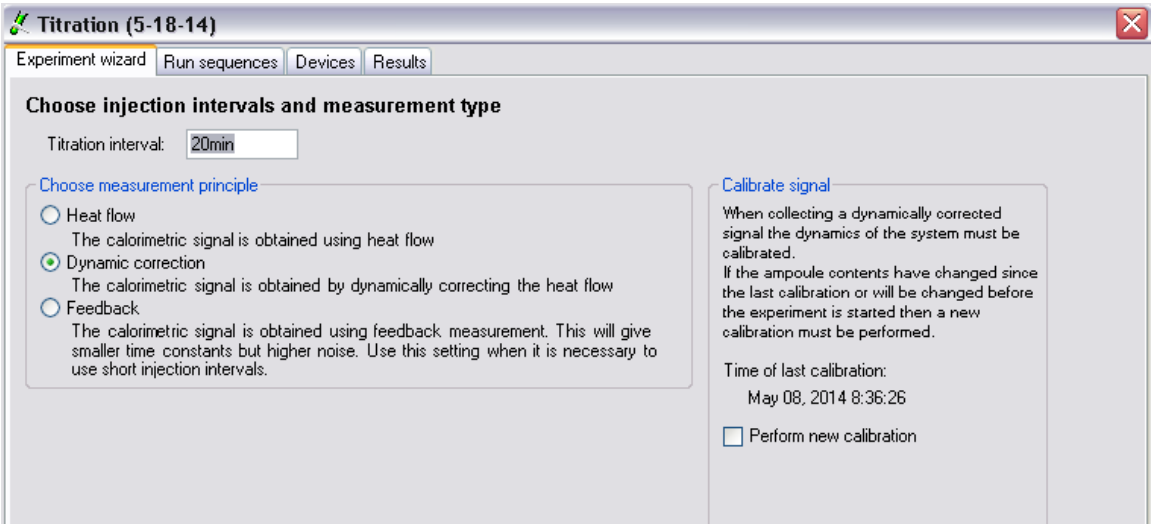

- Press start experiment to run the titration

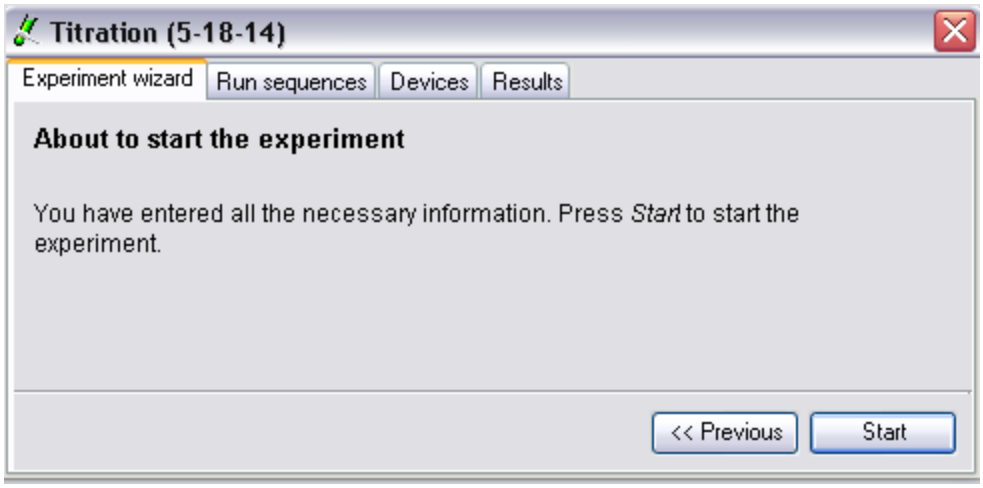

Identifying Suitable Experimental Conditions

- I looked in the literature to get a ballpark range for the concentrations of reactants
    - For my system I started with 0.25mM GNP solution (moles of gold) and 2.5mM Ligand solution.
- If the initial concentration is too high, the heat flow will saturate in the first injection, if this happens try decreasing your concentration by one order of magnitude
- The time between injections should be long enough for the instrument to reach baseline before another injection is perform.
    - If the baseline is not straight, or there is a lot of "noise" between injections, increase the time between injections.
    - I increased the time between injections by 5 minutes until I obtained a stable baseline

APPENDIX E

INDUCTIVELY COUPLED PLAMSA –MASS SPECTROSCOPY

Getting Started

- Ensure that the chiller is on and that the argon gas pressure is between 85 and 95 psi
- Ensure that the feed lines are in 2 % HNO_3 to flush the tubing
- Turn the instrument on and allow the ICP to warm up for at least 30 minutes
- Prepare and save an experiment file. The sample list should contain standards for calibration ranging from 0.01 ppb to 100ppm, and wash cycles every 10 to 15 samples, to ensure that sample material is not being carried over from one sample to the next
- Ensure that the samples are listed in the correct rack positions and that the instrument is set to the type of rack you are using

ICP Tuning Procedure

- Place both feed tubes into the high purity tuning solution and allow the ICP to intake the solution for about 5 minutes
- Perform a 1X Daily test
- Turn on He gas to 3.5 mL/min
- Tune:
    - Set Pole Bias to -14 V
    - Set Hexapole Bias to -8 V
    - Set the Focus to 1
    - Set D1 to -48 V
- Ensure that the counts from the tuning solution are high enough
- Place sample feed tube into autosampler
- Place internal standard feed into high purity standard solution
- Click “Queue”
- Append: vacuum
- When experiment finished be sure to release tubing and place into 2 % HNO_3 wash solution and dispose of waste

APPENDIX F

PROTONIC HYPΔH MODELLING SOFTWARE

- Integrated heat data from ITC experiments should be converted to .txt files in order to be imported into modelling software
- Open HypDeltaH software and click "create new project"

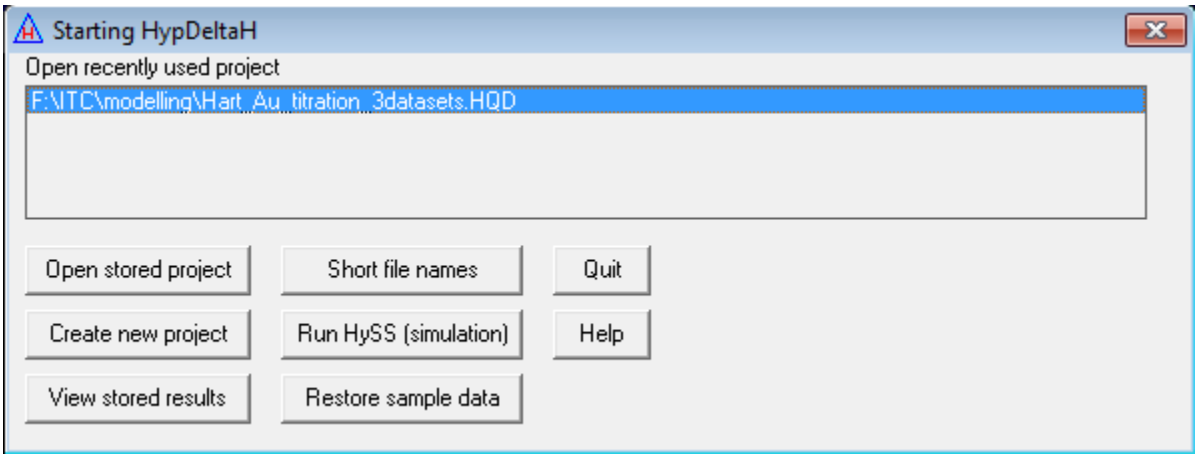

- Enter a unique project title
- Click "Copy model from HQD file" and select the model you will use
- Click "Experimental data file" and select the .txt file with calorimetry data you are trying to model

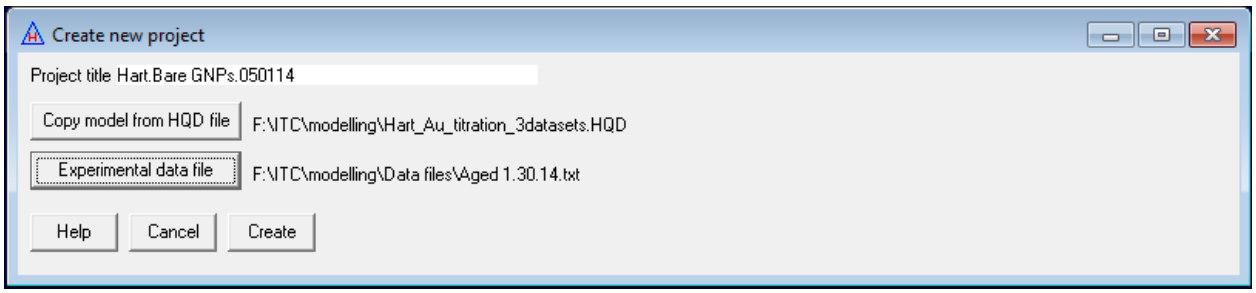

- Click "Create"
  - A window will pop up that says "Check all default (zero or blank) values", click "OK"
- Ensure that the units selected match the data you are modelling. In this dissertation, units of J, mJ, µmol, and µL were used.
- Click "Add reagent" to input the reactants. In this dissertation, NP was added to represent nanoparticle binding sites, and SH to represent the thiol ligand molecule
- Enter an initial guess for Beta. Log(Beta) = K. The initial guess should be close to what the actual value should be

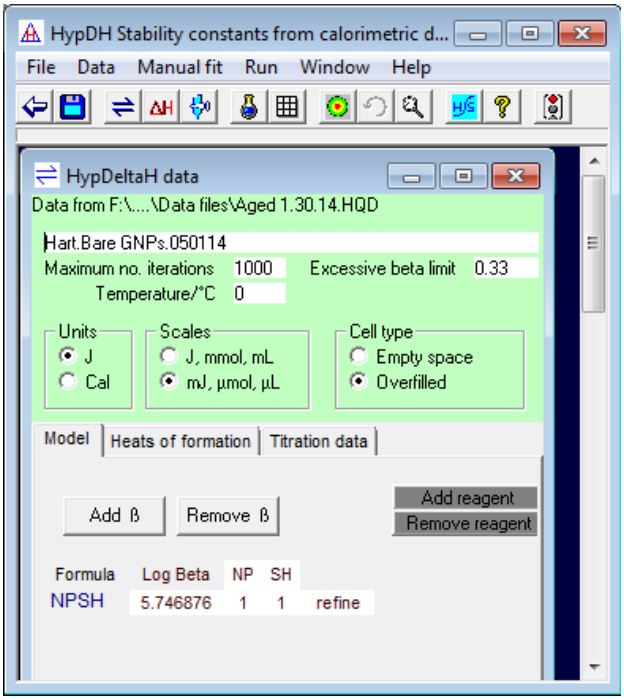

- Click the "Titration data" tab and enter a unique titration curve title for the data set already imported into the software, and enter the experimental parameters

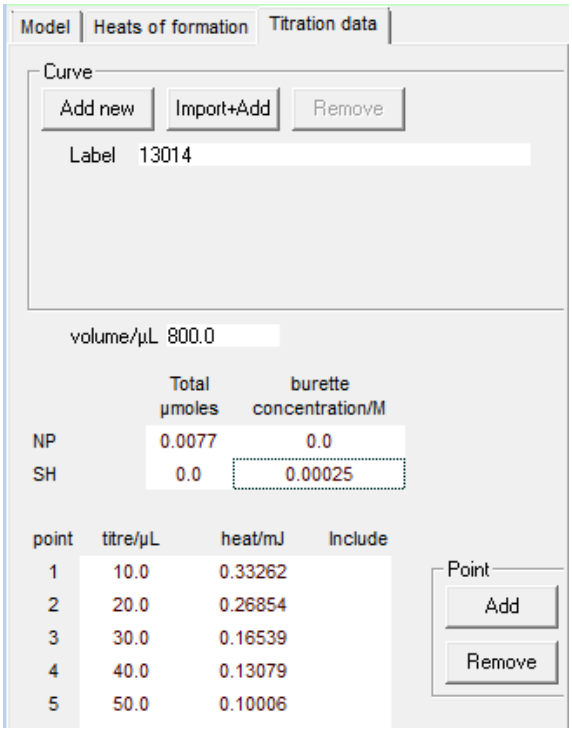

- Click “Import+Add” to import additional data sets for simultaneous modelling, and repeat previous step
- Once all data sets are imported and experimental parameters are entered, click the Green and red circle at the top of the screen

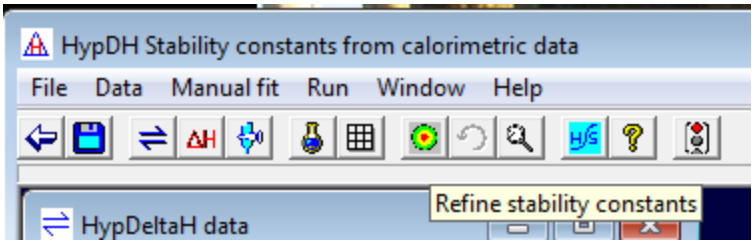

- A window should pop up with the calculated beta and enthalpy values:

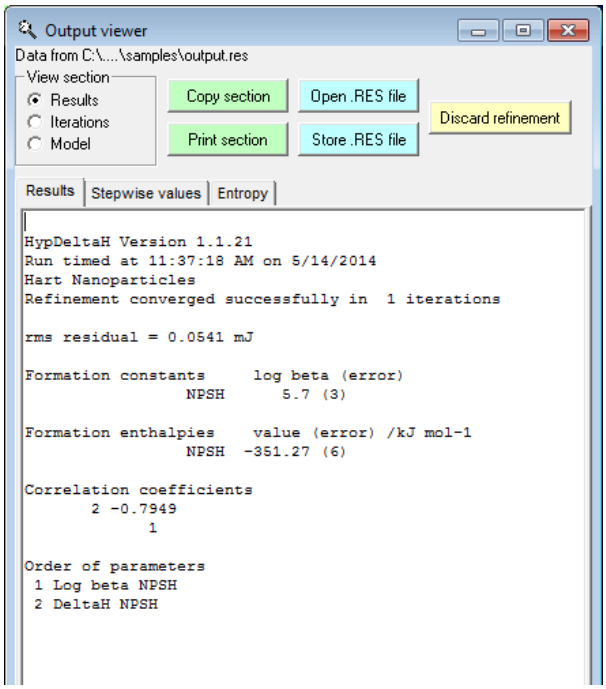

- Click “ Manual fit” in order to view plots of the modelled data;

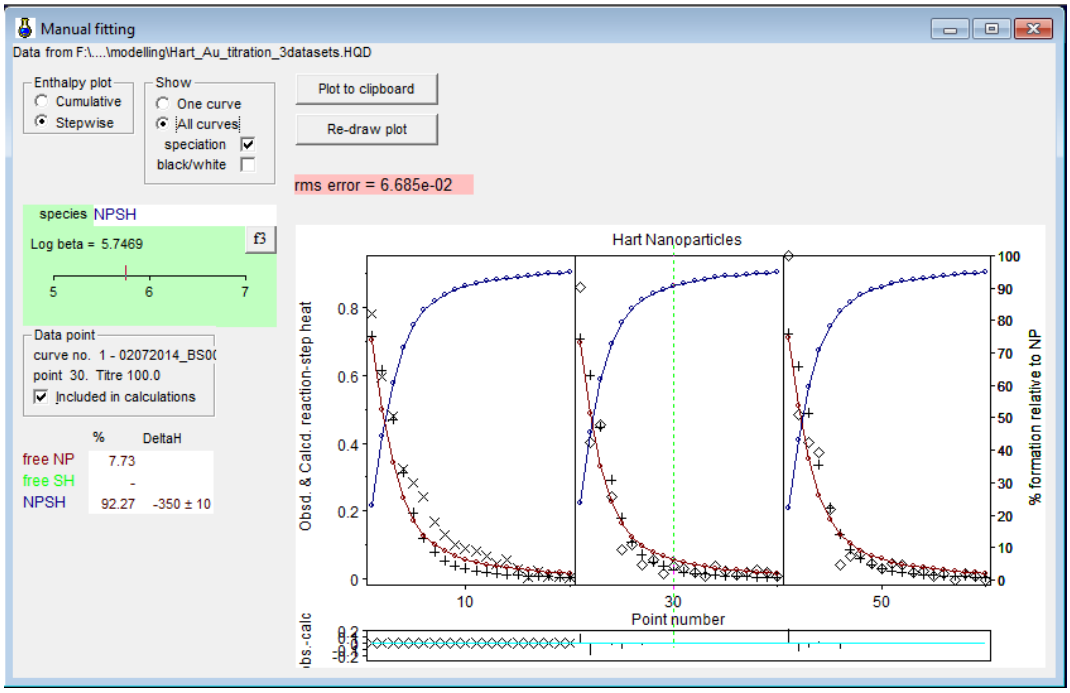

- Reduce the rms error by adjusting the Beta value.
- Once the rms error is minimized, export the data by click the “DeltaH and Concentrations” button. It looks like an empty table.

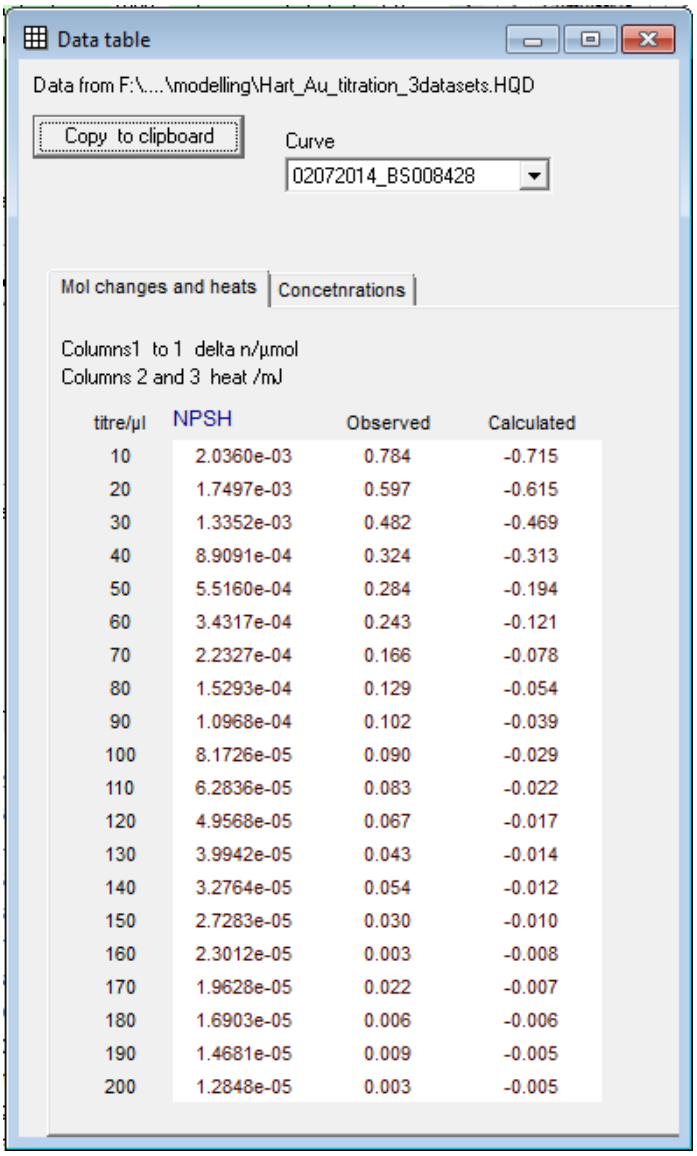

titre/µl	NPSH	Observed	Calculated
10	2.0360e-03	0.784	-0.715
20	1.7497e-03	0.597	-0.615
30	1.3352e-03	0.482	-0.469
40	8.9091e-04	0.324	-0.313
50	5.5160e-04	0.284	-0.194
60	3.4317e-04	0.243	-0.121
70	2.2327e-04	0.166	-0.078
80	1.5293e-04	0.129	-0.054
90	1.0968e-04	0.102	-0.039
100	8.1726e-05	0.090	-0.029
110	6.2836e-05	0.083	-0.022
120	4.9568e-05	0.067	-0.017
130	3.9942e-05	0.043	-0.014
140	3.2764e-05	0.054	-0.012
150	2.7283e-05	0.030	-0.010
160	2.3012e-05	0.003	-0.008
170	1.9628e-05	0.022	-0.007
180	1.6903e-05	0.006	-0.006
190	1.4681e-05	0.009	-0.005
200	1.2848e-05	0.003	-0.005

- Click “Copy to clipboard” and copy the data into excel or another data analysis program. This should be done for each curve fitted